CIVIL ENGINEERING STUDIES

STRUCTURAL RESEARCH SERIES NO. 271

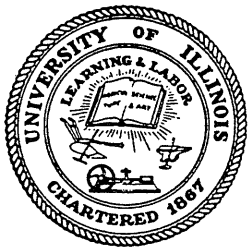

PRIVATE COMMUNICATION
NOT FOR PUBLICATION

THE EFFECT OF REINFORCEMENT ON ANCHORAGE ZONE CRACKS IN PRESTRESSED CONCRETE MEMBERS

by
PETER GERGELY
METE A. SOZEN
and
CHESTER P. SIESS

Issued as a Part
of
PROGRESS REPORT NO. 12
of the
INVESTIGATION OF PRESTRESSED REINFORCED CONCRETE
FOR HIGHWAY BRIDGES

UNIVERSITY OF ILLINOIS
URBANA, ILLINOIS
JULY 1963

THE EFFECT OF REINFORCEMENT ON ANCHORAGE ZONE CRACKS IN PRESTRESSED CONCRETE MEMBERS

by

Peter Gergely
M. A. Sozen
C. P. Siess

Prepared as a Part of an Investigation
Conducted by

THE ENGINEERING EXPERIMENT STATION
UNIVERSITY OF ILLINOIS

In cooperation with

THE DIVISION OF HIGHWAYS
STATE OF ILLINOIS

and

U. S. DEPARTMENT OF COMMERCE
BUREAU OF PUBLIC ROADS

Project IHR-10

INVESTIGATION OF PRESTRESSED REINFORCED CONCRETE
FOR HIGHWAY BRIDGES

Urbana, Illinois

July 1963

TABLE OF CONTENTS

TABLE OF CONTENTS (Continued)

LIST OF TABLES

LIST OF FIGURES

LIST OF FIGURES (Continued)

LIST OF FIGURES (Continued)

LIST OF FIGURES (Continued)

LIST OF FIGURES (Continued)

1. INTRODUCTION

1.1 Introductory Remarks

Considerable attention has been paid to the problem of anchorage zone stresses in recent years. Surveys have reported that more than half of the prestressed concrete girders inspected had visible longitudinal cracks in the end blocks. The majority of the authors concerned with the question, has treated the problem in terms of elastic stresses in homogeneous bodies. There has not been a general design method of transverse reinforcement, satisfactory for the use in the design office or for the inclusion in a code. A review of the relevant references constitutes Appendix A of this study.

The analytical and experimental investigation, reported in this work, resulted in a simple design procedure that bypasses the use of a hypothetical elastic stress distribution.

The anchorage zone (or lead-in zone) of a prestressed concrete beam is the portion of the beam where the prestressing forces disperse into the beam to a section where the stresses are linear. Due to the curvature of the flow of the prestressing forces into the beam, there are transverse tensile stresses of considerable magnitude. Without reinforcement, these stresses induce large cracks in the beam and may thus be detrimental to the performance of the beam.

1.2 Object and Scope

The main object of this study was the investigation of the behavior of the anchorage zones of prestressed concrete beams after the first crack has formed.

The first part of the work centered around the problem of crack initiation. A series of tests (three rectangular and seven I-beams) was

conducted to study the strain distribution and the propagation of cracks in specimens without reinforcement. A finite difference solution was made to obtain the elastic stress distribution in a specific case.

The second part of the work was concerned with the arrest of the longitudinal crack with the purpose of developing a procedure for the design of transverse reinforcement. A series of tests (14 rectangular and 11 I-beams) was conducted to study the effect of reinforcement on the propagation of cracks and to corroborate the analytical method. The basic differences between the behavior of anchorage zones of rectangular and I-shaped sections was examined. A few bond tests were also made to obtain force-slip relationships for the reinforcement used in the beams.

A large part of the previous experimental work had been done on concentrically loaded specimens, in which case the highest transverse stresses occur along the line of the load. In the present investigation, high eccentricity was employed to study the critical zone away from the load.

The design specifications developed in this investigation are presented in Chapter 6, including some illustrative design examples.

1.3 Acknowledgments

This study was carried out as a part of the research under the Illinois Cooperative Highway Research Program Project IHR-10, "Investigation of Prestressed Reinforced Concrete for Highway Bridges." The work on the project was conducted by the Department of Civil Engineering of the University of Illinois in cooperation with the Division of Highways, State of Illinois, and the U. S. Department of Commerce, Bureau of Public Roads.

On the part of the University, the work covered by this report was carried out under the general administrative supervision of W. L. Everitt,

Dean of the College of Engineering, Ross J. Martin, Director of the Engineering Experiment Station, N. M. Newmark, Head of the Department of Civil Engineering, and Ellis Danner, Director of the Illinois Cooperative Highway Research Program and Professor of Highway Engineering.

On the part of the Division of Highways of the State of Illinois, the work was under the administrative direction of R. R. Bartelsmeyer, Chief Highway Engineer, Theodore F. Morf, Engineer of Research and Planning, and W. E. Chastain, Sr., Engineer of Physical Research.

The program of investigation has been guided by a Project Advisory Committee consisting of the following:

Representing the Illinois Division of Highways

W. E. Chastain, Sr., Engineering of Physical Research, Illinois Division of Highways

W. J. Mackay, Bridge Section, Bureau of Design, Illinois Division of Highways

C. E. Thunman, Jr., Bridge Section, Bureau of Design, Illinois Division of Highways

Representing the Bureau of Public Roads

Harold Allen, Chief, Division of Physical Research, Bureau of Public Roads

E. L. Erickson, Chief, Bridge Division, Bureau of Public Roads

Representing the University of Illinois

C. E. Kesler, Professor of Theoretical and Applied Mechanics

Narbey Khachaturian, Professor of Civil Engineering

Fred Kellam, Bridge Engineer, Bureau of Public Roads and George S. Vincent, Chief, Bridge Research Branch, Bureau of Public Roads, also

participated in the meetings of the Advisory Committee and contributed materially to the guidance of the program.

The investigation was directed by Dr. C. P. Siess, Professor of Civil Engineering, as Project Supervisor and as ex-officio chairman of the Project Advisory Committee. Immediate supervision of the investigation was provided by Dr. M. A. Sozen, Professor of Civil Engineering, as Project Investigator.

Acknowledgment is due to W. A. Welsh for his invaluable assistance in the conducting of the experiments.

This report was written as a thesis under the direction of Profess M. A. Sozen.

1.4 Notation

a = height of the loading plate

A = cross-sectional area of rectangular beams

A_s = cross-sectional area of one reinforcing bar

b = width of rectangular cross section

c = distance between longitudinal section and the bottom of the beam

e = distance between the resultant prestressing force and the bottom of the beam

e_t = eccentricity of the total prestraining force

E = modulus of elasticity of the stirrups

f'_c = compressive strength of concrete determined from 6 by 12 control cylinders

f_s = steel stress in stirrups

F = force in stirrup

F = two dimensional Airy stress function

F_T = total stirrup force

g = unit bond defined as force per unit length

h = height of beam

T = designation of beams with I-shaped cross section

l = crack length

m = ratio of g and $\sqrt{f'_c}$

M = moment induced by prestressing forces on transverse sections

M_m = the maximum unbalanced moment caused by forces acting on a free body bounded by a transverse section and a longitudinal section

P = resultant of a group of prestressing forces immediately after release

r = radius of gyration for the gross plain section

R = designation of rectangular beams

s = slip of bars in pull-out tests

w = crack width

x = transverse coordinate axis

y = longitudinal coordinate axis

z = distance between the end of the beam and the centroid of the areas of the stirrups that are within h/2 from the end

τ_{xy} = shear stress in anchorage zone

σ_x = normal stress on longitudinal planes

σ_y = normal stress on transverse planes

μ = Poisson's ratio

2. ANALYSIS OF ANCHORAGE ZONE STRESSES

2.1 Introductory Remarks

The computed elastic stress distribution in an end block is presented in this chapter. There are numerous solutions available but the agreement among them is not very good. Different authors have used different approximations and assumptions. A finite difference solution was made in this investigation to attempt to establish the correct stress distribution.

The elastic stress distribution is affected by the eccentricity of the load, the distribution of the applied forces in the three principal directions with respect to the axis of the end block, and the geometry and material properties of the end block.

When the load is concentric, the tensile stresses along the line of the load dominate. As the eccentricity increases, the stresses away from the line of the load and near the end face increase. In this investigation, solutions were obtained for large eccentricities to explore the latter case.

2.2 Analysis of Stresses

The analytical investigation that was carried out to determine the stresses in a specific case is described in this section. The results will be compared with those obtained by others in Section 2.4.

The region considered had a width of 12 inches. A single eccentric load was applied at 4.5 in. from the center line. It was spread over a distance of 1.5 in. The load was considered to be a line load normal to the plane of the region, that is, the problem was treated as two-dimensional. Homogeneity, isotropy and linear elasticity were assumed for this solution. The consequences of these assumptions are discussed in Chapter 4 and in Appendix A.

The solution was based on the two-dimensional Airy stress function method. The stress function has to satisfy the biharmonic differential equation $\nabla^4 F = 0$ throughout the region. The stresses are given by the second derivatives of the stress function.

The region can be seen in Fig. 2.1 where the boundary conditions are also shown.

All existing solutions indicate that St. Venant's principle holds, that is, the stress distribution reaches the one predicted by conventional methods at a distance equal to the depth of the section, or sometimes less. In this investigation a larger region was considered to confirm the principle. The width of the region was 12 in. and the length was 20 in. At this distance from the end face the longitudinal stresses were taken to be equal to the linear stress distribution obtained from elementary methods and the shear stresses were put equal to zero. Hence,

$$F_{xx} = \sigma_y = \frac{P}{A} + \frac{My}{i} = -\frac{4.5}{12} x + 1.25$$

and

$$F_{xy} = \tau_{xy} = 0$$

where the subscripts on F indicate derivatives.

The two integration constants were ignored since they do not influence the second derivatives of the stress function. Thus,

$$F = -\frac{4.5}{72} x^3 + 0.625 x^2$$

where $P = A = 72$ has been used for simplicity.

On the longitudinal boundaries of the region $F_{yy} = \sigma_x = 0$ and $F_{xy} = \tau_{xy} = 0$. Also the general boundary conditions of the theory of

two-dimensional elasticity require that on a side parallel to the x-axis (1),*

$$\int \tau_{xy}\, ds = F_y \qquad \text{and} \qquad \int \sigma_y\, ds = F_x$$

Therefore, on free boundaries F_x and F_y are constant. At the corners the values, as calculated on the two sides, must agree. This yields relations to evaluate the integration constants.

The boundary values of the stress function and its normal derivatives are shown in Fig. 2.1. With these values known, the stresses inside the region can be computed by one of several methods.

In the present investigation, the biharmonic differential operator was replaced by the corresponding finite difference operator. The region was divided into 1/2 by 1/2 in. grid systems, yielding 897 internal grid points. The value of the stress function at grid points on the boundary is calculated from the functions shown on Fig. 2.1. The normal derivatives give the necessary relationships between the imaginary grid points immediately outside the boundary and grid points immediately inside it. The resulting system was solved by iteration. The computation and the computer program are described in Appendix C.

2.3 Results of Analysis

The computer calculated and printed the transverse, longitudinal and shearing stresses and the transverse strains for a Poisson's ratio of 0.10. The Young's modulus was taken as 3,900,000 psi. For some points in the critical parts of the region, the principal stresses were calculated to

---

* Numbers in parentheses refer to entries in the List of References.

obtain a quantitative idea of their variation from the longitudinal and transverse stresses. Solutions were also obtained at points of maximum stress in the critical regions for values of Poisson's ratio equal to 0.15 and 0.20.

Contours of equal transverse stress are plotted in Fig. 2.2. The tension and the compression zones are indicated. The tensile stresses under the load occur at a distance from the end face and are called bursting stresses while the tensile stresses at the top of the region are called spalling stresses.

In the case considered in the present investigation, the spalling stresses are higher than the bursting stresses and the first crack is expected correspondingly at the surface near the centerline. When the eccentricity decreases, the bursting stresses become relatively more important.

The longitudinal stresses on transverse sections and the transverse stresses on longitudinal sections will be presented in the next section.

The total tensile forces on longitudinal sections are plotted in Fig. 2.3 separately for the bursting and spalling stresses. It can be seen that the maximum values of these forces due to the two kinds of stresses are about equal. However, the spalling stresses are more concentrated as shown in Fig. 2.2.

The centers of gravity of the tensile stresses on longitudinal sections are also shown in Fig. 2.3. The forces are close to the end face in the spalling zone while they are at a distance from the edge in the bursting zone.

The study of the effect of the variation of Poisson's ratio showed that it has considerable influence on the transverse strains only close under the load where the longitudinal stresses are high. The maximum bursting

stresses, about one inch under the load, are changed by about 20 per cent due to a variation in the Poisson's ratio from 0.10 to 0.15 (see Fig. 2.4). This difference is larger where the transverse stresses are small and, hence, the effect of the longitudinal stresses become more important. The consequence of the alteration of Poisson's ratio is negligible in the spalling zone where the longitudinal stresses are small.

The principal stresses differ appreciably from the transverse and longitudinal stresses only in regions where the latter stresses are about equal (and small) and opposite in sign, and the shearing stresses are large. This can be seen from the Mohr's circle of stresses. These conditions exist near the top of the region, about one inch away from the line of the load. The principal tensile stress is substantially larger than the transverse stress at few points only. The increase is 100 per cent half an inch from the edge, between the load and the center line. However, the stresses are small there, hence the increase is not significant. At points of large stress, the difference is less than 2 per cent.

More information will be given about the stress distribution in the following section and in the next chapter.

2.4 Comparison with Results Obtained by Various Investigators

The most comprehensive sets of curves and tables were given by Guyon (2). His results are used by most designers but some researchers have questioned his approach. Recently, Gerstner and Zienkiewicz verified Guyon's calculations by using a different method of calculation (3) and Iyengar confirmed his results at least for the symmetric case using different boundary corrections (4).

The longitudinal stress distribution from the finite difference solution is compared with Guyon's results in Fig. 2.5. The agreement is good. The stresses close to the unloaded corner of the region are small, and, therefore, the solutions are probably less accurate there. The principle of St. Venant is demonstrated.

The transverse stresses are shown in Fig. 2.6. The stresses calculated by Guyon are smaller than those resulting from the finite difference solution. Part of this difference is due to the fact that the plots of Guyon in Fig. 2.6 are for a concentrated load while the finite difference method considered distributed load. The shape of Guyon's stress curve under the load is not known with good accuracy since interpolation does not yield the maximum values that occur between published values. Also, the maximum compressive stress at the end face (under the load) is not given.

Most other solutions differ considerably from the above results. Bleich's boundary corrections were not as good as Guyon's and hence Bleich's stresses are not correct. The method by Magnel gives reasonable stress distribution only along the line of the load (Fig. 2.7). Along other lines the stress distribution does not resemble a cubic parabola that Magnel assumed. It can be seen that the length of the "lead-in zone" in his analysis must be assumed correctly. At L/4 from the loaded end, the stresses are zero. The transfer length should be at least 8 in. which would put the point of zero stress at a distance of 2.5 in. from the loaded end. The computer solution indicated 0.7 in. for this distance. Also, the position of maximum tensile stress (fixed at L/2 in Magnel's approach) is much shorter in the finite difference solution and in other solutions mentioned above. To get a stress distribution similar to those given by the "exact" methods, Magnel's method requires a lead-in length that is unreasonably short.

The principle of partitioning (symmetrical prism method), advanced by Guyon, results in very good approximations to the bursting stresses. This method considers an imaginary prism "cut" from the eccentrically loaded block in such a way that the load acts concentrically on the prism. The widths of the prisms are determined by the distances to the nearest boundaries or by the distance to the neighboring prism. There are many solutions available for the axially symmetric case and the agreement among them is good. The stress distribution calculated by the symmetrical prism method is compared with the finite-difference solution in Fig. 2.8. It can be seen that in the case where the actual distribution of the load is taken into account, it gives a good approximation. However, this method does not offer any information about the spalling stresses.

Most authors emphasize the importance of the size of the loading plate. This is especially justified in the case of a concentric load. The spalling stresses (primarily when caused by eccentric loads) are not as much affected by the relative size of the loading plate. In this investigation the eccentricity was large and the spalling stresses controlled. Hence, the size of the loading plate was not considered to be a major variable.

There are significant differences between the magnitude and distribution of transverse tensile stresses along the line of the load for concentric and eccentric loads. A specific comparison is shown in Fig. 2.9. The distribution of transverse stresses for concentric loading is taken from Reference 4. The distribution for an eccentricity of 0.375h is obtained from the finite difference solution. The curves in Fig. 2.9 show that the depth of the tensile zone for eccentric loading is smaller than that for concentric loading while the maximum stress is larger for eccentric loading. The total tensile force acting on the line of the load is 0.12P for eccentric loading and 0.23P for concentric loading.

3. RESULTS OF TESTS ON SPECIMENS WITHOUT REINFORCEMENT

3.1 Introductory Remarks

In methods of design based on elastic conditions, the tensile forces in end blocks are calculated from a theoretical stress distribution and reinforcement is provided to resist all or part of this force. There are three drawbacks to this approach:

(a) There is no rigorous solution for stresses in the anchorage zone. In relation to design, this is a minor disadvantage, since the differences in the magnitudes of the tensile force based on different solutions are small compared with other uncertainties involved.

(b) There is inelastic action in the end block almost immediately upon application of the load and certainly in advance of cracking.

(c) The reinforcement cannot act effectively before cracking. After cracking, the force distributions based on elastic analysis of a continuous medium are invalid.

The tests presented in this chapter were carried out to serve two purposes: to compare the strain distribution in a concrete end block with distributions based on elastic analyses and to study the conditions following the initiation of the crack.

Two kinds of specimens were tested: rectangular beams and I-beams. The dimensions of the specimens are given in Appendix B and are shown in Fig. B.1. The average concrete strength was about 5000 psi. The loading arrangement is sketched in Fig. B.6. The specimens were tested to failure or up to 50 kips of load, whichever came first.

Three rectangular and seven I-beams were tested without reinforcement. One of the beams (I7) consisted of the bottom half of the regular section (inverted T-section).

In all tests the cracks were observed using a magnifying glass. Gages were mounted on the sides, along longitudinal lines, on three rectangular and three I-beams. A typical gage pattern on a rectangular beam is shown in Fig. B.4. The line of gages at 3.5 in. from the center-line was not employed on I-beams. The gages were on the "test end" of the beams, that is, where the height of the bearing area was 1.5 in.

The behavior of the specimens without reinforcement is discussed in the next section in terms of load-strain curves, strain distributions and cracking. There were no visible cracks at 20 kips, hence the strains will be studied at 10 and 20 kips. The measured strains will be compared with the computed values in Section 3.3.

3.2 Behavior of Specimens without Reinforcement

(a) Rectangular Beams

The transverse stresses in the spalling and bursting zones were studied by strains measured along longitudinal lines. In particular, the lines along the axis of the load and along the center line were used to compare some aspects of the behavior of the two zones.

The study of the change of strains at certain points with the applied load discloses the initiation of inelastic action. Figure 3.1 shows the variation of strains with load at points 0.5, 1.0, 1.5, 2.0 and 3.0 in. under the center of the loading plate in Specimen R1. It can be seen that nonlinear response started at a load of about 15 kips. The first visible crack occurred at about 24 kips. Probably there were microcracks at lower loads as indicated by the high tensile strains measured. It should be noted that "strain" refers to the unit deformation measured over the length of the strain gage which was 0.75 in. Measured strains of 0.0006 do not

necessarily indicate strains in the intact concrete, which must have cracked at a strain less than 0.0002. This was reached at about 17 kips of load. No cracking was noticed at this load under examination with a magnifying glass.

The curves in Fig. 3.1 are representative for rectangular beams. Similar plots for Beams R2 and R3 are shown in Figs. 3.2a and 3.3a.

Figure 3.2b shows load-strain curves at points 0.5, 1.0, 1.5 and 2.0 in. from the edge, along the center line of Specimen R2. The reversal of strain must indicate cracking elsewhere in the specimen. First, the gage nearest the edge reversed at about 14 kips, followed by the other gages in turn, evincing the progress of cracking. The crack became visible about 0.5 in. below the center line at a load of about 24 kips. Thus, the gages were near the crack on the top half of the specimen. The contraction indicated is attributable to transverse shrinkage stresses that are released when the crack forms near the gage. The shrinkage stresses are largest near the surface of the beam, hence the gage nearest the surface shows the largest contraction. Similar curves for Specimen R3 are shown in Fig. 3.3b.

The comparison of Figs. 3.2a and 3.2b indicates that the cracking in the spalling zone had little effect on the load-strain curves at points in the bursting zone. This fact substantiates the principle of partitioning given by Guyon (Section 2.4). Since the bursting stresses are not sensitive to the behavior of the spalling zone, the bursting zone can well be approximated by conditions in a symmetric prism.

Representative load-strain curves at points along the lines 1.0 in. from the line of the load and along a line 1.5 in. from the center line are shown in Fig. 3.2c. The strains off but near the line of the load are small and show no definite trend. The gages off the line of the center line

registered a sudden increase of strain at about 16 kips when a crack must have formed across the gages.

The distribution of strains along longitudinal lines will be studied later in this chapter. Representative curves in Fig. 3.4 show that the transverse strains along the line of the load are distributed in the manner of bursting strains. A maximum value is reached at about one inch from the end and the strains decrease toward the end of the specimen. The strains along the center line are typical of spalling strains. The transverse strains increase steadily toward the end of the beam. These curves were measured in Specimen R2. Similar curves will be shown at the end of this section and in the next section.

The development of cracks was carefully observed in all tests. There were three types of cracks: those in the spalling zone started at about mid-height at the end face of the specimen. The second kind of cracks initiated under the load at a distance of one to two inches from the loaded edge. The third group of cracks were flexural cracks at the top of the beam and were of no interest in this investigation. They were controlled by a No. 3 bar placed near the top of the specimens.

In Specimen R3 (as in Specimens R1 and R2) the first crack appeared 5.5 in. from the bottom starting at both ends and extending 3 in. (Fig. 3.5). This occurred at a load of 24 kips. One flexural crack also started near the center of the beam at the top. The progress of the cracks is shown in this figure. The failure was due to a wedge type of bearing failure under the 1.5 in. bearing block. There was no observable crack under the loading plate before this occurred. The measured strains were the highest in this region. It is probable that the glue and the strain gages prevented the vision of cracks.

It can be seen that there is symmetrical behavior. On the left end of the beam (as shown in Fig. 3.5) the loading block was 1.5 in. high ("test end") and 3.0 in. on the right end. The size of the loading plate influences the stresses under the load but has little effect away from the load. The bearing failure is induced under the smaller loading block.

(b) I-Beams

The strains were measured in two I-shaped beams. In order to check the participation of the top part of the beam, a half I-beam (inverted T-shape) was also tested.

The load-strain curves for I-beams give information similar to that of rectangular beams, as discussed above. The load-strain curves shown in Figs. 3.6a and 3.6b for Specimen T2 are representative for I-beams. In Fig. 3.6a the load-strain curves are plotted for points along the line of the load. Nonlinear response started about 7 kips. Similar curves for points along the center line and along a line 1.5 in. from the center line are plotted in Fig. 3.6b. There is no reversal of the strains along the center line shown in Fig. 3.6b, implying that there was no longitudinal cracking in the specimen up to a load of 20 kips. The first visible crack occurred at about 30 kips. The corresponding sets of curves for Specimen T3 are plotted in Figs. 3.7a and 3.7b. The observations made above hold in general with the exception that in this beam the crack became visible at 15 kips that corresponds to the early reversal of strains along the center line as can be noted in Fig. 3.7b. (The difference in cracking load was caused by a manufacturing defect discussed later in this section). Since the strains were very small at points 1.5 in. below the center line, the values along this line in Fig. 3.7b are erratic.

Specimen T7 was a half I-beam or an inverted T-beam. The strains were measured along the line of the load. The load-strain curves are shown in Fig. 3.8. In this case the largest strains were measured at the gage 0.5 in. from the edge while in the regular I-beams the largest strains were measured farther from the end. There is nonlinear action starting at about 10 kips. This can not be due to cracks in the web, since in this specimen there was no active web.

The transverse strains along the center line of Specimen T2 are shown in Fig. 3.9. The distribution resembled the spalling stress distribution. The strains along the line of the load (shown in Fig. 3.10) followed the typical distribution of bursting strains.

Specimen T3 failed prematurely by crushing under the loading plate, probably due to local irregularities. Beam T2 had a very small crack on one side of the junction of the web and the flange as shown in Sketch 3.1. There

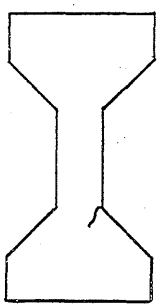

Sketch 3.1

was antisymmetric action due to this accidental crack. The strains in the flange were large on the other side, while in the web they were small on the side of the crack. The large strains on the opposite side in Specimen T2 increased the average as shown in Fig. 3.10.

The typical development of the cracks in the I-beams is demonstrated in Fig. 3.11. On the right hand side the height of the end block

was 3 in. and, therefore, it covered half of the tapered part of the flange. This caused the longer cracks in the right-hand end of the beam. The crack occurred at 5.5 in. from the bottom in Beams T3, T4, T5 and T6 and at 4.5 in. in Specimens T1 and T2.

At high loads the crack progressed 15 to 20 in. from the ends. To get an idea of the participation of the top part of the beam, Specimen T7 was tested. It was a half I-beam (inverted T-shape) with strain gages placed along the line of the load. The strains are plotted in Fig. 3.12. Again, there was considerable nonlinear behavior. The distribution of strains resembles that for spalling strains since there is no measurable decrease in the tensile strains near the end face. The compression zone was evidently small enough not to be detected by the first gage that was 0.5 in. from the edge.

(c) Comparison of the Behavior of the Specimens

Some important conclusions, valid for single loads acting in the flange, can be drawn from the comparison of the behavior of the above specimens. The main question is the difference between the behavior of the rectangular and I-beams. Is the I-beam much weaker than the rectangular beam because of the smaller section of the web that may fail sooner under the spalling stresses? The comparison of the transverse strains and the crack patterns for the rectangular and I-beams is discussed in the following paragraphs.

The measured transverse strains along the line of the load for the rectangular beam R3 and the I-beam T3 are compared in Fig. 3.13. The difference in the strains is small, especially at higher loads. The larger increase of transverse strains in the I-beam is due to the nonlinear response

that started earlier in the I-beam than in the rectangular beam (as it was seen in Figs. 3.1, 3.2a, 3.3a, 3.6a and 3.7a). The faster increase of strains in I-beams cause the diminishing of the difference that can be observed in Fig. 3.13. The explanation of the earlier nonlinear response of the I-beam as compared with the response of the rectangular beam will be given later in this section.

The measured transverse strains along the center line for Specimens R3 and T2 are shown in Fig. 3.14. The strains in the rectangular beam are somewhat higher, but the difference is small. The strains did not increase at the end of Beam T2 at about 20 kips of load. This indicates cracking near the gages as it was discussed earlier in this section in connection with the consideration of Figs. 3.2b and 3.3b.

The development of cracks was different in the rectangular and I-beams (Figs. 3.5 and 3.11). There were more flexural cracks in the rectangular beam than in the I-beam. The tensile bending stresses on the top surface are smaller in an I-beam. The length of the cracks in the web were of similar magnitude, except that at the right-hand end of the I-beam, where the loading plate covered part of the tapered part of the flange, the cracks were longer. This shows that if part of the loading acts in the web, there is greater participation of the web in carrying the load.

The comparison of transverse strains and the crack patterns in rectangular and I-beams has shown that the presence of the web does not weaken the I-beam if the load acts in the flange. The smaller forces in the web of an I-beam as compared with the web portion of a rectangular beam can be explained by the different manner in which the load disperses into the main part of the beam. In a rectangular beam the stresses flow at a rapid

pace into the "web" portion of the specimen. The upmost of these stress flow trajectories becomes almost vertical at a point close to the edge of the end block. This results in larger stresses in the area around the mid-height of the rectangular beam than in the web portion of the I-shaped block. In an I-beam most of the force is confined to the flange. As a result of this concentration, the web portion of the end block close to the end face is stressed less than the corresponding area of the rectangular beam. The curvature of the trajectories is small, hence the transverse stresses are expected to be smaller in I-beams.

This difference in response explains the small difference between the transverse strains in rectangular and I-beams (Figs. 3.13 and 3.14). The strains in the I-beam were smaller, except at higher loads when, due to cracks in the spalling zone, the web portion of the rectangular beam (without reinforcement) could not carry the extra force that caused the difference in strains at smaller loads. Thus, in the cracked state the responses of the two kinds of beams become similar and, correspondingly, the strains in the cracked beams were almost equal.

The longer cracks on the end of I-beams where the loading plate was larger are due to the fact that greater part of the load goes into the web. Thus, on this end the behavior is between that of rectangular and I-beams.

The approximately equal strains in the web portion of the rectangular and I-beams correspond to the smaller forces in the web of I-beams. The comparison of forces will be given in Chapter 5 in connection with the discussion of the tests on beams with reinforcement.

Comparison of the strains in Specimens T3 and T7 (half beam) shows that the distributions of transverse strains along the line of the

load are similar in the two beams. Hence, the flange can be considered to act independently from the web for the purpose of analyzing bursting stresses. The behavior of the flange is not influenced much by the presence of the web if the load acts in the flange. This suggests that the symmetrical prism method is feasible.

3.3 Comparison of Analytical and Experimental Results

The measured strains follow the theoretical distribution of bursting and spalling strains in general. The strains along the line of the load (bursting zone) reach the maximum at a distance of one to two inches from the end and indicate that there is a compression zone under the load. The measured strains along the center line increase toward the end face, agreeing with the theoretical distribution of spalling stresses.

The measured strains along the line of the load are compared with the results of the finite difference solution in Fig. 3.15. The two bands for the finite difference solution represent strains calculated using two sets of values of the modulus of elasticity and Poisson's ratio. If Poisson's ratio is changed from 0.10 to 0.20, the maximum strain (47×10^{-6}) will increase about 34 per cent (to 63×10^{-6}). The actual value of Poisson's ratio is between the above values, hence the variation of this parameter may cause about 15 per cent change in the strains.

One of the curves in Fig. 3.15 represents the results of the finite difference solution using 3,800,000 psi for the modulus of elasticity. This is about the value estimated for compressive stresses. In tension, however, the modulus of elasticity becomes considerably smaller with increasing stresses. The maximum transverse tensile stress at 10 kips of load is about 100 psi. At this stress the modulus could reduce by as much

as 50 per cent. Using this value as a conceivable limit, the strains are plotted for a modulus of elasticity of 1,900,000 psi in Fig. 3.15. The combined effects of the changes of the modulus of elasticity and Poisson's ratio may change the maximum strain from 47×10^{-6} to 126×10^{-6}.

The measured transverse strains fall between the two sets of values obtained from the finite difference solution. Since the two sets represent probable extreme values, the measured strains agree reasonably well with the results of the finite difference solution. More information is needed about the basic behavior of concrete in tension, especially under sustained loads, to permit good estimation of the modulus of elasticity.

Measured transverse strains along the center line of the beam are compared with the results of the finite difference solution (for a Poisson's ratio of 0.10 and a modulus of elasticity of 3,800,000 psi) in Fig. 3.16. The measured strains follow the calculated ones but are somewhat larger. A small decrease of the modulus of elasticity would bring the calculated strains to close agreement with the measured values. Since the compression in the longitudinal direction is small, the effect of Poisson's ratio on the strains is small in the spalling zone.

It was found in these experiments that minute initial irregularities (cracks, voids) may have substantial effect on the strain distribution in the highly stressed regions.

The microcracks in the bursting zone are distributed and cause general increase of strains. In the spalling zone, due to the concentration of stresses, one large crack forms.

4. ANALYSIS OF END BLOCKS WITH TRANSVERSE REINFORCEMENT

4.1 Introductory Remarks

The object of this chapter is to analyze the forces and the extent of cracking in reinforced end blocks in order to develop a method of arresting cracks due to transverse stresses. The presence of the crack has to be admitted a priori when the action of reinforcement is investigated.

A common method of designing reinforcement for end blocks is to compute the tensile stresses and forces according to some elastic solution and then to provide steel at an arbitrary working stress to carry the total tensile force or part of it. This approach ignores some important aspects of the behavior of end blocks. There is inelastic action at relatively low loads that changes the stress distribution. The concrete must be cracked before the reinforcement comes into action. The formation of a crack invalidates the elastic stress distribution. An initial crack (for example, at the junction of the web and the flange, as found in Beam T2 of the present investigation) also modifies the elastic conditions. Even for an assumed elastic case, there is no generally accepted solution, as it was mentioned in Chapter 2. In addition, the tensile strength of the concrete under complex conditions is not known sufficiently.

The analysis presented in this chapter investigates the conditions in a cracked end block in order to limit the length and width of the crack. A method is presented that estimates the position of the first crack. The equilibrium of the free body bounded by the crack is investigated in order to estimate the internal forces. The relationship between the width and length of the crack and the stirrup is also examined.

4.2 Equilibrium Conditions in the End Block

The equilibrium of a cracked end block with rectangular cross section is considered. The admitted longitudinal crack and the inside end face of the lead-in zone cut out the free body. The following quantities enter the analysis: applied force, stirrup force, the length and width of the crack and the dimensions of the end block.

The forces acting on the free body are shown in Fig. 4.1. The crack and the applied load are at distances of "c" and "e" from the bottom of the end block, respectively. The sketch on the top part of the figure illustrates the beam with the free body marked in full lines. The prism is shown enlarged in the bottom part of the figure.

The applied force P produces a linear stress distribution at a distance L from the end. To maintain equilibrium, there must be a moment M and a shearing force acting on the top part of the prism. The moment is to be supplied by the tensile force T in the reinforcement and by the compression C in the concrete. The height of the free body (that is the position of the crack) will be determined from the condition that on that longitudinal section the moment will be the largest.

The moment on the longitudinal section is:

$$M = P\left[c - e - \left(\frac{c}{h}\right)^2 \left(2h - 3e - c + \frac{2ec}{h}\right)\right] \qquad \text{if } c > e$$

This moment (and, hence, T and C) changes with the height of the free body (c). The moment takes extreme values for the following two values of c:

$$c_1 = \frac{h^2}{3\ (h - 2e)} \qquad \text{and} \qquad c_2 = h \qquad \text{for } 3e < h$$

The first of these gives the maximum moment, the second gives the zero moment on the top surface. The magnitude of the former is:

$$M_{max} = P\left[\frac{h^2}{27} \cdot \frac{4h - 9e}{(h - 2e)^2} - e\right]$$

If $3e \geq h$, the maximum moment occurs along the line of the load. This moment can be obtained from the general expression of the moment by setting $e = c$. This yields

$$M_e = 2P \frac{e^2}{h^3} (h - e)^2 \qquad \text{for } c = e$$

Knowing the moment, the forces can be calculated if the distance between the forces can be estimated. The position of the tensile force is given by the center of gravity of the stirrup forces. The position of the compressive force is not known. It is somewhere between the end of the crack and the end of the lead-in zone. This interval is small under working conditions. In designing reinforcement for the end block, the lever arm must be estimated. The length and width of the crack is limited by serviceability requirements. If the position of the compressive force is assumed to be at the end of the crack, the design will be on the safe side. Thus, the length of the crack must be known.

The direct analysis of the length of the crack is not practical because of the many factors that are involved. The stress conditions are complex at the tip of the crack. The situation is sketched in Fig. 4.2. A moment and a force act on the left end of the bottom part of the beam. The stirrups apply tensile forces on both halves of the beam. The top part offers resistance by tensile stresses at the end of the crack and by compression following the tensile zone. The situation somewhat resembles a

beam (the bottom part in this case) on elastic foundation. An analysis along this line is elaborate and can give the length of the crack only approximately. The spring constants, that is the elasto-plastic resistance supplied by the top part, is not known. The top part of the beam also bends and, thus, complicates the interaction of forces. The effect of shearing stresses can not easily be considered. The propagation of the crack is caused by local, time-dependent effects. For these reasons the calculation of crack length is not attempted in this study. The numerical procedure that would yield an approximation is too lengthy to be worth the unreliable results it may give.

In addition to the relationships between the moment on the free body, the stirrup force and the crack length, the stirrup force and the crack width must also be connected. Force-slip relations can be obtained from bond tests. The crack width will be twice the slip, assuming that the bar is anchored similarly on both sides of the crack. The elongation of the steel between the surfaces of the crack is small compared with the slip.

The analysis presented in this chapter involves relationships between the loading and the position of the crack, the stirrup force and the crack length and between the stirrup force and the crack width. In order to obtain quantitative information, a series of tests was made on reinforced end blocks.

5. RESULTS OF TESTS ON SPECIMENS WITH REINFORCEMENT

5.1 Introductory Remarks

A series of tests were made on reinforced end blocks to substantiate the method of analysis presented in Chapter 4.

A total of 14 rectangular and 11 I-beams were tested. The description of the specimens and the method of testing are presented in Appendix B of this study. The end blocks can be classified into three groups according to the information obtained. The first group of specimens yielded most of the data used in this discussion. These specimens all had strain gages to measure the strain in the reinforcement and dials to determine the crack width, (from R11 to R17 and from T13 to T18, inclusive.) The specimens in the second group either did not have sufficient instrumentation to yield enough numerical data or were single exploratory specimens with properties different from that of the first group of beams (R5-R10, T9-T12). The specimens in the third group did not have No. 3 bars on the top of the beams. These specimens failed in bending at early loads (R4, T8).

The forces in the stirrups were measured in most specimens. Strain gages were mounted on the steel at a position where the crack was to form, as explained in Appendix B. The crack width was measured by 0.0001 in. dials at points along the beam. In some beams, mechanical gages were used to check the linear stress distribution. The instrumentation for the specimens is listed in Table B.1.

Some bond tests were also made to obtain the force-slip characteristics of the bars used as reinforcement. "Twin pull-out" specimens were designed to simulate the conditions in the end block. The measured average bond stress was very low. In order to investigate the effect of confinement

on the slip of the bars, companion "single pull-out" specimens were also tested. Both kinds of specimens are described in Appendix B.

The behavior of the specimens with reinforcement is discussed in the next section in terms of the variation of stirrups strains with the load and in terms of the development of the cracks.

5.2 Rectangular Beams

The group of specimens (R11-R17), that will be the subject of the main part of the discussion, had either one bar at 0.5 in. or two bars at 0.5 and 2.0 in. from the end face. No. 2 deformed bars or No. 7 USSWG were used in the specimens. (Sometimes the wires will also be called "bars", for simplicity).

The variation of strains in the stirrups at 0.5 in. from the end face in Specimens R11, R12, R14 and R17 is shown in Fig. 5.1. The relationship is linear up to about 16 kips of load when the wires started to yield. The cracks began to open at about 10 kips (at 20 kips in Beam R14). The difference between the strains in the No. 2 bars (having a yield force of 2.5 kips) and in the No. 7 USSWG (yield force 0.80 kips) is not large.

The stirrup forces are plotted against the applied load for the above mentioned four rectangular beams in Fig. 5.2. The wires yielded at 0.80 kips, the bars did not reach the yield stress. The forces carried by the two kinds of reinforcement are about equal. The larger reinforcement had the larger force. The opening of the cracks (at about 10 kips) had no noticeable effect on the stirrup forces. The relationship between the stirrup force and the crack width will be studied in Section 5.5. No conclusion can be made now about the relative performance of the bars without the consideration of the deformations.

Three rectangular specimens had reinforcement placed both at 0.5 and 2.0 in. from the end face. The variation of stirrup strains with the applied load for Specimens R8 and R15 are shown in Fig. 5.3. (R13 had strains nearly equal to those in R8 and the curve for this beam is therefore omitted.) It can be seen that the stirrups in different positions had about equal strains. The two stirrups carried equal share of the transverse force. The strains in the wires were about the same as in the bars. The forces carried by these stirrups (in the same beams) are shown in Fig. 5.4. The observations made above in connection with the discussion of the curves in Fig. 5.2 also apply to this figure. The wires carried smaller forces than the bars, while the strains were about equal to those in the bars.

The comparison of the beams with one stirrup with those with two stirrups shows (Figs. 5.1 and 5.3) that the strain (before yield) in each of the stirrups was about the same. The force in each of the bars or beams with two stirrups was approximately the same as the force in single bars. This difference must be associated with different crack lengths.

The strains and forces in the first group of rectangular specimens (given in Section 5.1) have been presented above. Before discussing the development of cracks in these beams, the strains and forces will be considered in some of the specimens of the second group. The steel strains were not measured in the two specimens of the third group.

The rectangular Specimen R7 had one stirrup (No. 2 bar) at one inch from the end. Specimen R9 had two No. 2 bars at 0.5 and 3 in. from the end. The variation of strains in these stirrups is shown in Fig. 5.5. The strains in the single stirrup at 1 in. are about equal to those in single stirrups at 0.5 in. from the edge (see Fig. 5.1).

The first part of this section has dealt with measured stirrup strains in rectangular specimens. The performance of the end block is gaged mainly by the magnitude of the cracks. That will be examined in the next paragraphs. The development of cracks and the variation of the crack width along the beam is discussed here, while the relationship between the stirrup force and the crack width at the end of the beam is presented in Section 5.5.

The development of cracks in rectangular beams, representative of the specimens of the first group, is shown in Figs. 5.6 and 5.7. It can be seen that the No. 2 single bars restricted the cracks more efficiently than the No. 7 USSWG. At higher loads there was about 50 per cent reduction in the crack length. The application of a second bar had a similar effect. The same information is given in Fig. 5.8, where the crack length is plotted versus the applied load. The crack length was measured with the help of a hand magnifying glass, therefore the measurements were somewhat erratic. The plots were smoothed out to give the relationships shown in Fig. 5.8. The effect of the size and number of bars is clearly demonstrated. The influence of the reinforcement on the crack width will be discussed later in this section.

The variation of the crack width along rectangular beams is shown in Fig. 5.9 for a load of 20 kips. It can be seen that the effect of the amount of reinforcement on the crack width is similar to that on the crack length as noted above.

Both the crack length ℓ and the crack width w increase with the load. The rate of increase depends on the amount of reinforcement. The relative rate of increase of the crack width (one inch from the end of the beams) and the crack length in rectangular beams is illustrated in Fig. 5.10. It can be seen that up to a load of about 20 kips the ratio w/ℓ increases

linearly with the load. This means that the crack width increases faster than the crack length. For the rectangular beams the ratio of crack width to crack length is $0.11 \times 10^{-4} \cdot P + \text{const.}$, provided that the applied load P is less than 20 kips. For larger loads the crack width for the smallest amount of reinforcement increases much faster than the crack length as the load goes up. The rate of increase gets smaller as more reinforcement is used. With two No. 2 bars the ratio d/ℓ remains practically constant. For more reinforcement the trend may reverse.

5.3 I-Beams

The presentation of the tests and the description of the behavior of I-beams will parallel that of rectangular beams. The reinforcement used in these beams were similar to those in rectangular beams, to permit comparison. The comparison of the behavior of the two kinds of sections will be made in Section 5.4.

The variation of strains in the stirrups at 0.5 in. from the end face of Specimens T13, T14, T16 and T18 are shown in Fig. 5.11. The wire started to yield at a load of 35 kips in Specimen T16. The relationship is linear up to this load. The strain gage in Beam T18 did not give reliable results above a strain of 0.0011. The stirrup forces in the same four specimens are shown in Fig. 5.12, while in Fig. 5.13 the stirrup forces in the two bars of Beam T15 are plotted against the applied load. Similar relationships are given in Fig. 5.14 for beams T10 and T12, both having one No. 2 bar at one inch from the end. The comparison of Figs. 5.11, 5.12 and 5.13 shows that at low loads (before yield) the forces were about equal, except in Specimen T15, which had two No. 2 bars. The force in each of the bars in Beam T15 was about 25 per cent smaller than the forces in single bars.

The development of cracks in Specimens T14, T16 and T18 is shown in Fig. 5.15. It can be seen that the No. 2 bar restricted the cracks much more efficiently than the wires.

The variation of crack width along I-beams is shown in Fig. 5.16 for a load of 20 kips. The effect of the amount of reinforcement is reflected in this figure.

The relationship between the applied load, the crack length and the crack width is of special interest in this study, since the interaction of these quantities is the basis of the analysis presented in Chapter 4. Curves showing these relationships for rectangular beams were shown in Figs. 5.9 and 5.10. There is less information about the relationships among the above quantities in I-beams. In Specimens T12, T13 and T14 the measurement of crack length was not reliable, and in Beam T10 the dial used to measure the crack width had a dial division of 0.001 and did not permit measurements that were accurate enough. The measured crack length is plotted against the applied load for Specimens T15 and T16 in Fig. 5.17, while the variation of the ratio of the crack width to the crack length is shown in Fig. 5.18. The observations made about the corresponding relationships for rectangular beams are also valid here. In the case of single wires the crack width developed at an increasingly faster rate than the crack length.

5.4 Comparison of the Behavior of Rectangular and I-Beams

The comparison of the behavior of specimens without reinforcement in Chapter 3 resulted in some important conclusions about the basic difference between the action of rectangular and I-beams. The behavior of the reinforced specimens will be compared in this section. The basic differences will be summarized in Section 5.6. Some remarks will also be

made at the end of this section about particular problems associated with the performance of reinforced end blocks.

The comparison of Figs. 5.2 and 5.12 shows that the stirrup forces in single No. 2 bars in rectangular beams were about 1.5 times as large as those in I-beams. The same ratio was found to be 1.7 for beams with two bars (Figs. 5.4 and 5.13), 1.1 for specimens with one wire (Figs. 5.2 and 5.12) and 1.6 for beams reinforced with one bar at one inch from the end fact (Figs. 5.5 and 5.14). For the specimen reinforced with wire, the applied force versus stirrup force relationship became nonlinear at 13 kips. For the other specimens, a load of at least 28 kips was applied before nonlinearity was observed.

In the specimens reinforced with two bars (or wires), the force in each of the bars was about 3/4 of the force of the stirrup in a companion specimen with single reinforcement. The forces in the bars of specimens reinforced with two bars were about equal.

The development of cracks was markedly different in the two kinds of beams (Figs. 5.6 and 5.15). The cracks in rectangular beams were about 1.5 times wider than in I-beams (at a point one inch from the end of the beams) as would be implied by the differences in the forces. The crack lengths in rectangular specimens were about 2.2 times as large as those in I-beams in the case of beams with single wire reinforcement, while the same ratio was about 2.5 for the other specimens. Thus, the cracks were wider and longer in the rectangular beams.

So far in this section the behavior of the rectangular and I-beams has been discussed and compared in terms of the crack length, crack width and the stirrup force. The influence of the amount of reinforcement was also investigated. The relationship between the stirrup force and the

crack width will be presented in Section 5.5. In the remainder of this section some particular observations will be made concerning the behavior of the specimens.

The effect of a larger loading plate (3.0 in. instead of 1.5 in.) on the stresses and strains in the spalling zone was very small. This was ascertained by measuring the strains in bars at both ends of Beam R17. The loading jack and the dynamometer were also reversed to see if there was bond of the loading rod. It was found that the difference in applied force at the two ends was negligible. The crack pattern was similar at the two ends in most tests, except that the crack length was somewhat larger in I-beams at the end with the larger loading plate. This was discussed in Section 3.2.

In some beams mechanical gages were used to check the linearity of the stress distribution away from the end block. The accuracy of the measurements was not sufficient to detect the distance from the end face where the distribution of longitudinal strains began to deviate from the straight line.

The plastic strip that was used to insure that the crack would pass through the gage, influenced the behavior of the end blocks. The effect of the pre-crack was that cracking and the stirrup force reached a certain stage at a lower load. The first crack became visible much earlier, but as the cracking progressed, the difference in the behavior became smaller.

The anchorage of the stirrups was found to be very important. On the top part of the beams, the seven inches of cover length was sufficient for anchorage, there was no slip detected on the top. In Beam R1 the stirrup was bent in a loop around the loading rod, but, unlike in the other specimens, it was not welded together. At failure, the bent portion of

the bar was partially straightened out, indicating the need for good anchorage.

The variation in concrete strength did not show any influence on either the cracking or on the failure load. The consistency of the concrete is more important. Careful casting of the end blocks is essential to prevent local irregularities (voids, cracks) that are much more detrimental in an end block than in most other areas of concrete construction.

5.5 Bond

The principal role of the reinforcement in anchorage zones is the arrest of cracks. In order to estimate the width of the longitudinal crack, a relationship is needed between the stirrup force and the crack width. This relationship was determined in 11 of the 25 tests on reinforced specimens. Independent pull-out tests were also carried out to study the bond-slip relationships of the reinforcement under different conditions.

The measured relationships between the stirrup force and the crack width are plotted in Fig. 5.19 for specimens with single No. 2 bars, in Fig. 5.20 for specimens with single No. 7 wire and in Fig. 5.21 for specimens with two No. 2 bars. The crack width was measured at a point one inch from the end of the beams. The comparison of these figures shows that, below yield, the crack width at a given load was approximately inversely proportional to the area of the bars. The crack width for two bars was less than half of that for one bar. There was no appreciable difference between the measured crack width at a given stirrup force in rectangular and I-beams.

The crack width is related to the stirrup force, the bond characteristics of the bar, the quality of the concrete and to the stress conditions around the bar. Bond tests give relationships between the slip and the force in the bar. Since results of bond tests are more readily

available than measurements of crack width, a connection is needed between the slip of the bars in bond tests and the crack width in beams. The extension of the stirrup bars between the surfaces of the crack is small in relation to the crack width, hence the crack width in the beams was compared with twice the measured slip in bond tests under similar conditions.

To determine the bond characteristics of the reinforcement under conditions similar to that existing in the end block, twin pull-out tests were made. Companion simple pull-out tests were also cast and tested to serve for comparison. The specimens and the testing procedure are described in Appendix B.

There were seven twin pull-out specimens and seven single pull-out specimens tested. Three of the latter kind of tests produced erratic results and are not reported. The results of five twin pull-out tests and four single pull-out tests will be discussed in the following paragraphs. It should be noted that the slip-measuring system did not permit reliable measurements upon first application of load. Hence, bond-slip curves are drawn through the origin.

The results or bond tests on No. 2 bars are shown in Fig. 5.22 and on No. 7 wire in Fig. 5.23. The slip values were doubled to permit direct comparison with the crack width. The single pull-out tests gave results similar to the twin pull-out tests, as it can be seen in these figures.

The comparison of the relationships between the measured force and the crack width in the end block and twice the measured slip in the bond tests (Figs. 5.19, 5.20, 5.22 and 5.23) shows that the results of the bond tests on specimens with bars (Fig. 5.22) agree well with the curves in Fig. 5.20. The crack width measured in specimens reinforced with wires was smaller than the corresponding values in the bond tests (Figs. 5.20 and 5.23).

Since the anchorage length in the case of the wires was larger than in the case of the deformed bars, the anchorage of the lower end of the wires around the loading rod could reduce the amount of slip. Therefore, the crack width is less than twice the measured slip in the bond tests in the case of wires.

The design method developed in this investigation requires the knowledge of a relationship between the stirrup force and the crack width. The relationship is approximated by the force-slip relation from bond tests. When no such data are available, the slip can be estimated from an assumed distribution of bond stresses. For simplicity, the force per unit length g will be assumed to be constant over the anchorage length of the bar. It is usually expressed in terms of the concrete strength. If the relation $g = m\sqrt{f'_c}$ is assumed, the integration of the strains in the bar along the anchorage length gives:

$$s = \frac{F^2}{2mEA\sqrt{f'_c}},$$

where A is the area of the bar and F is the force in the bar. Twice this value is plotted in Fig. 5.24 for $f'_c = 4900$ psi, $E = 30 \times 10^6$ psi and for the two kinds of reinforcement used in this investigation. For the wires $m = 3$ and for the bars $m = 4$ is used. The curves are second degree parabolas. Since the measured relationships have a smaller curvature, the approximation can be good in one interval only. Different values for m have to be selected according to the size of the load (or crack width) that is to be approximated. In the analysis presented in this investigation, the segment that is of importance centers around the crack width of 0.005 in. This requires that m should be about 4. In other areas of application of this method of approximation, much larger forces are dealt with, hence,

as it can be seen in Sketch 5.1, a higher value of m is required. For example, if a stirrup force in the No. 2 bar is 2.4 kips, then m = 6 would

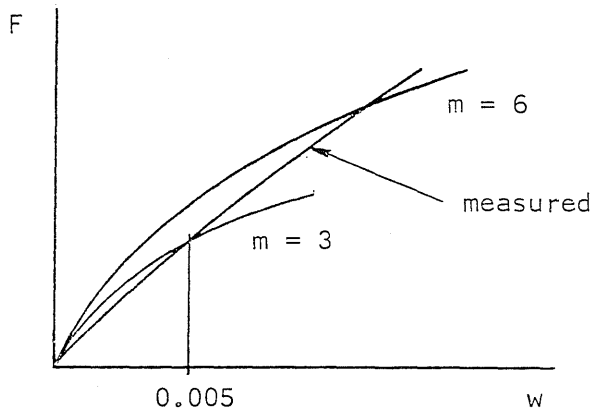

Sketch 5.1

be required for close approximation around this magnitude of the force. This "stepwise" dependence on m is the reason for the low values used here. Since the slip corresponding to tolerable crack width is low, the associated average bond force is also low. A value of m = 4 was found to yield relationship between stirrup force and crack width that approximates the measured relationships closely for specimens with No. 2 deformed bars. The bond tests on deformed bars reported in Reference 5 indicated that the unit bond stress is a linear function of the reciprocal of the diameter. Accordingly, the unit bond force (defined as the product of the unit bond stress and the nominal diameter) is independent of the diameter. Although the tests in Reference 5 did not include bars of small diameter, it is plausible to project the conclusion that the unit bond force is independent of the diameter of deformed bars with diameters ranging from 1/4 to 5/8 in., bars which are used as stirrups. Therefore, until further data are available, a value of m = 4 can be used for larger bars than the No. 2 bars used in the tests reported here.

5.6 Conclusions

The behavior of rectangular and I-beams has been described and compared in the first four sections of this chapter. The relationship between the stirrup force and the slip (or crack width) has been presented in the previous section. The behavior of all specimens and the interaction of the variables will be summarized in this section. Especially, the basic differences between the action of the two kinds of specimens will be discussed.

The strains measured in the spalling zones of rectangular specimens without reinforcement were about equal to the transverse strains in I-beams. An explanation was given in Section 3.2, according to which the load is more confined to the flange in the I-beam and, thus, the web portion of the rectangular specimen carries higher loads. The test results presented in this chapter substantiate this explanation, as it will be described in the following paragraphs.

The ratio of measured stirrup forces in rectangular beams to that in I-beams were the following: for two bars, 1.7; for one bar (at 1.0 in.), 1.6; for one bar (at 0.5 in.), 1.5; and for one wire, 1.1. For adequately reinforced beams the force can be transmitted into the web portion of the rectangular beams, and there is a difference between the stirrup forces in the two kinds of beams. If the rectangular beam is under-reinforced (by one wire, for example), the crack opens earlier, and the load is more confined to the bottom part, since the top part of the beam does not bend as much as in the case of adequately reinforced beams. Then the action of the rectangular beam becomes similar to that of the I-beam as reflected by the 1.1 ratio above. Therefore, if an adequate amount of reinforcement is used, the stirrup force is larger in the rectangular beam, and the web part is participating in carrying the load.

Corresponding to the difference in the stirrup force, the ratio of the measured crack width in the rectangular beams to that in I-beams is about 1.4 for equal applied loads. The ratio of the lengths is about 2.5 for specimens reinforced with two No. 2 bars and about 2.1 for beams with one wire. Thus, the cracks are wider and longer in the rectangular beam. The crack length is very much affected by irregularities and its measurements by surface conditions. In the identical Specimens R8 and R13 the crack widths were about equal, while the observed crack length in Beam R13 was about twice as large as that in Specimen R8.

The comparison of the results of single pull-out and twin pull-out tests indicated that the lack of confinement was not the cause of the low bond stresses. The force-slip relationships were similar in the two specimens.

5.7 Reconciliation of Theoretical and Experimental Results

The method of analysis of end blocks (Chapter 4) was based on the investigation of the equilibrium of forces acting on a free body formed by a longitudinal crack in the anchorage zone (Fig. 4.1). An expression was derived to predict the position of the crack. In this section, the equations and the parameters of the analysis will be used to examine the interaction of forces and deformations of the specimens used in this investigation.

The expression for the position of the crack (Chapter 4) yields $c = 5.3$ in. for the dimensions used in the present investigation for rectangular beams ($e = 1.5$ in., $h = 12$ in.). The section where the moment reaches a maximum value has to be determined by trial and error in the case of I-beams. For the cross section and loading used in the present investigation the crack is predicted to occur at 5.5 in. from the bottom.*

* As described in Section 3.2, the crack was observed to occur at about 5.5 in. from the bottom in seven of the nine test specimens without reinforcement.

The maximum moment, acting on a section at 5.3 in. from the bottom, for a load, say, 20 kips is 15.4 k-in. For the I-beam the corresponding moment at 5.5 in. from the bottom is 8.6 k-in.

The ratio of the maximum moment in the rectangular beam to that in the I-beam is 1.8. For an assumed equal moment arm, this ratio is equal to the ratio of the total stirrup forces. This agrees well with the test results on specimens with adequate reinforcement (two No. 2 bars), where this ratio was 1.7. For less reinforcement, the measured ratio was less, as discussed in the previous section.

Two approaches were considered for the basis of design of reinforcement in anchorage zones. One method is a successive approximation that involves the adjusting of the steel force, the stresses in the concrete, the crack length and the crack width to satisfy equilibrium and force-deformation conditions. The other method is a simplified analysis of the forces and the crack width for an assumed limiting length of the lead-in zone.

The first approach approximates the crack length and the distribution of the stresses in the concrete beyond the tip of the crack by trial and error. These stresses and the crack length are related to the tensile force and to the known applied moment. The stirrup force is, in turn, related to the crack width by the bond characteristics of the reinforcement. The procedure is very laborious and the accuracy of the results is uncertain at present, because the relationship involved is not known in sufficient detail. There are numerous assumptions to be made in this method regarding the geometry of the crack and the stress-strain properties of the concrete. This method can not yet be considered for design purposes.

The second approach is a straightforward method, suited for use in the design office. The maximum moment acting on a longitudinal section is calculated (Chapter 4). In order to estimate the moment arm of the stirrup forces and the compressive force of the concrete, the crack length has to be known. There is no practical way of estimating this quantity. Measurements of the crack length are erratic. Since linear stress distribution is reached at a distance of h (or less) from the end face (Chapter 2 and Appendix A), this value is taken as the upper limit for the distance between the compressive force and the end face. The stirrup force can be calculated by dividing the known moment by this assumed moment arm, to obtain the total stirrup force. Bond-slip relationships are used to check if the crack width is less than a prescribed limit. If the actual moment arm is smaller than the one defined above, the stirrups will be overstressed. Then the limitation on the crack width will modify the design. This method will be applied to the specimens of the present investigation in the following paragraphs. It will be the basis of the design specifications presented in Chapter 6.

The selection of the reinforcement for the I-beam under a load, say, 120 kips includes the following steps: The total stirrup force is calculated from the maximum moment, using a moment arm equal to the height of the beam less the distance between the resultant of the stirrup forces and the end of the beam. Hence, $F = 8.6/11.5 = 0.75$ kips, if the center of gravity of the stirrup forces is assigned to a point 0.5 in. from the end face. This force would produce a stress of 14.4 ksi in one bar and 29 ksi in the case of one wire. The corresponding crack widths are (Figs. 5.19 and 5.20) 0.004 in. for one wire and 0.002 for one bar. The average measured stirrup force was 0.63 kips.

If two No. 2 bars are considered, placed at 0.5 in. and 2.0 in. from the end, the moment arm is 10.25 in. Hence, the total stirrup force is F = 8.6/10.25 = 0.84 kips and the crack width is 0.0011 in. The measured stirrup force was 0.88 kips in this case.

For rectangular beams a similar analysis gives a total stirrup force of 1.50 kips and, (using two No. 2 bars) a crack width of about 0.002 in. The measured stirrup force was 1.54 kips.

The interaction of the applied load, the stirrup force and the crack width is plotted for the measured values and for the values predicted by the above analysis in Figs. 5.25 and 5.26. The calculated stirrup forces (represented by the broken lines) are larger than the measured values. This indicates that the assumed moment arm gives conservative results. The measured crack widths agree well with the values predicted by the analysis if a uniform bond value of $4\sqrt{f'_c}$ (300 lb/in.) is used for the bars and $3\sqrt{f'_c}$ (200 lb/in.) for the wires. These approximations agree best with the measured values at a crack width of about 0.005 in., which is the limiting crack width proposed in this investigation. For smaller cracks, the predicted values are lower than the measured crack widths, but the difference is small. Since this deviation occurs at small cracks, it is not consequential.

The above discussion illustrates the basic relationships that are involved in the analysis presented in Chapter 4. This procedure is used in the design recommendations given in the next chapter.

6. DESIGN RECOMMENDATIONS

6.1 Introductory Remarks

The design method presented in this chapter is based on the method of analysis introduced in Chapter 4 and discussed quantitatively in Section 5.7. In essence, it admits the presence of a longitudinal crack in the anchorage zone and is concerned with the equilibrium of the beam portions on either side of the crack. Transverse reinforcement is provided to satisfy equilibrium for any possible position of the longitudinal crack. The force in the reinforcement is calculated from the maximum of these moments, using an assumed moment arm. The steel stress is controlled by a limiting crack width through an approximate force-slip relationship.

The pivotal assumption is that there is a longitudinal crack in the anchorage zone. The prime role of the reinforcement is to confine the crack. The test series presented in Chapter 5 was designed to test the basic hypothesis and to determine the force-slip relationships for the transverse reinforcement.

The method is best suited for the analysis and design of anchorage zones with loads of high eccentricity. In such cases the conditions of anchorage do not influence the forces in the spalling zone. If the load has small eccentricity, the size of the loading plate influences the forces along the line of the load, though the results given by this method are on the safe side.

There are no limitations to the design method, as far as its areas of application are concerned. The lack of sufficient data on the force-slip relationship of reinforcement of different sizes prevents the precise determination of the crack width. However, there is neither need nor justification for precision in predicting the crack width.

The expressions, used in the specifications below and for the magnitude of the maximum moment in rectangular single loads, were discussed in Chapter 4.

The approximate expression for the limit on the s given in the following specifications, is derived from the relationship presented in Section 5.5. In the relationship

$$F^2 = 4EA\sqrt{f'_c} \cdot w$$

or

$$f_s^2 = \frac{4E\sqrt{f'_c} \cdot w}{A}$$

for f'_c = 5000 psi, a representative concrete strength at re prestressed concrete, the value of the square root of $4E\sqrt{f}$ which can be taken conservatively as 1.0×10^5. Therefore,

$$f_s = 10^5\sqrt{\frac{w}{A_s}}$$

There is one aspect of the design of anchorage zc difficult to cover in a set of specifications prepared to m quirements. That is the importance of quality control in t placing of the concrete in the anchorage zone. The anchora be free of irregularities and, if possible, shrinkage crack these criteria are awkward to specify along with rules for transverse reinforcement, they could be anticipated in spec to the manufacture of prestressed concrete members.

6.2 Design Specifications

The following set of specifications is concerned with the proportioning of reinforcement in the anchorage zone of pretensioned and post-tensioned prestressed concrete members.

1. Transverse reinforcement shall be provided within a distance h/2 from the end of the beam to carry the total force F_T given in Eq. 1,

$$F_T = \frac{M_m}{h - z}$$

and the stress in the transverse reinforcement shall be

$$f_s \leq 10^5 \sqrt{\frac{w}{A_s}}, \quad \text{but not greater than 30,000 psi,}$$

where A_s = area of one stirrup

F_T = total stirrup force

h = height of the beam

z = distance between the end of the beam and the centroid of the areas of the stirrups that are within h/2 from the end

w = permissible nominal crack width, in.

M_m = the unbalanced moment caused by forces acting on a free body bounded by a transverse section and a longitudinal section within the member considered. The critical position of the longitudinal section is that which results in the maximum value for M_m. The internal stress distribution normal to the transverse section is computed using the elementary expression for stress due to combined axial load and bending:

$$f = \frac{P}{A}\left(1 + \frac{e_t \cdot y}{r^2}\right)$$

where P = total prestressing force immediately after release

A = gross area of concrete section

e_t = eccentricity of the total prestressing force

y = distance from centroidal axis

r = radius of gyration for the gross plain section

(a) For anchorage zones having a rectangular cross section loaded by a single group of prestressing forces, M_m is either on a plane containing the line of the resultant load and has a magnitude of

$$M_m = 2P \frac{e_b^2}{h^3} (h - e_b)^2$$

or on a section at a distance of $c = \frac{h^2}{3\ (h - 2e_b)}$ from the bottom of the beam with a magnitude of

$$M_m = P \left[\frac{h^2}{27} \cdot \frac{4h - 9e_b}{(h - 2e_b)^2} - e_b \right]$$

where e_b = distance from the resultant prestressing force to the bottom of the beam

c = distance between the longitudinal section of M_m and the bottom of the beam

P = resultant of the group of prestressing forces

(b) For other cases, the position of the longitudinal section and the magnitude of M_m acting on it shall be determined by trial and error.

(c) For draped pretensioned strands, the point of action of the resultant prestressing force shall be taken at 25 diameters along the strands from the end.

2(a). Closed stirrups shall be used, enclosing all the prestressing tendons. The stirrups shall extend from the top to the bottom of the section and satisfy the requirements for cover.

(b). The amount of transverse reinforcement over a distance h from the end of the beam shall not have a longitudinal spacing greater than h/5 and shall not be less than the minimum required for shear.

(c) The first stirrup shall be as close to the end of the beam as permitted.

6.3 Illustrative Examples

(a) Post-tensioned Highway Bridge Girder

The transverse reinforcement will be designed for the AASHO standard beam No. 1. The cross section is shown in Fig. 6.1a. The area and the moment of inertia are 276 $in.^2$ and 22,740 $in.^4$. The prestressing force is applied by 22 strands in the bottom part of the section and by two strands at the top of it. The center of gravity of all the forces (a total of 336 kips) is at 6.17 in. from the bottom, while the similar distance for the resultant of the bottom strands is 4.37 in. The center of gravity of the cross section is at 12.59 in. from the bottom. The stresses due to bending are 2.41 ksi compression and 0.24 ksi tension.

The forces in the bottom part of the section excluding the web are shown in the sketch below:

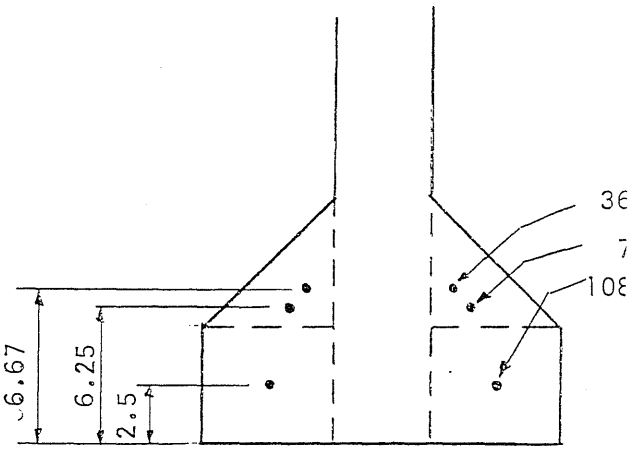

Sketch

As a first trial, it may be uniform. As a next trial, a section a The stress at that section is 0.99 ksi portion of the stress diagram in the w uniform stress it is 668.2 k-in. The 3035.8 k-in. The moment of the prestr 308 x 10.63 = 3274.0 k-in. Hence the calculations show that the moment at 1 the net moment is 231.7 k-in. Therefo 239.0 k-in.

The resultant of the stirrup end. Hence, the total stirrup force i bars, area 0.20 in.^{2}. The allowable s

$$f_s = 10^5 \sqrt{\frac{w}{A}} = 10^5 \sqrt{\frac{0.005}{0.20}}$$

30,000 psi. The total stirrup area re 2 - No. 4 bars, closed stirrups, total

(b) Pretensioned Highway Bridge Beam

In the calculation of the moment on the longitudinal section the magnitude of the force is taken into account. As long as all the force is on one side of the section, it can be considered as an external force. The effective point of action of the pretensioning forces must be estimated (the distance between the resultant force and the bottom of the cross section).

The transverse reinforcement will be designed for the anchorage zone of the standard AASHO beam No. IV. The cross section is shown in Fig. 6.1b. The area and the moment of inertia of the section are 789 $in.^2$ and 260,700 $in.^4$. The prestressing force is applied by 48 strands, 16 of which are draped. The center of gravity of all the forces is at 11.9 in. from the bottom, while the corresponding distance for the loads in the lower half of the section is 10 in. The stresses due to the total force are 3.0 ksi compression at the bottom and 0.24 ksi tension at the top. The force in 46 strands (a total of 1160 kips) will be considered in the calculations. The remaining two strands act at the top of the section. The maximum moment is 1010 k-in. and occurs at a distance of 37 in. from the bottom of the section.

The center of gravity of the transverse reinforcement is assumed to be at 5 in. from the end face. The total stirrup force is F = 1010/49 = 20.6 kips. Try No. 4 bars, area 0.20 $in.^2$ f_s = 15,800 psi. The total area required is A_{req} = 20.6/15.8 = 1.31 $in.^2$, use 4 - No. 4 bars, closed stirrups, total area, A = 8 x 0.20 = 1.60 $in.^2$.

(c) Post-Tensioned Rectangular Beam

The transverse reinforcement will be designed for the I-section of example (a) with rectangular end blocks. The cross section has an area

of 28 x 16 = 448 in.^{2} and a moment of inertia of 29,269 in.^{4}. Again, the total force of 336 kips acts at a point 6.17 in. from the bottom, and the resultant of the forces in the lower part of the cross section is 308 kips and acts at 4.37 in. from the bottom.

The bending stresses are 2.0 ksi compression on the bottom and 0.51 ksi tension on the top. The net bending moment on a longitudinal section at 14 in. from the bottom due to these bending stresses and the forces acting in the lower part of the end face is 490 k-in.. The corresponding moment at 14.5 in. is 500 k-in. and at 15 in. the moment is 486 k-in. Hence, the maximum moment is 500 k-in. It is interesting to note, that if the forces at the top of the section (2 x 14 = 28 kips) are ignored, the moment is much smaller. The expression for the position of the maximum moment gives

$$c = \frac{28}{3\ (28 - 2 \times 4.37)} = 13.6 \text{ in.}$$

and the maximum moment is

$$M = 308 \left[\frac{28^2}{27} \cdot \frac{4 \times 28 - 9 \times 4.37}{(28 - 2 \times 4.37)^2} - 4.37 \right] = 410 \text{ k-in.},$$

hence, the two cables on the top increased the maximum moment from 410 k-in. to 500 k-in.

There is a large difference between the maximum moment in the rectangular and the I-beam. In example (a) the maximum moment was 239 k-in. compared with the 500 k-in. obtained for the rectangular section in this example.

The selection of the reinforcement involves steps that are similar to those given in examples (a) and (b) above.

7. SUMMARY

7.1 Object and Scope

The objectives of this investigation were to study the crack initiation and the action of transverse reinforcement in arresting cracks in the anchorage zone of prestressed concrete beams.

A detailed review of relevant references was made (Appendix A). The majority of the consulted works was concerned with elastic stress distribution in the anchorage zone. It was concluded from the study of the references that, though some definite results could be ascertained about the effect of certain variables, there was not sufficient information about the behavior of a cracked end block. Non-prestressed reinforcement can not prevent cracking. Therefore, in order to develop a direct method of designing transverse reinforcement with the realization of a crack, an analytical and experimental investigation was undertaken.

The first part of the investigation was concerned with the conditions of crack initiation. A series of tests was conducted on three rectangular and seven I-beams to determine the transverse strain distribution along certain longitudinal lines and the development of cracks. The specimens and the testing procedure were described in Appendix B. A finite difference solution was also made, based on the two-dimensional Airy stress function method, to determine the stresses and strains in a specific case. This solution was described in Chapter 2, while the details of the computer program were given in Appendix C.

In the second part of the investigation, an analytical study was made of the conditions of the equilibrium on the cracked end block. To corroborate the analysis, 14 rectangular and 11 I-beams with transverse reinforcement were tested. The behavior of these specimens was described

in Chapter 5. The force in the stirrups related to the crack width in the analysis. Bond tests were made on seven simple pull-out specimens on seven so called "twin" pull-out specimens. The latter kind of tests designed to simulate the conditions in the end block, where there is nc confinement of the bar.

7.2 Behavior of Specimens without Reinforcement

The measured transverse strains along the line of the load ar along the center-line of the specimens indicated two main tension zones (Figs. 3.2a and 3.2b). There are high tensile strains under the load ar distance of about one to two inches from the loaded end. In beams stre by forces of small eccentricity, the stresses under the load (the so-ca bursting stresses) are the highest. The majority of the references cor was concerned with these stresses. In the case of loads with larger eccentricities, the other tension zone (called the spalling zone) has h stresses that initiate a longitudinal crack close to the mid-height of beam. The specimens tested in this investigation had an eccentricity c 4.5 in. with a beam height of 12 in. The measured strains compared wel with the results of the finite difference solution if a possible variat in the modulus of elasticity of concrete in tension was allowed. The reversal of the gages indicated minute cracks at low loads.

The strains in the two kinds of beams were similar. This was explained by the different kinds of flow of forces in the two cases; ir I-beams the forces are more confined to the flange.

The longitudinal cracks close to the center line of the beam progresses deep into the beams (Figs. 3.5 and 3.11). The beams failed a splitting wedge type of failure under the loading block.

It was noted that initial irregularities (cracks and voids) lower the strength of the anchorage zone without reinforcement.

7.3 Behavior of Specimens with Reinforcement

The strains were measured at an induced longitudinal crack in three kinds of transverse reinforcement (one No. 7 USSWG, one No. 2 bar and two No. 2 bars). The measured forces were proportional to the applied load up to yield. The crack width increased at a faster rate than the crack length with increasing applied load.

The comparison of the performance of the rectangular and I-beams substantiated the hypothesis that the forces would be larger and the cracks longer and wider in rectangular beams than in I-beams. This indicates that the performance of the I-shaped beams is better if most of the prestressing forces act in the flange.

7.4 Bond-Slip Relationship

Both the crack width and the stirrup force were measured in eleven specimens. The relationship between these quantities was needed in the analytical investigation on which the design procedure was based. The comparison of the measured relationships (Figs. 5.19, 5.20 and 5.21) shows that the crack width was approximately inversely proportional to the stirrup area. There was no appreciable difference between the measured crack width at a given stirrup force in the rectangular and I-beams.

The two kinds of bond tests gave force-slip curves that were similar to those in the beams, assuming that the crack width was about twice the slip.

In the design method, a uniform unit bond (force per length) was used. It was found to be $4\sqrt{f'_c}$ from the bond tests for bars. The reason

for this low bond value was that the slip for tolerable crack widths is small.

7.5 Results of Practical Significance

Although the major part of this study was concerned with the reconciliation of theoretical and measured stresses in a rather idealized test specimen and the experimental work was limited, it was possible to present some of the results in a form suitable for immediate application, since the hypothesis developed for the action of transverse reinforcement involves simple assumptions which can be projected on the basis of intelligible principles to cover practical cases.

The investigation brought out the importance of spalling stresses, transverse tensile stresses away from the line of the load, and showed that for an eccentric load these stresses would be larger for a rectangular than for an I-shaped end block.

A new approach to the problem of transverse reinforcement predicated on the admission of a longitudinally cracked anchorage zone was developed. A simple design method for transverse reinforcement was based on this approach and presented in a format which can be incorporated readily in a building code.

REFERENCES

1. Timoshenko, S., J. N. Goodier, "Theory of Elasticity," McGraw-Hill Book Company, Inc., 1951, pp. 483-490.

2. Guyon, Y., Prestressed Concrete, 1st Edition, J. Wiley and Sons, Inc., New York, 1953.

3. Gerstner, R. W., O. C. Zienkiewicz, "A Note on Anchorage Zone Stresses," Journal of the American Concrete Institute, Vol. 59, July 1962.

4. Iyengar, K. T., "Two-Dimensional Theories of Anchorage Zone Stresses in Post-Tensioned Beams," Proc., ACI, Vol, 59, 1962, p. 1443.

5. Ferguson, P. M., J. N. Thompson, "Development Length of High Strength Reinforcing Bars in Bond," Proc., ACI, Vol. 59, July 1962.

6. Douglas, D. J., N. S. Trahair, "An Examination of the Stresses in the Anchorage Zone of a Post-Tensioned Prestressed Concrete Beam," Magazine of Concrete Research, Vol. 12, No. 34, March 1960.

7. Bleich, F., "Der gerade Stab mit Rechteckquerschnitt als ebenes Problem," Der Bauingenieur, No. 10, 1923.

8. Sargious, M., "Beitrag zur Ermittlung der Hauptzugspannungen am Endauflager vorgespannter Betonbalken, Thesis, Technische Hochschule Stuttgart, 1960.

9. Huang, T., "A Study of Stresses in End Blocks of Post-Tensioned Prestressed Beam," Thesis, University of Michigan, 1961.

10. Sievers, H., "Die Berechnung von Auflagerbanken und Auflagerquadern von Bruckenpfeilern," Der Bauingenieur, Vol. 27, 1952.

11. Sievers, H., "Uber den Spannungszustand im Bereich der Ankerplatten von Spanngliedern vorgespannter Stahlbetonkonstrucktionen," Der Bauingenieur, Vol. 31, 1956.

12. Morsch, E., "Uber die Berechnung der Gelenkquader," Beton und Eisen, No. 12, 1924.

13. Magnel, G., "Design of the Ends of Prestressed Concrete Beams," Concrete and Constructional Engineering, Vol. 44, 1949.

14. Ramaswamy, G. S., H. Goel, "Stresses in End Blocks of Prestressed Beams by Lattice Analogy," Proc., World Conference on Prestressed Concrete, San Francisco, 1957.

15. Ross, A. D., "Some Problems in Concrete Construction," Magazine of Concrete Research, Vol. 12, 1960.

16. Hiltscher, R., G. Florin, "Die Spaltzugkraft in einseitig eingespannten, am gegnuberliegenden Rande belasteten rechteckigen Scheiben," Die Bautechnik, Heft 10, 1962.

17. Christodoulides, S. P., "A Two-Dimensional Investigation of the End Anchorages of Post-Tensioned Concrete Beams," The Structural Engineer, Vol. 33, 1955.

18. Christodoulides, S. P., "The Distribution of Stresses Around the End Anchorages of Prestressed Concrete Beams," International Association for Bridge and Structural Engineering, Publications, Vol. 16, 1956.

19. Christodoulides, S. P., "Three-Dimensional Investigation of Anchorage Zone Stresses," The Structural Engineer, 1957.

20. Marshall, W. T., A. H. Mattock, "Control of Horizontal Cracking in the Ends of Pretensioned Prestressed Concrete Girders," Journal of the Prestressed Concrete Institute, Vol. 7, No. 5, 1962.

21. Zielinski, J., R. E. Rowe, "An Investigation of the Stress Distribution in the Anchorage Zones of Post-Tensioned Concrete Members," Cement and Concrete Association, Research Report 9, 1960.

22. Ban, S., H. Muguruma, Z. Ogaki, "Anchorage Zone Stress Distribution in Post-Tensioned Concrete Members," Proc., World Conference of Prestressed Concrete, San Francisco, 1957.

23. Zielinski, J., R. E. Rowe, "The Stress Distribution Associated with Groups of Anchorages in Post-Tensioned Concrete Members," Cement and Concrete Association, Research Report 13, 1962.

24. Mahajan, K. D., "Analysis of Stresses in a Prestressed Beam Using Araldite Models," Indian Construction News, August 1958.

25. Goodier, J. N., "Compression of Rectangular Blocks," American Association of Mechanical Engineers, Tran., Vol. 54, 1932.

26. Abeles, P. W., F. H. Turner, Prestressed Concrete Designer's Handbook," Concrete Publications, Ltd., London, 1962.

27. Hawkins, N. M., V. Srinivasagopalan, M. A. Sozen, "Anchorage Zone Stresses in Prestressed Concrete Beams," Structural Research Series No. 207, University of Illinois, 1960.

28. Chaikes, S., "Calcul des Abouts des Poutres en Beton Precontraint," International Congress of Prestressed Concrete, Ghent, 1951.

29. Keuning, R. W., M. A. Sozen, C. P. Siess, "A Study of Anchorage Bond on Prestressed Concrete," Structural Research Series No. 251, University of Illinois, 1962.

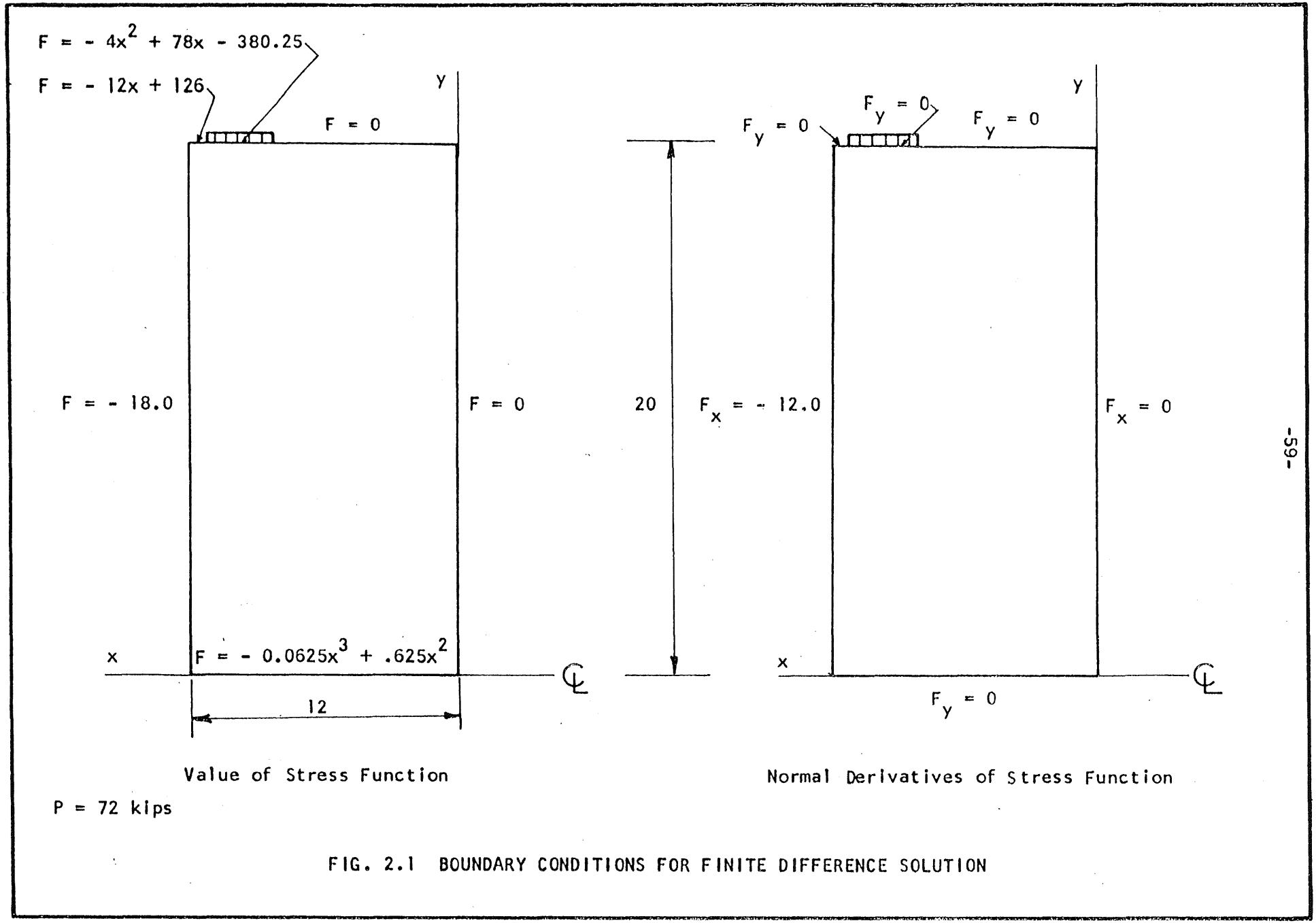

FIG. 2.1 BOUNDARY CONDITIONS FOR FINITE DIFFERENCE SOLUTION

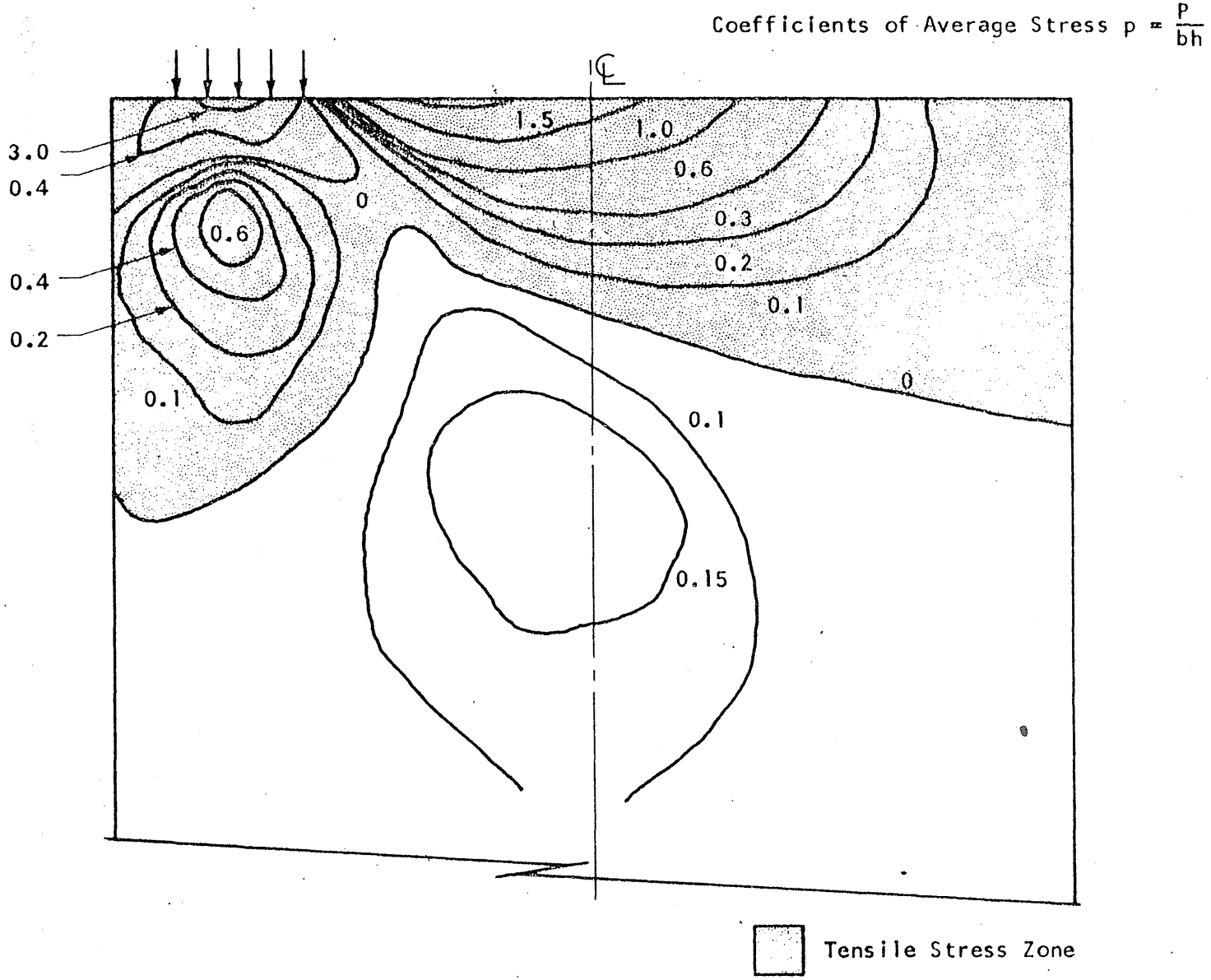

FIG. 2.2 CONTOURS OF EQUAL TRANSVERSE STRESS

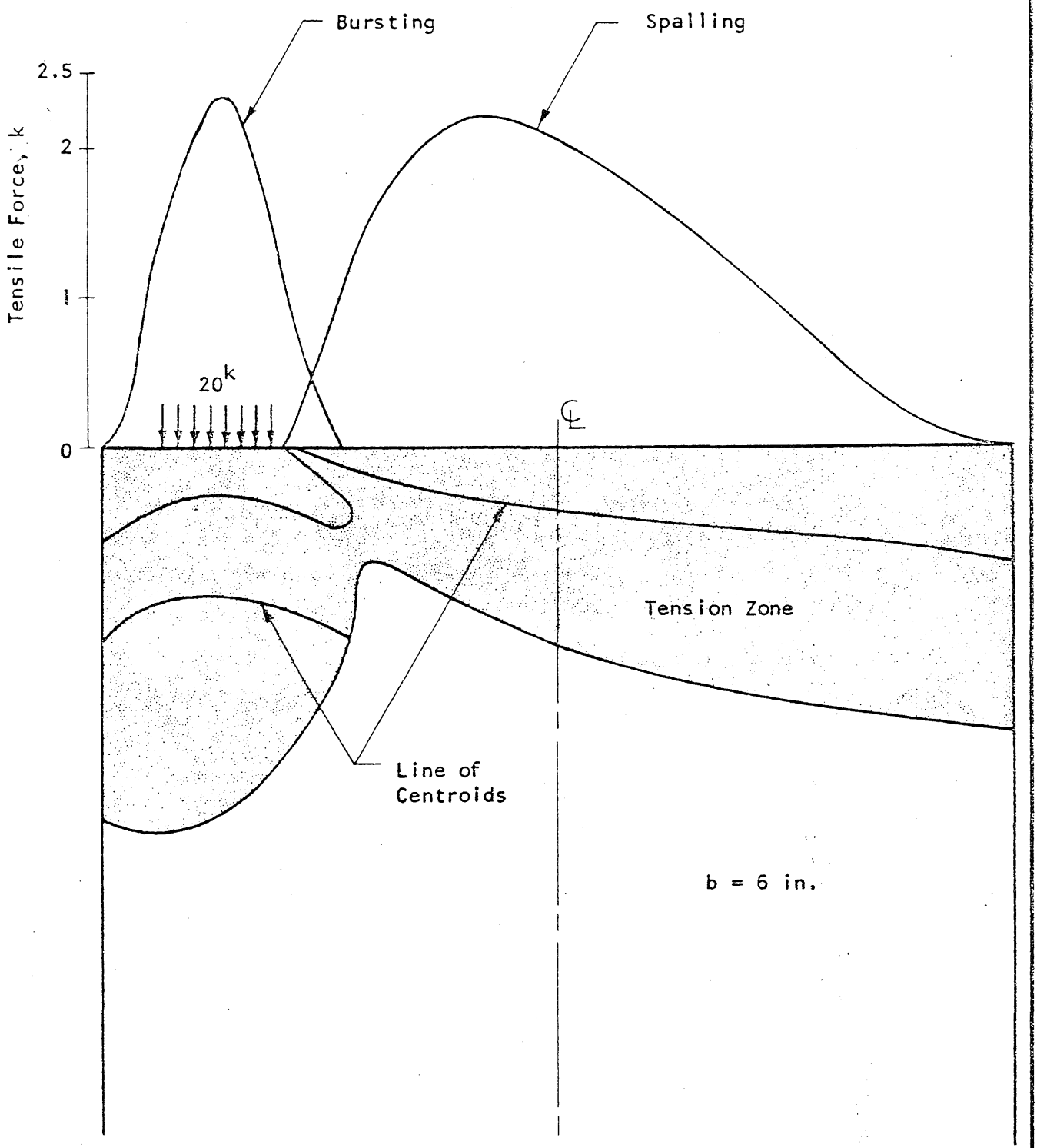

FIG. 2.3 MAGNITUDES AND POINTS OF ACTION OF TENSILE FORCES ON LONGITUDINAL SECTIONS IN THE TENSION ZONE

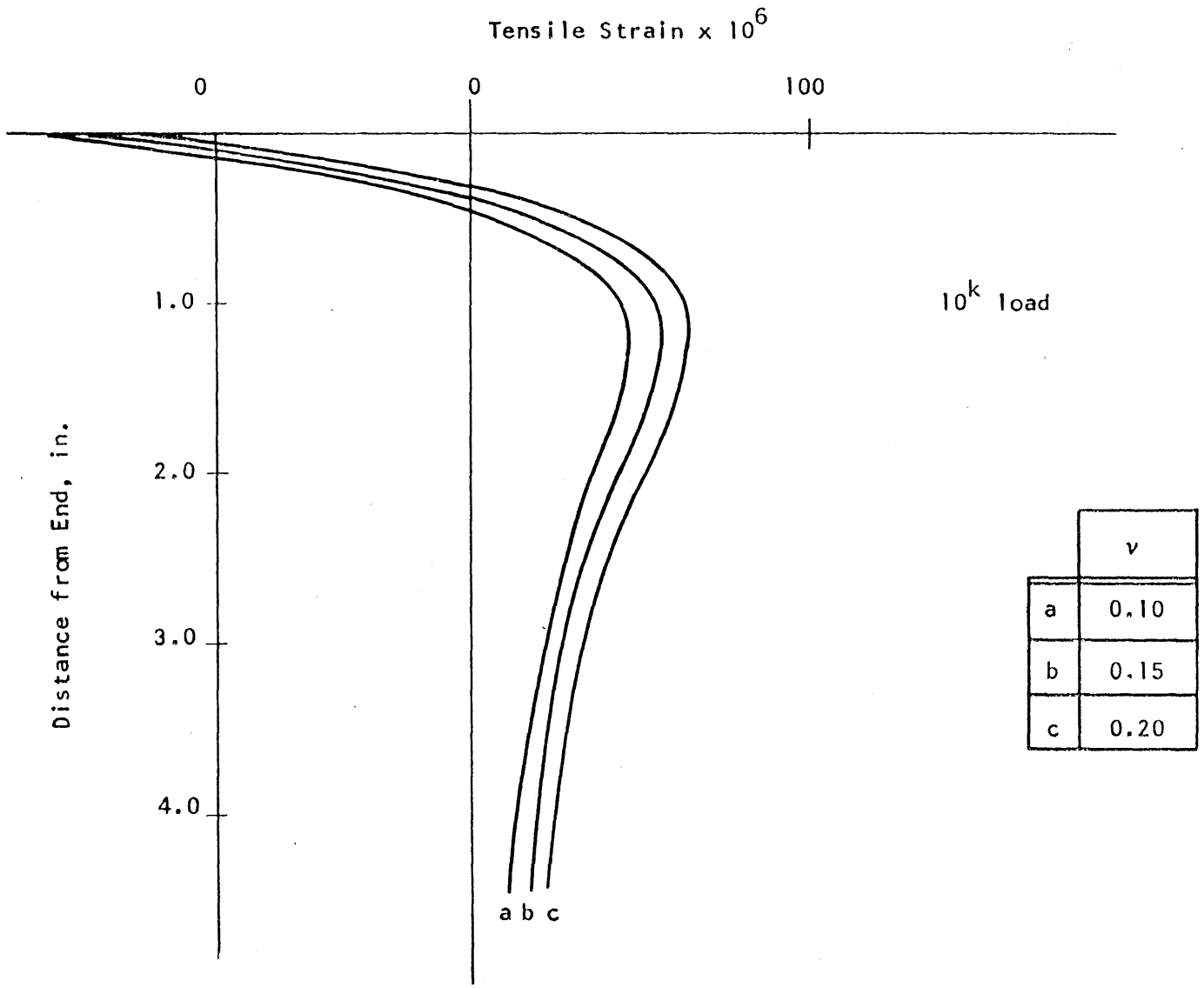

FIG. 2.4 EFFECT OF POISSON'S RATIO ON TRANSVERSE STRAINS

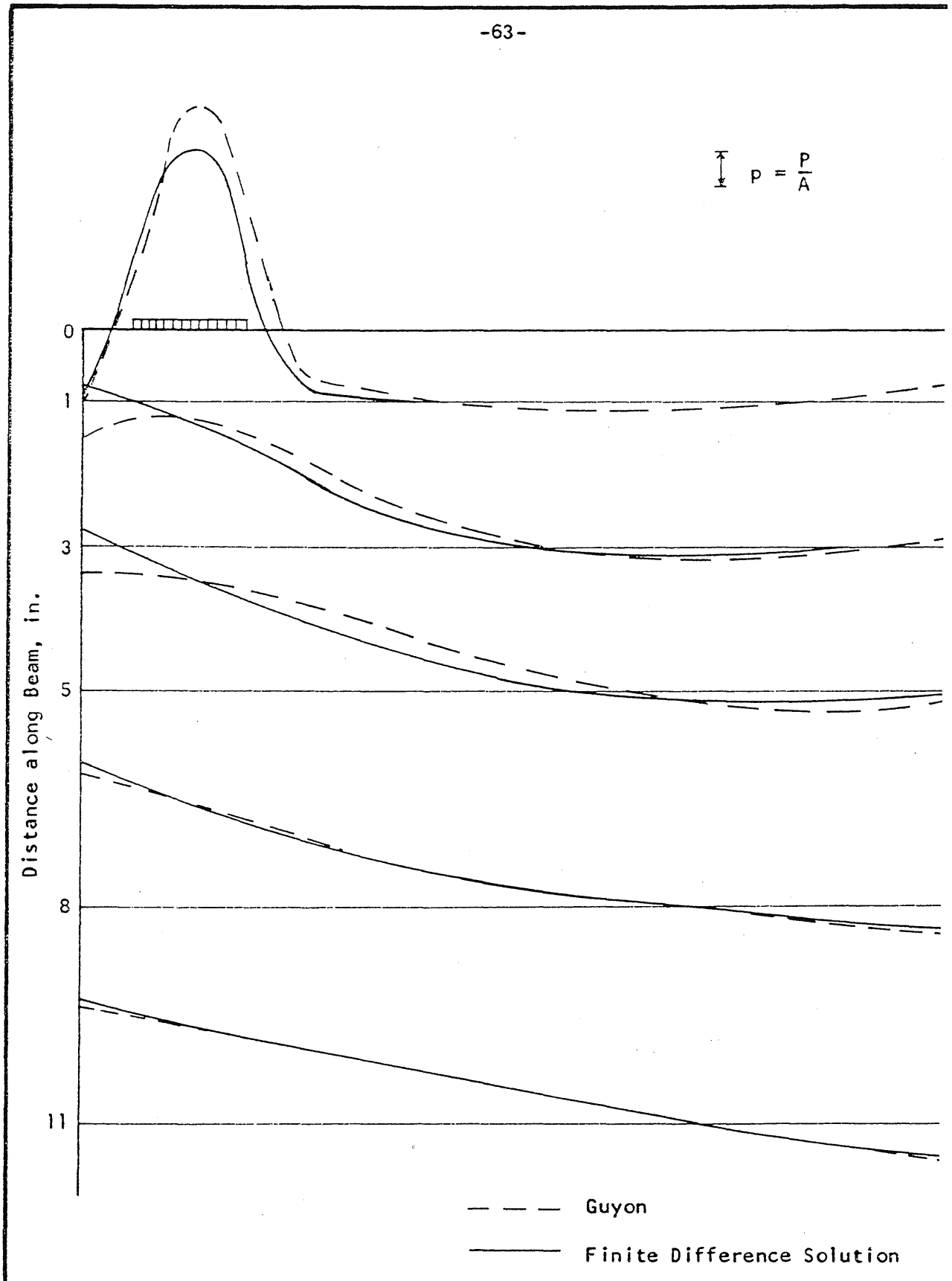

FIG. 2.5 LONGITUDINAL STRESSES FROM GUYON'S SOLUTION AND FROM THE FINITE DIFFERENCE SOLUTION

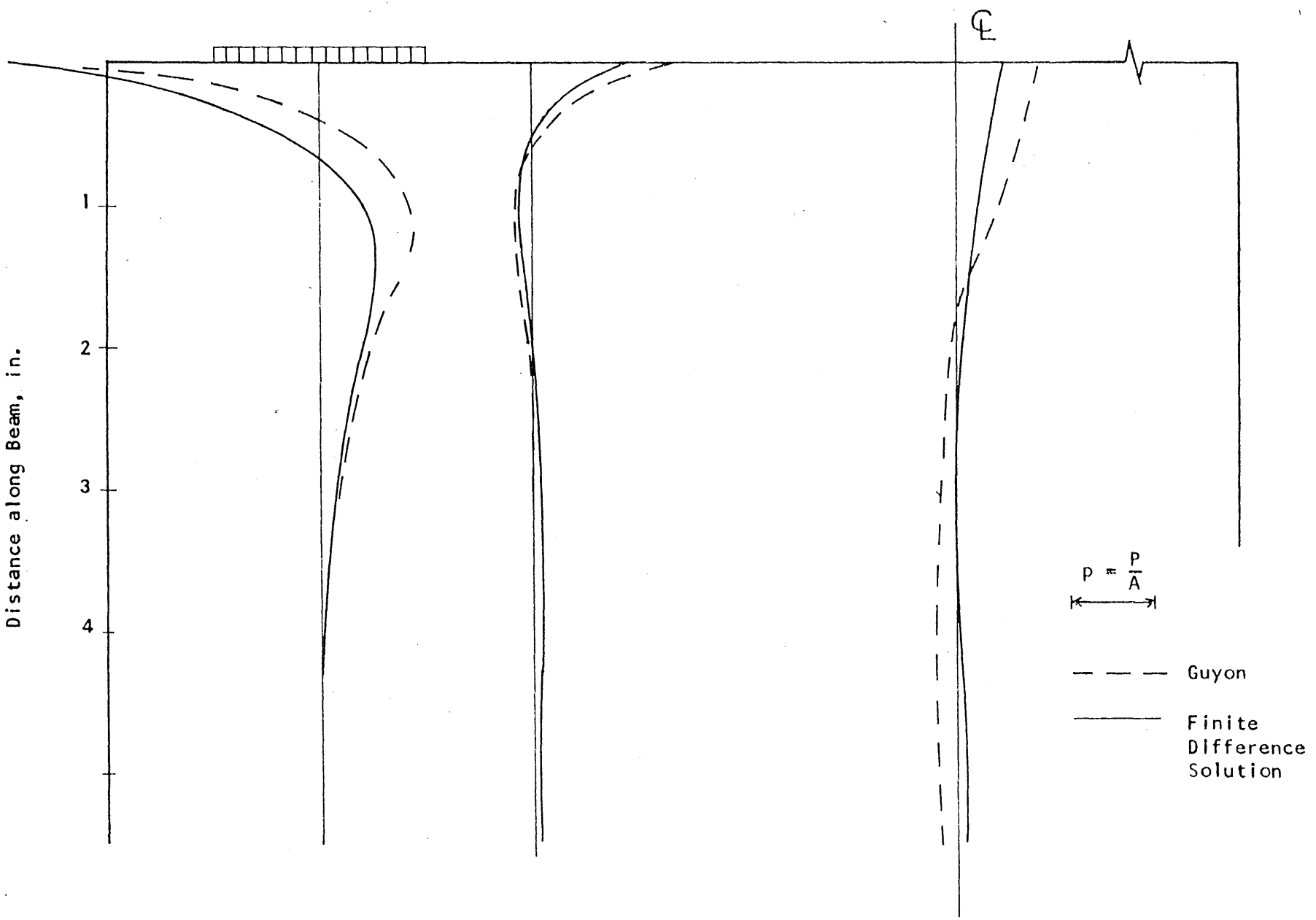

FIG. 2.6 TRANSVERSE STRESSES FROM GUYON'S SOLUTION AND FROM THE FINITE DIFFERENCE SOLUTION

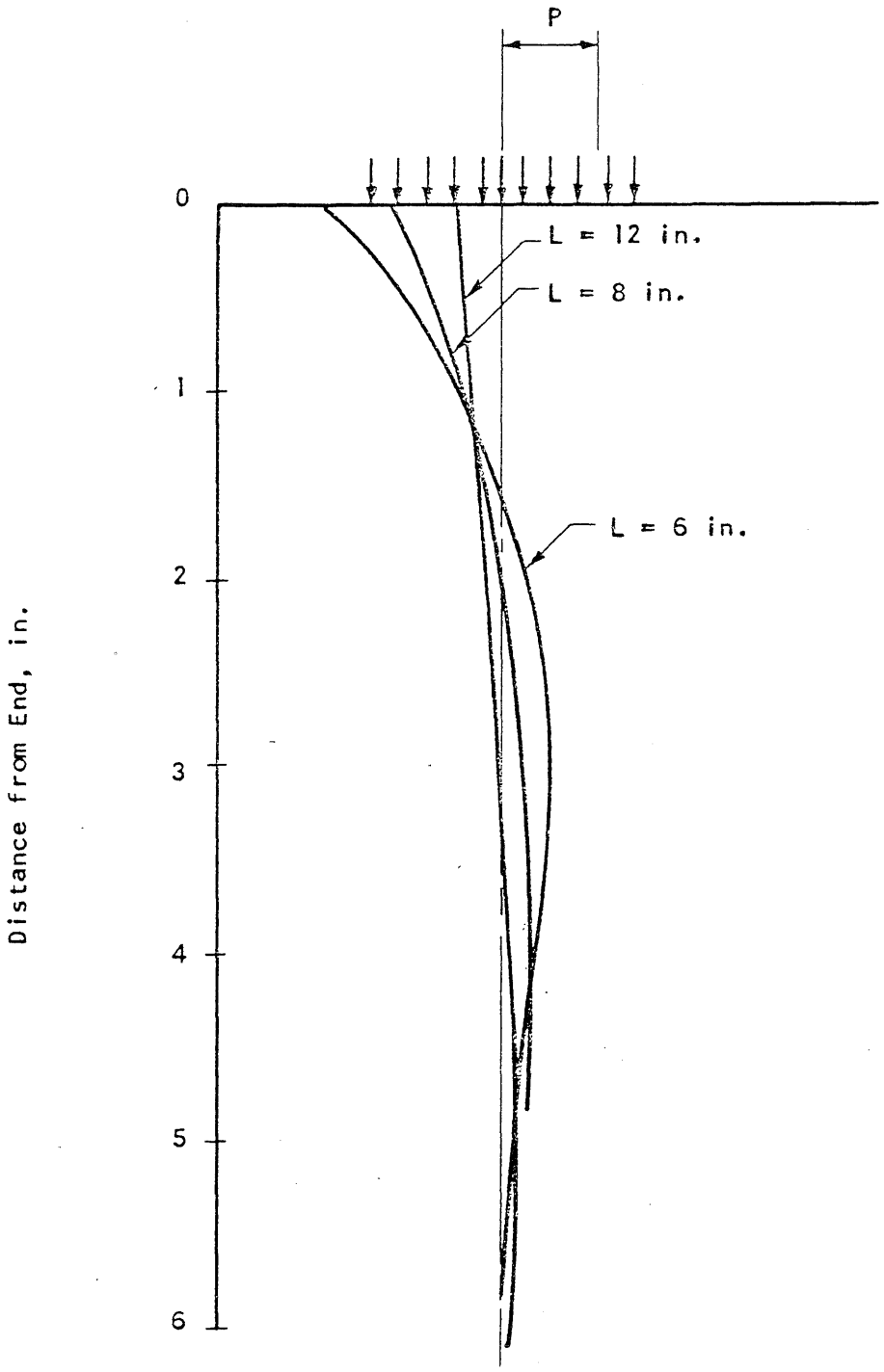

FIG. 2.7 MAGNEL'S SOLUTION

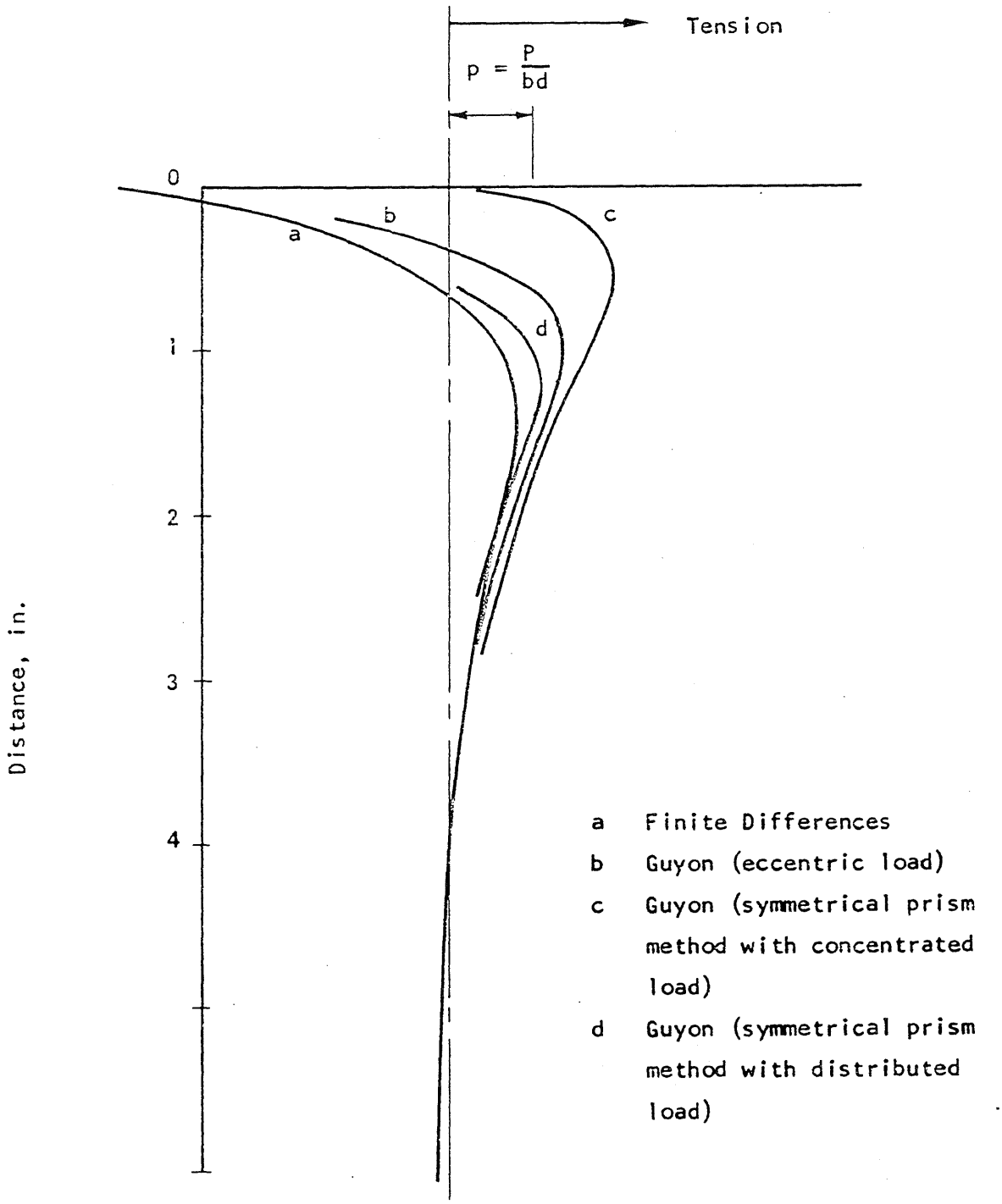

FIG. 2.8 TRANSVERSE STRESSES COMPARED WITH THE RESULTS OF THE SYMMETRICAL PRISM METHOD

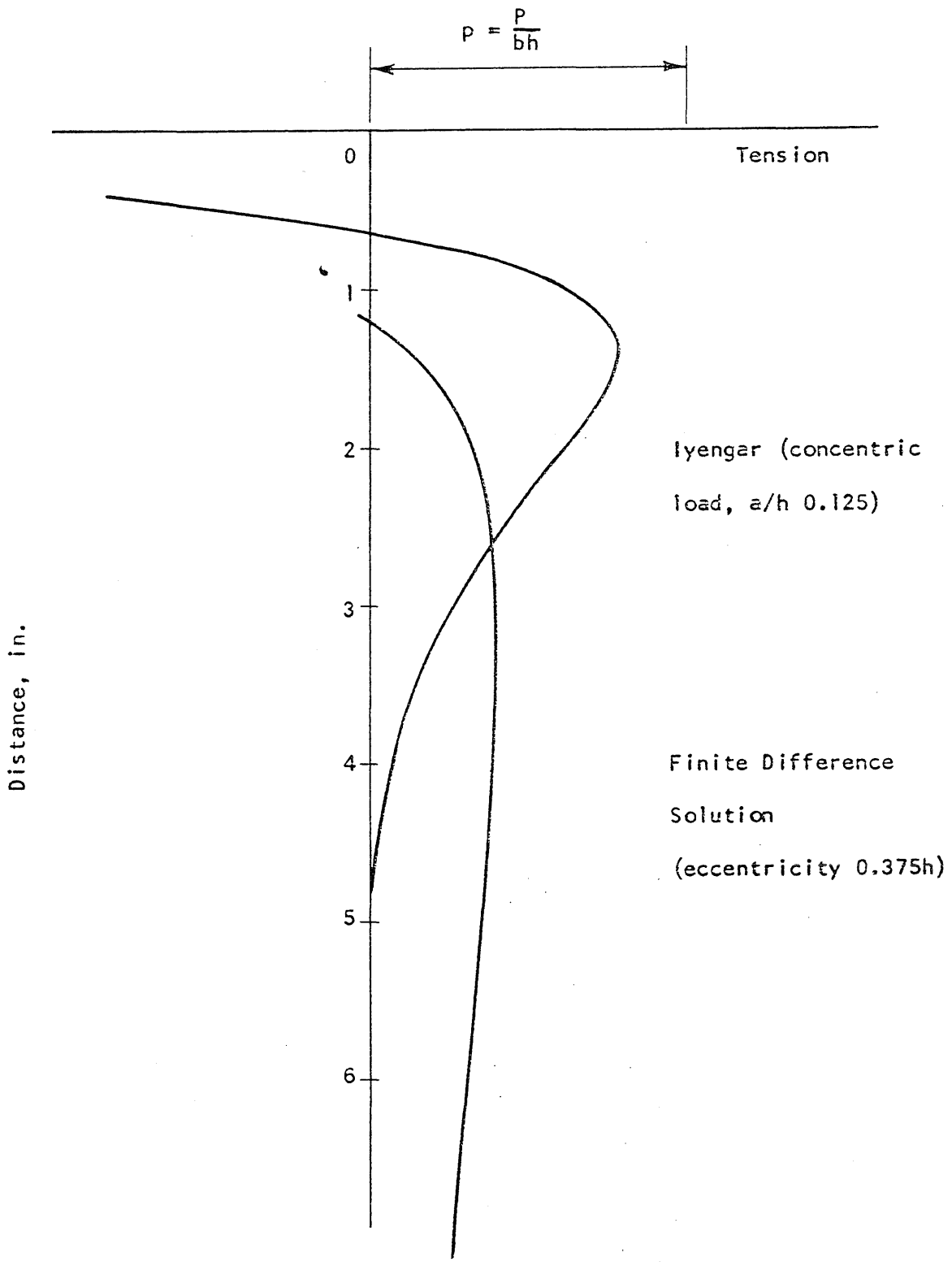

FIG. 2.9 STRESSES ALONG LINE OF LOAD BY IYENGAR AND FROM THE FINITE DIFFERENCE SOLUTION

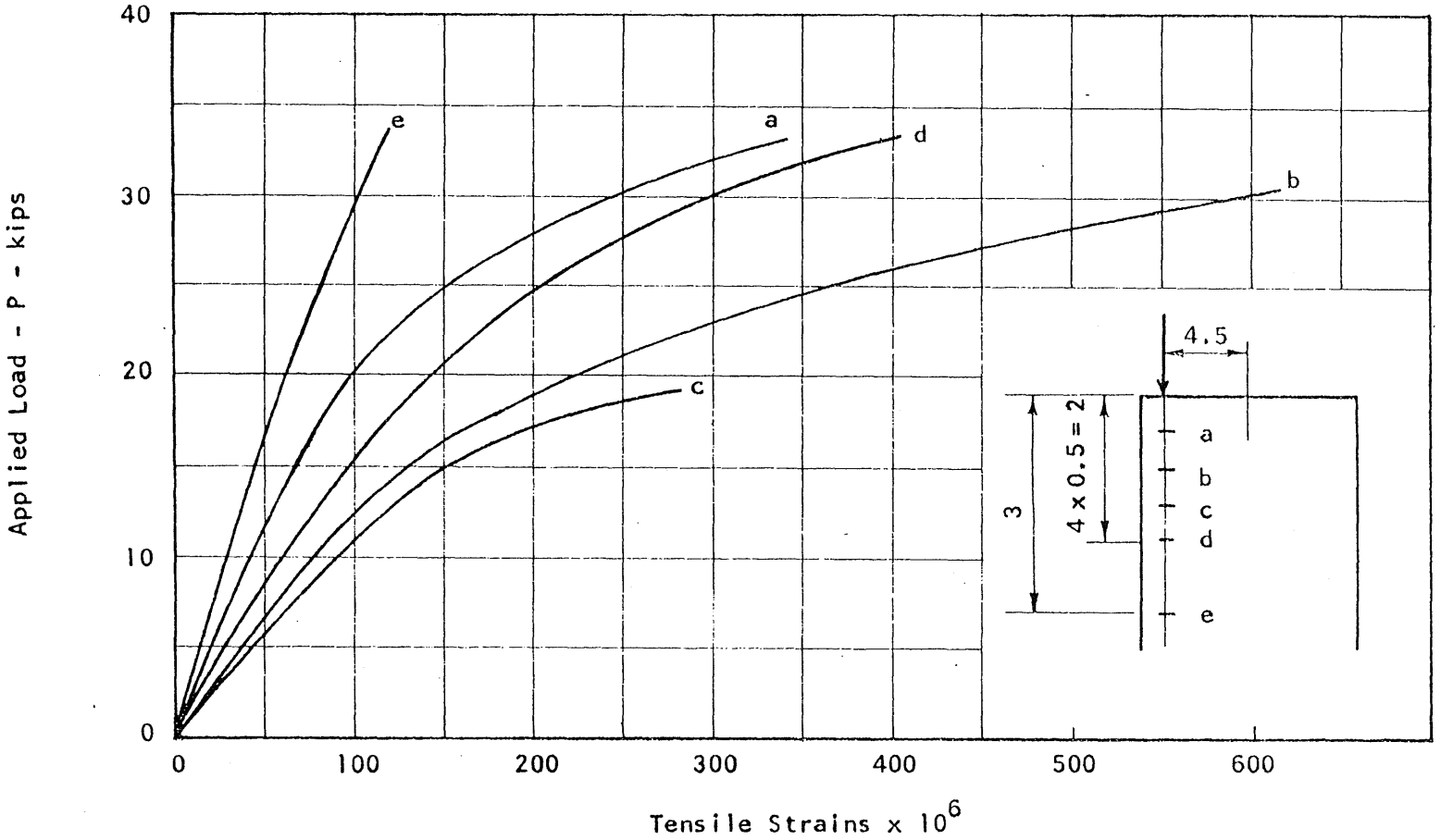

FIG. 3.1 MEASURED RELATIONSHIPS BETWEEN LOAD AND TRANSVERSE STRAIN FOR SPECIMEN R1

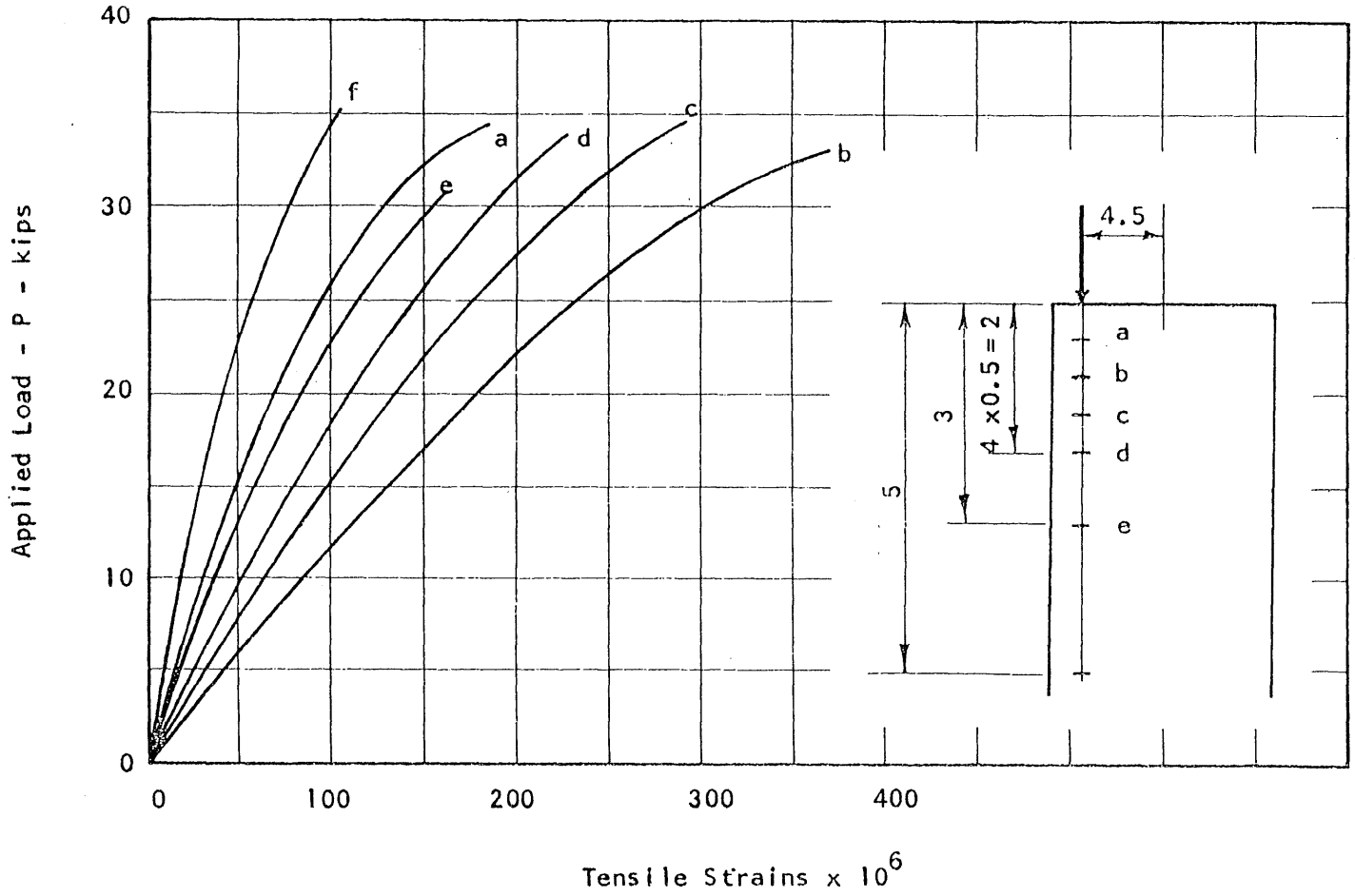

FIG. 3.2a MEASURED RELATIONSHIPS BETWEEN LOAD AND TRANSVERSE STRAIN FOR SPECIMEN R2

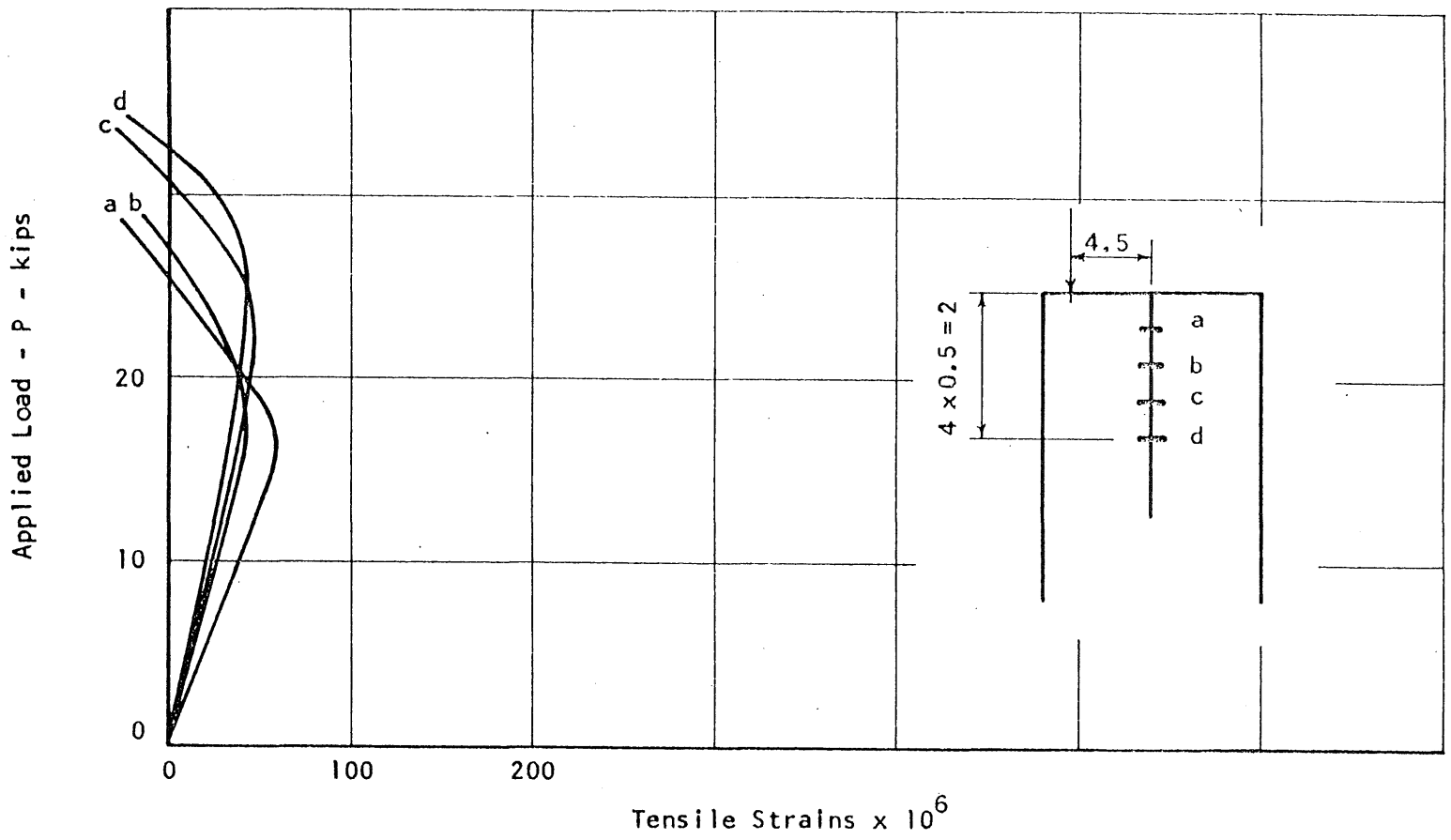

FIG. 3.2b MEASURED RELATIONSHIPS BETWEEN LOAD AND TRANSVERSE STRAIN FOR SPECIMEN R2

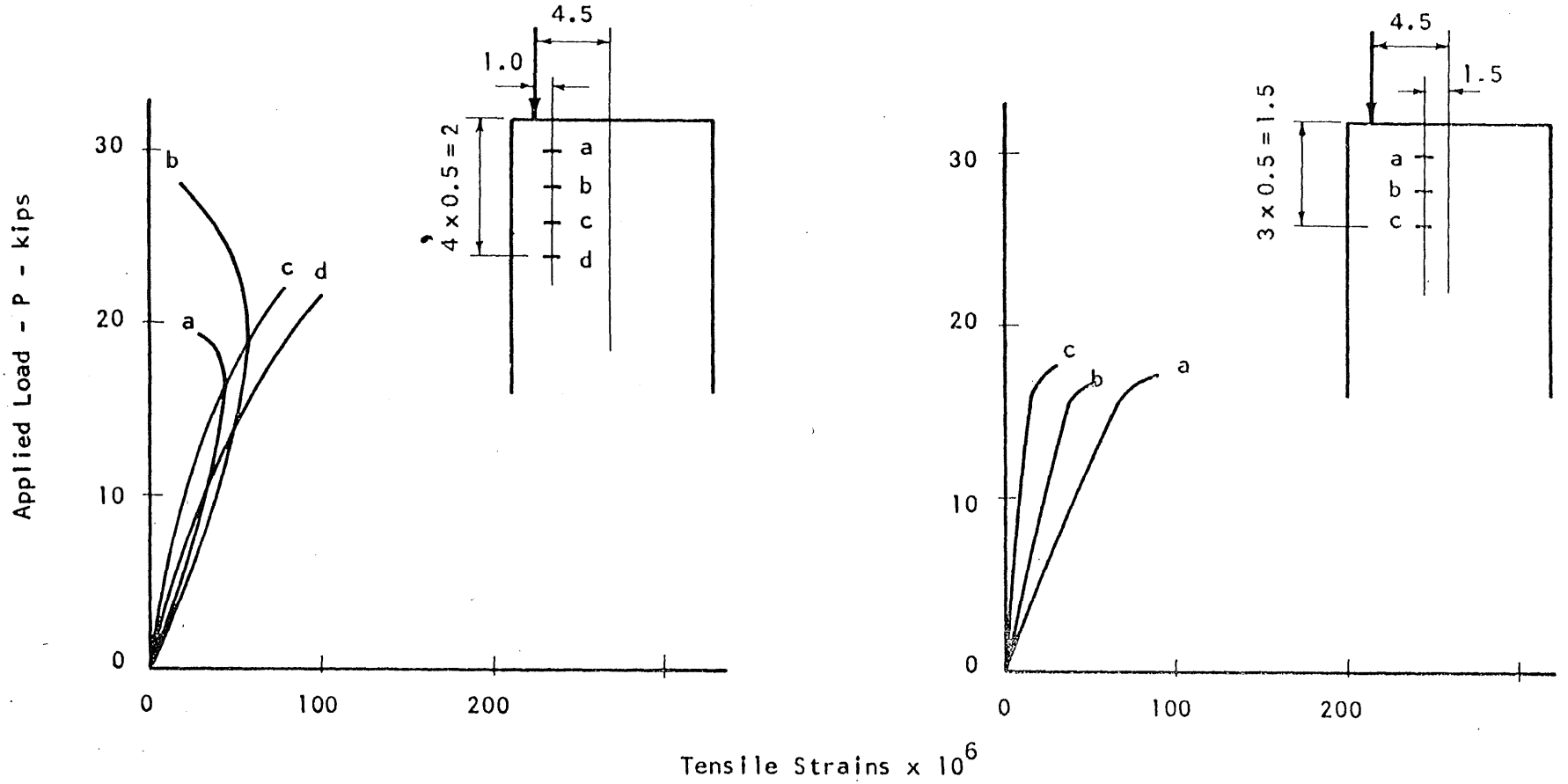

FIG. 3.c MEASURED RELATIONSHIPS BETWEEN LOAD AND TRANSVERSE STRAIN FOR SPECIMEN R2

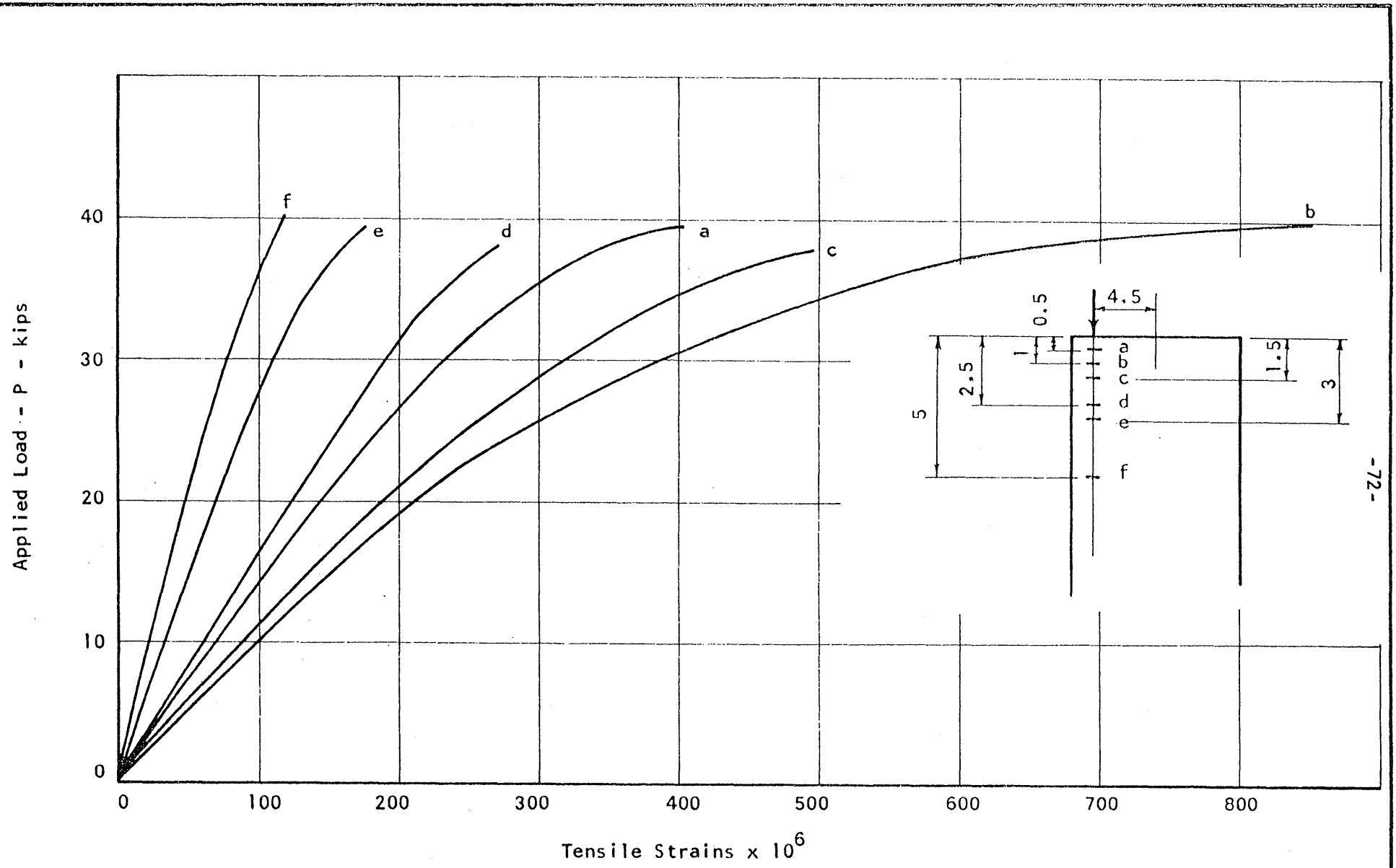

FIG. 3.3a MEASURED RELATIONSHIPS BETWEEN LOAD AND TRANSVERSE STRAIN FOR SPECIMEN R3

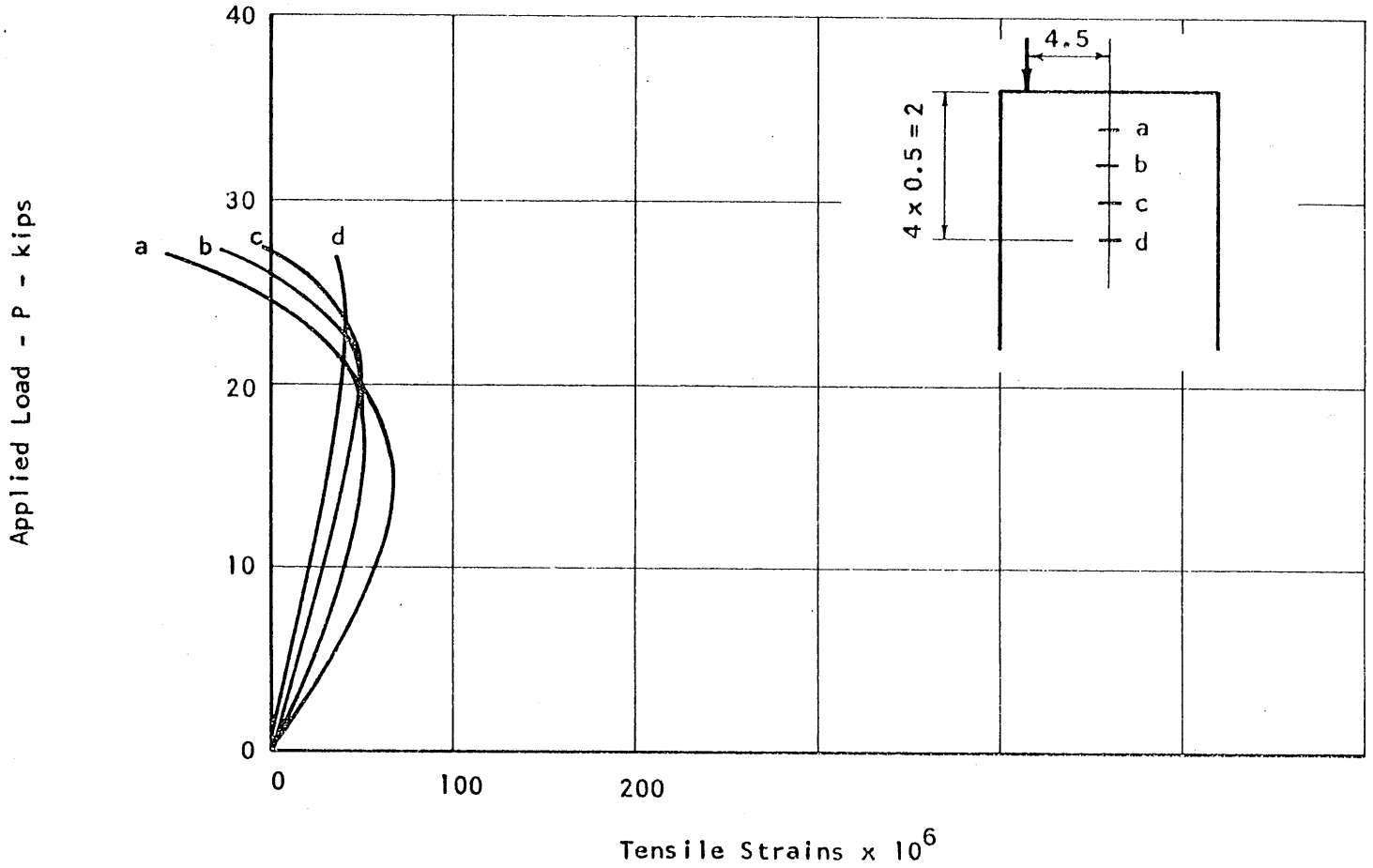

FIG. 3.3b MEASURED RELATIONSHIPS BETWEEN LOAD AND TRANSVERSE STRAIN FOR SPECIMEN R3

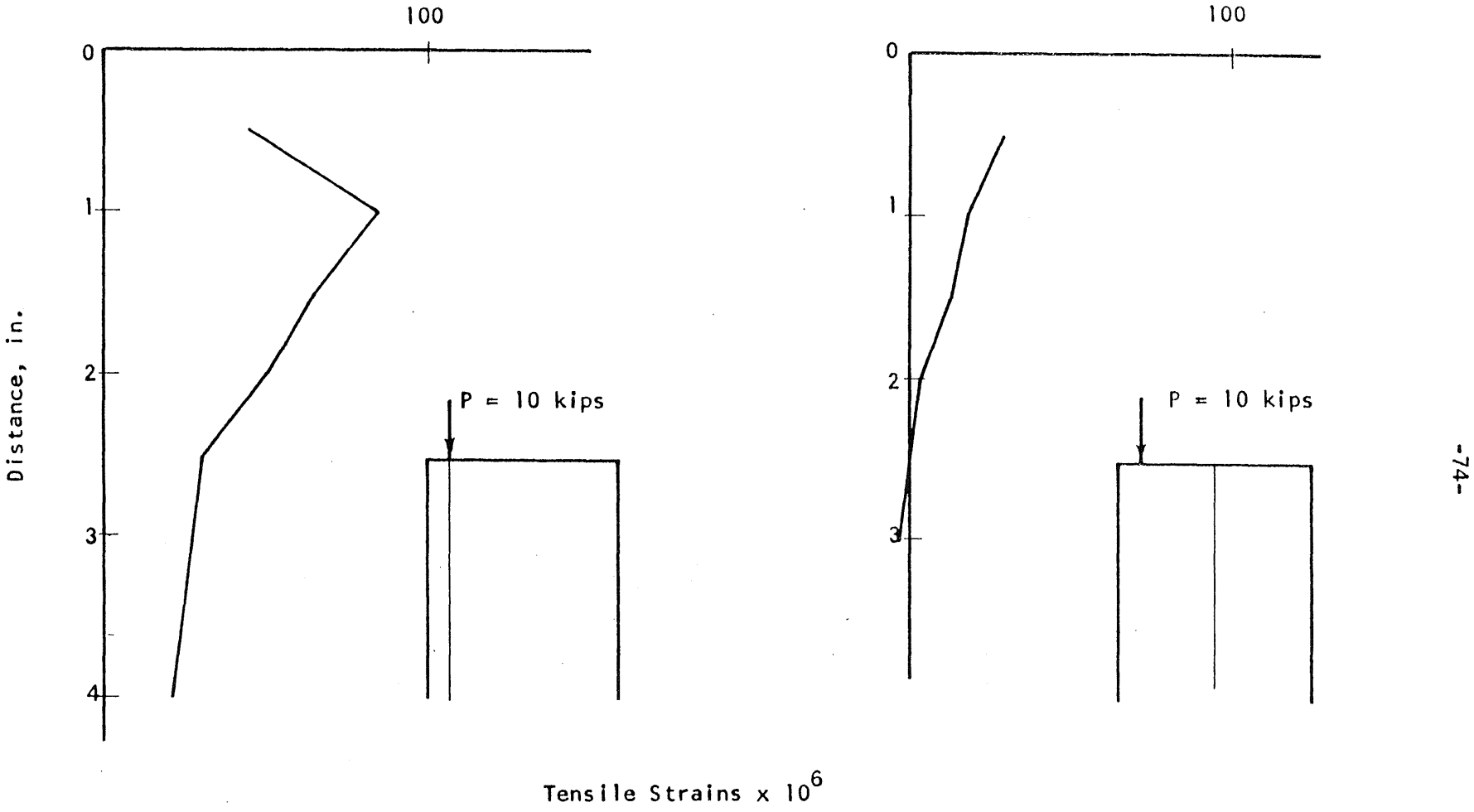

FIG. 3.4 MEASURED DISTRIBUTION OF TRANSVERSE STRAINS ALONG LINE OF LOAD AND ALONG CENTER LINE FOR SPECIMEN R2

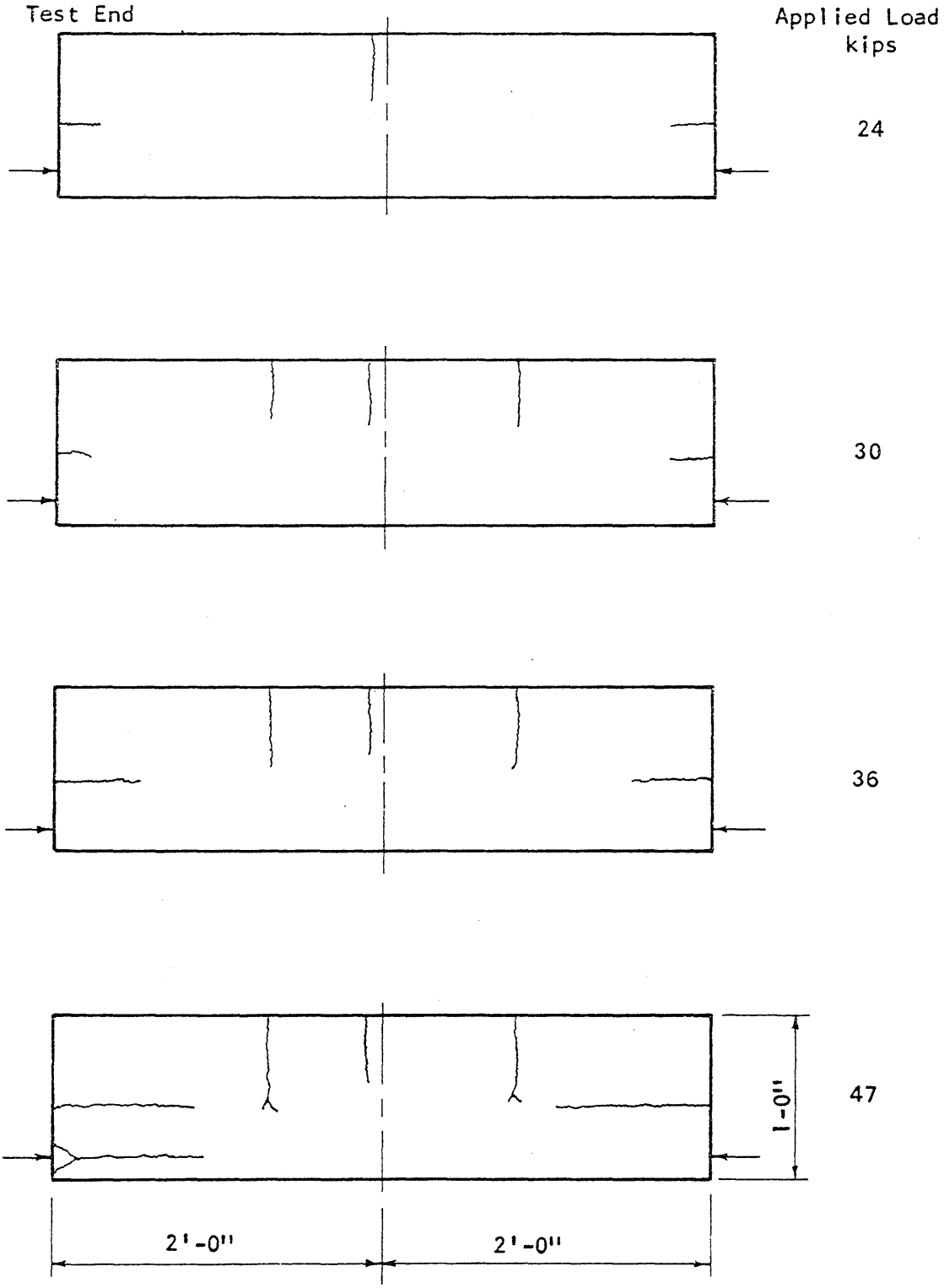

FIG. 3.5 DEVELOPMENT OF CRACKS IN SPECIMEN R3

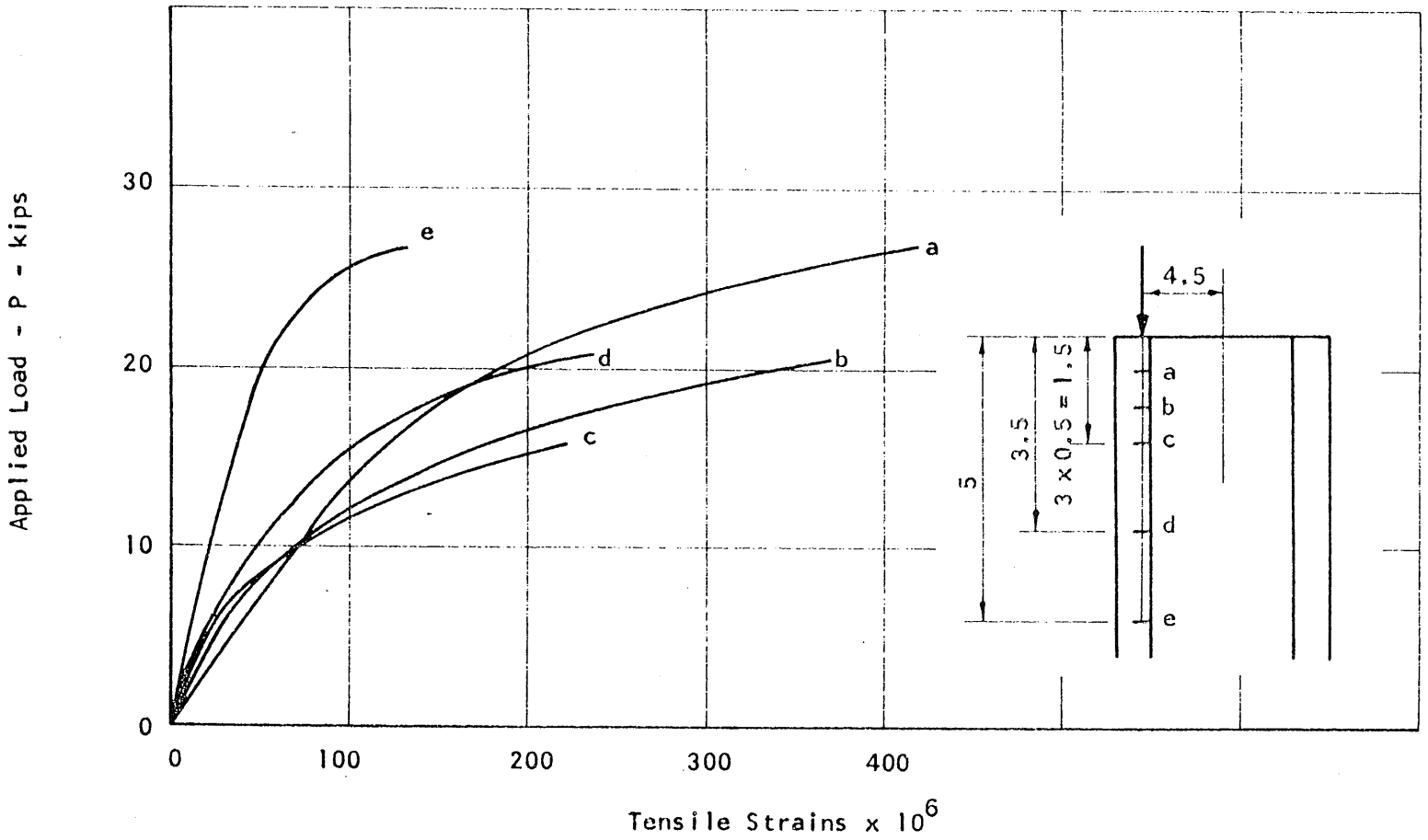

FIG. 3.6a MEASURED RELATIONSHIPS BETWEEN LOAD AND TRANSVERSE STRAIN FOR SPECIMEN T2

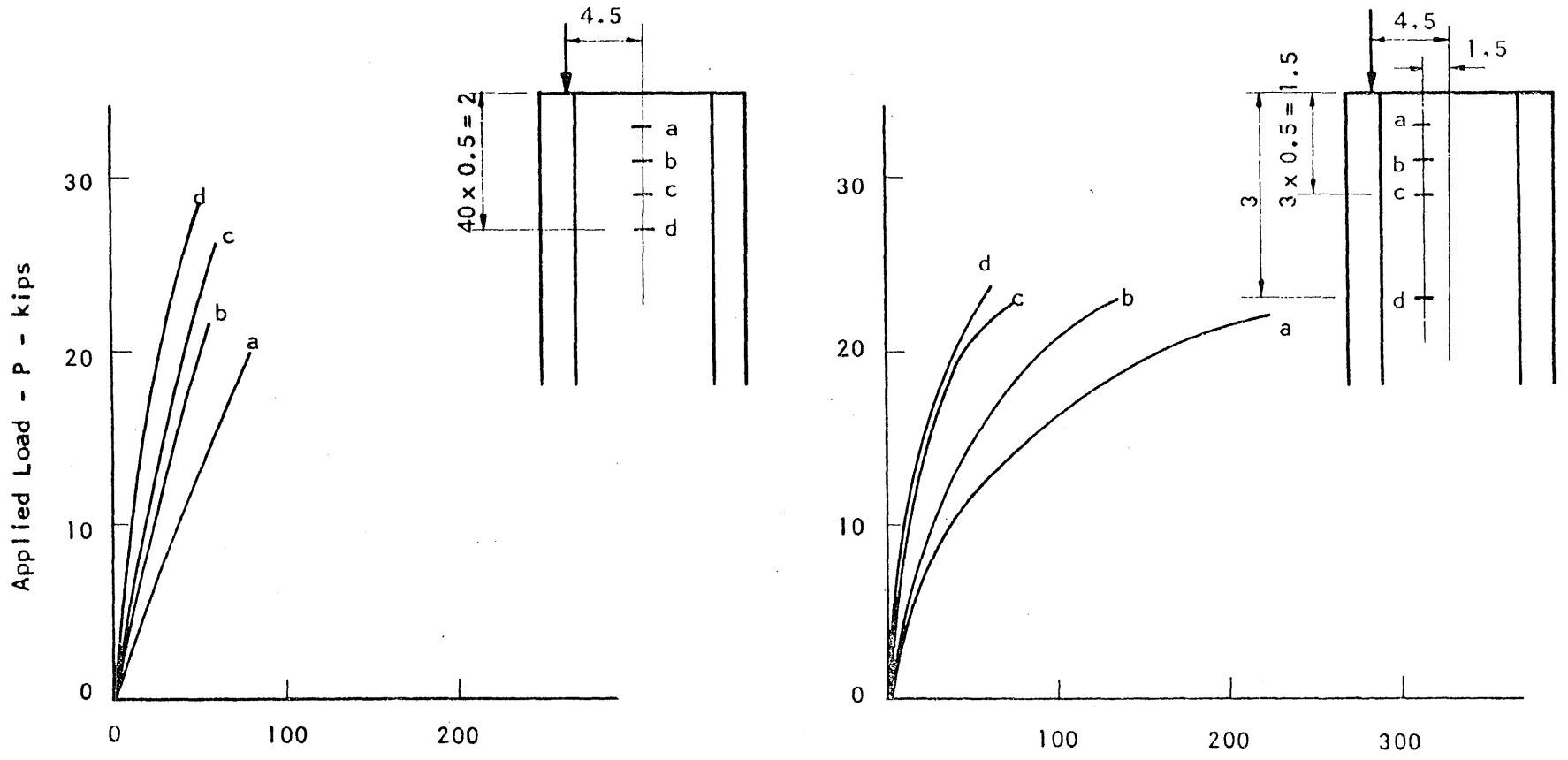

FIG. 3.6b MEASURED RELATIONSHIPS BETWEEN LOAD AND TRANSVERSE STRAIN FOR SPECIMEN T2

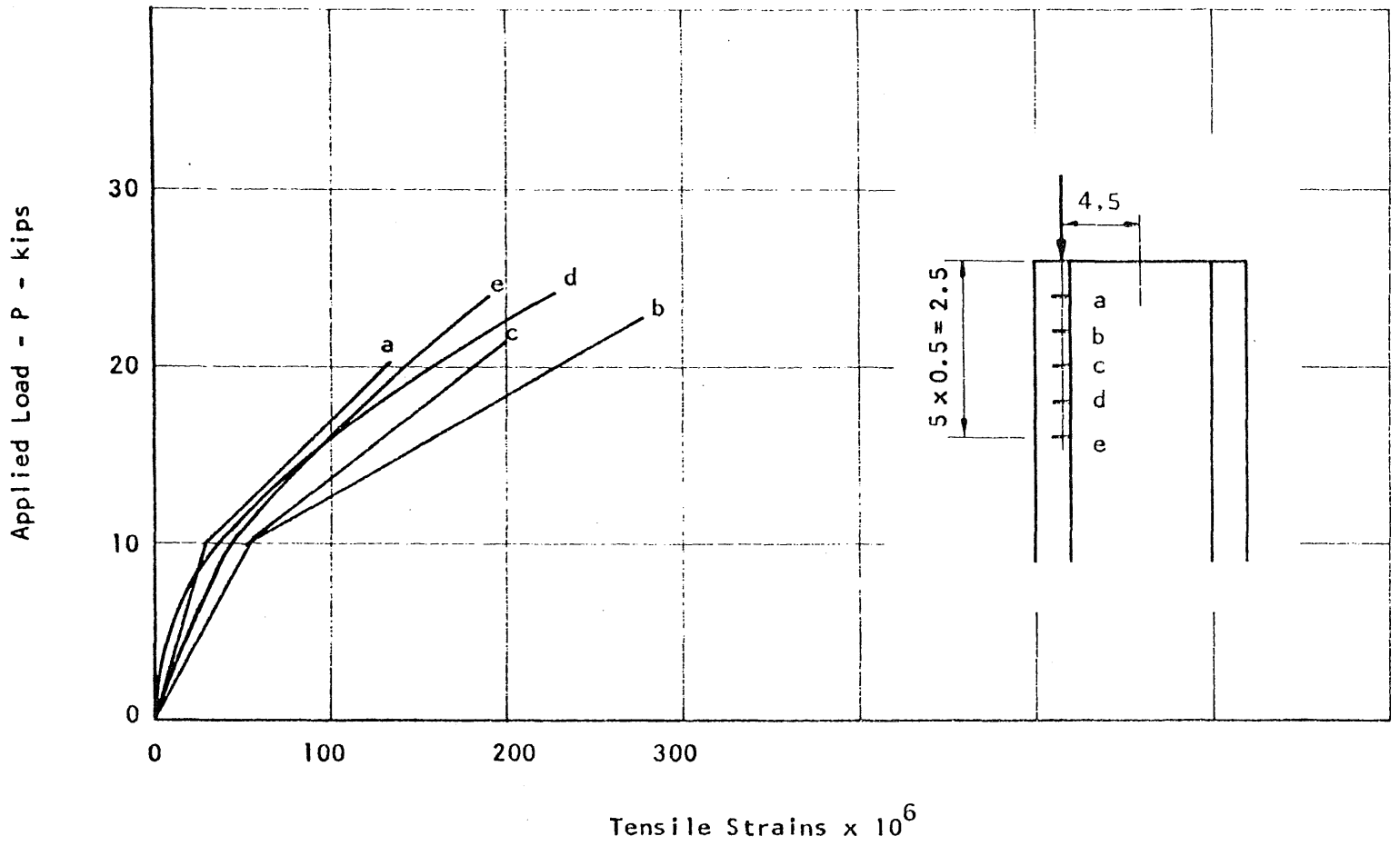

FIG. 3.7a MEASURED RELATIONSHIPS BETWEEN LOAD AND TRANSVERSE STRAIN FOR SPECIMEN T3

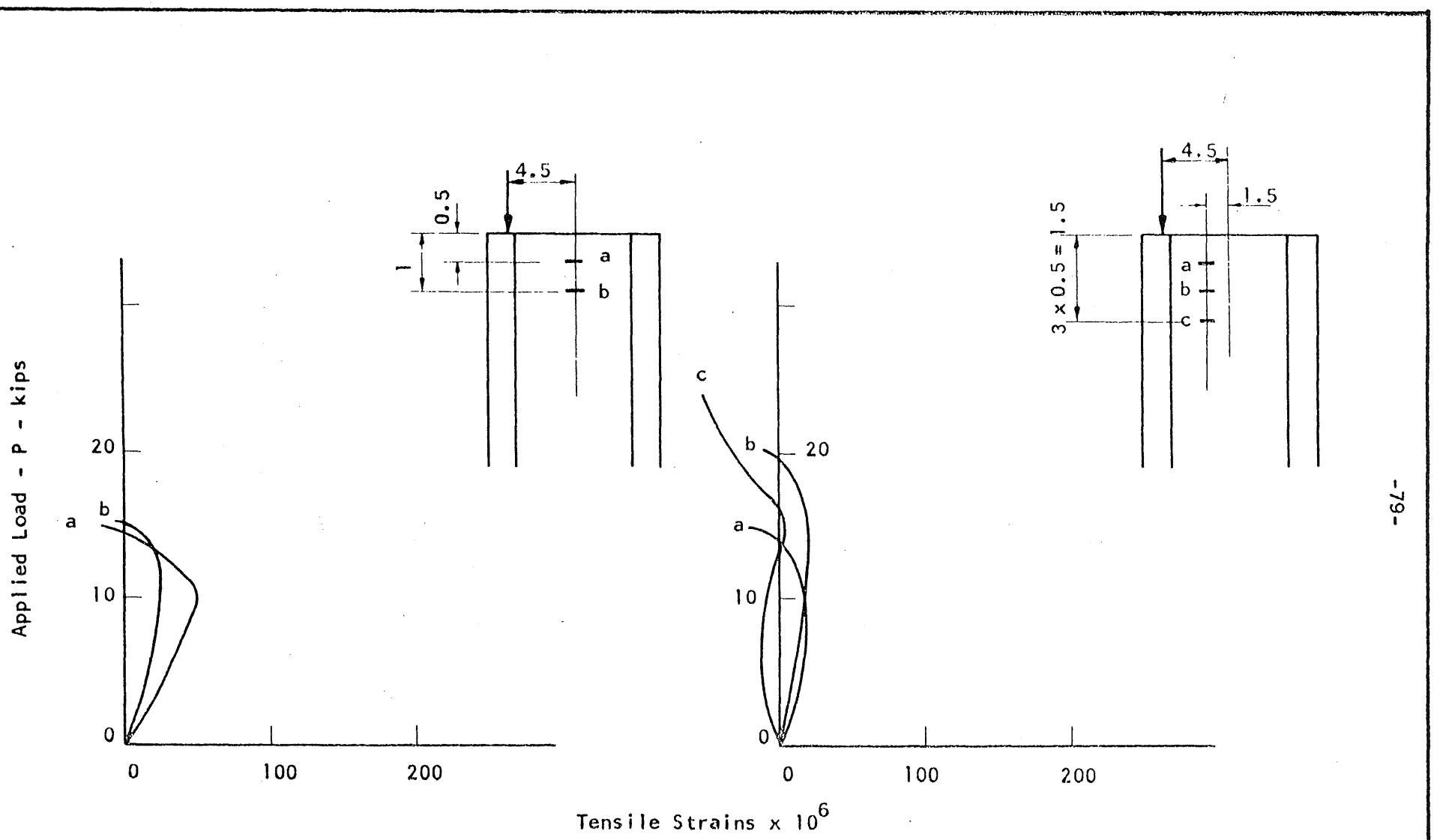
Applied Load - P - kips
20
10
0
a
b
0
100
200
4.5
0.5
1
a
b
c
4.5
1.5
3 x 0.5 = 1.5
a
b
c
Tensile Strains x 10^6

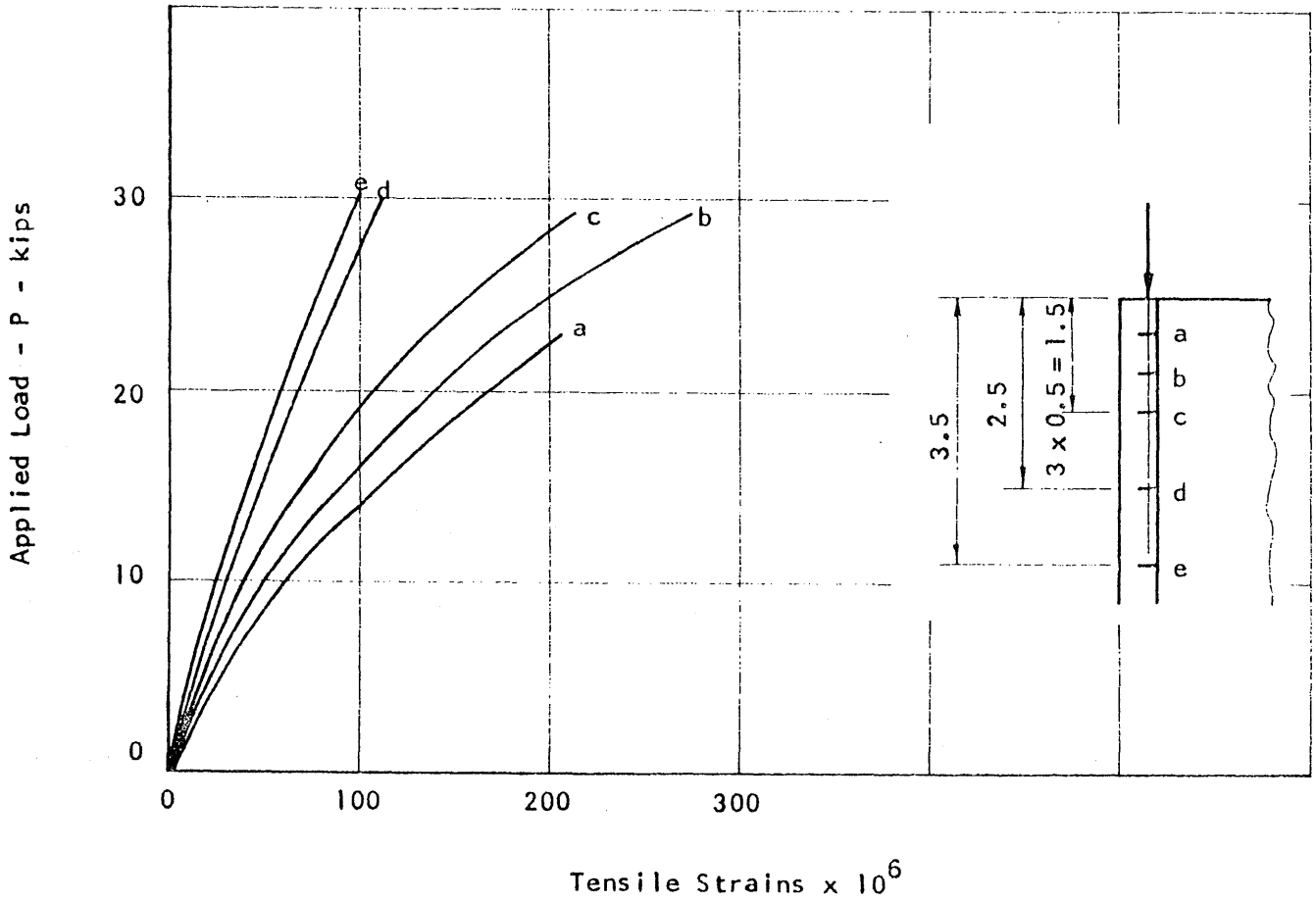

FIG. 3.8 MEASURED RELATIONSHIPS BETWEEN LOAD AND TRANSVERSE STRAIN FOR SPECIMEN T7

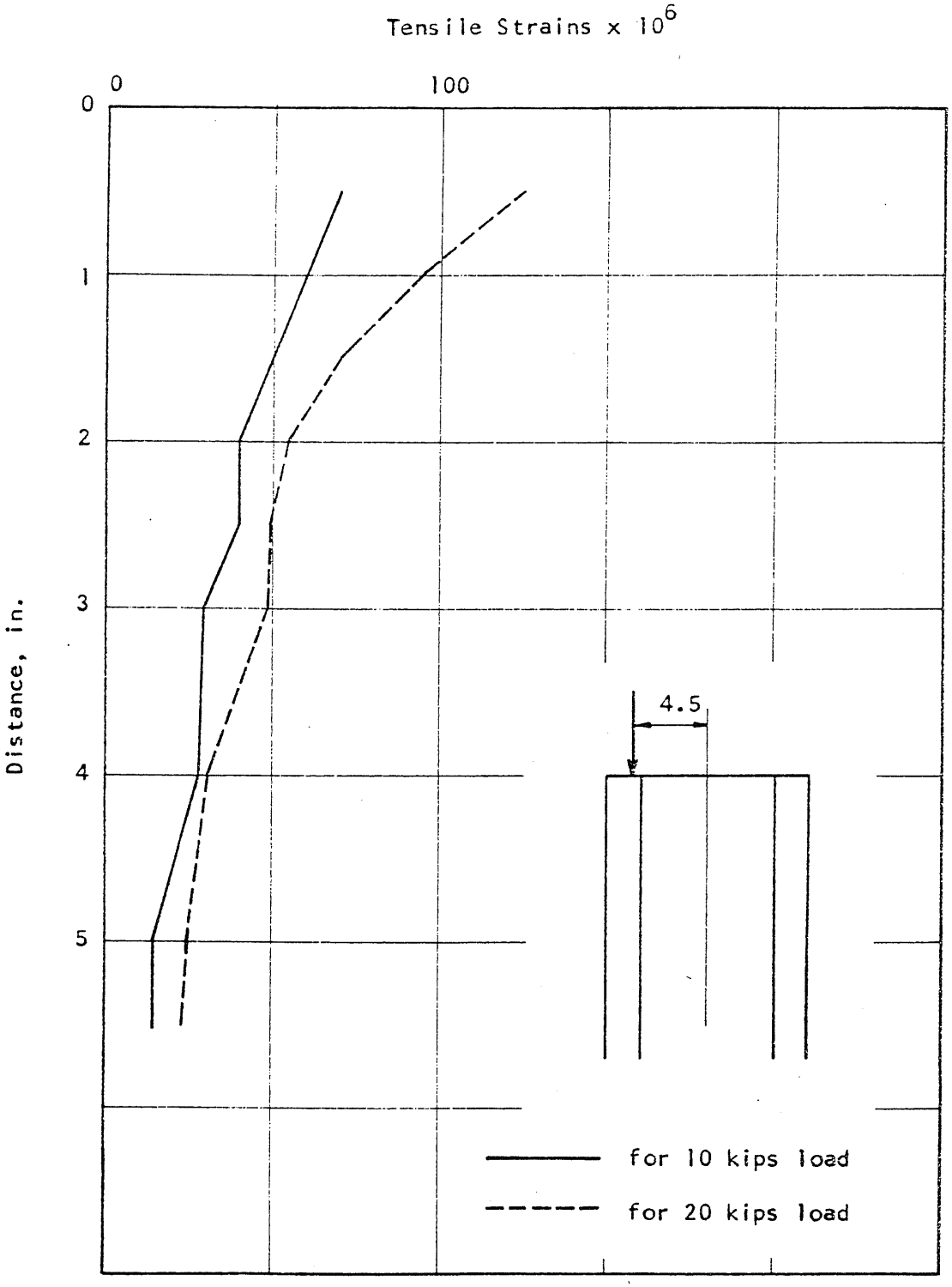

FIG. 3.9 TRANSVERSE STRAINS AT POINTS ALONG CENTER LINE FOR SPECIMEN T2

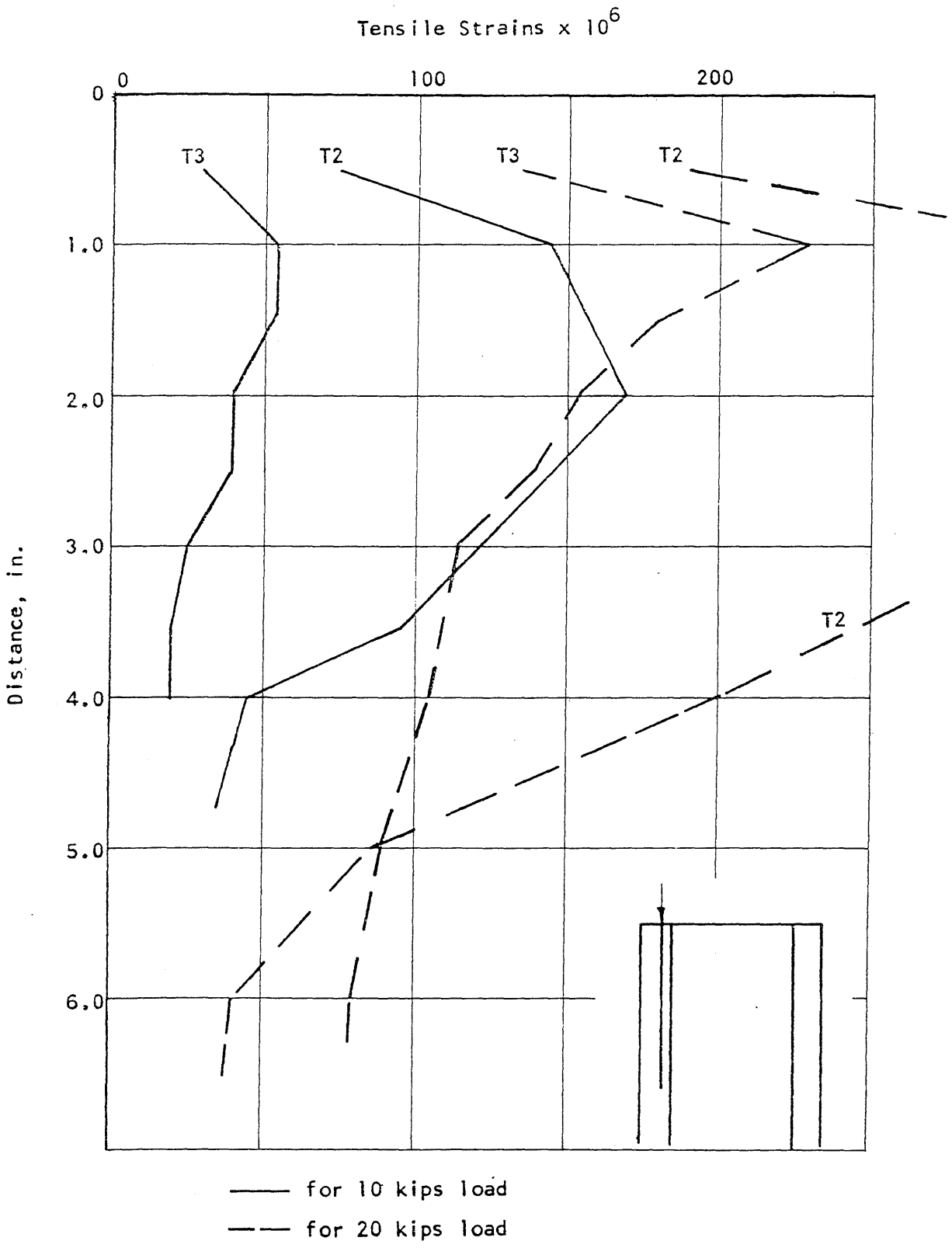

FIG. 3.10 TRANSVERSE STRAINS AT POINTS ALONG THE LINE OF LOAD FOR SPECIMENS T2 and T3

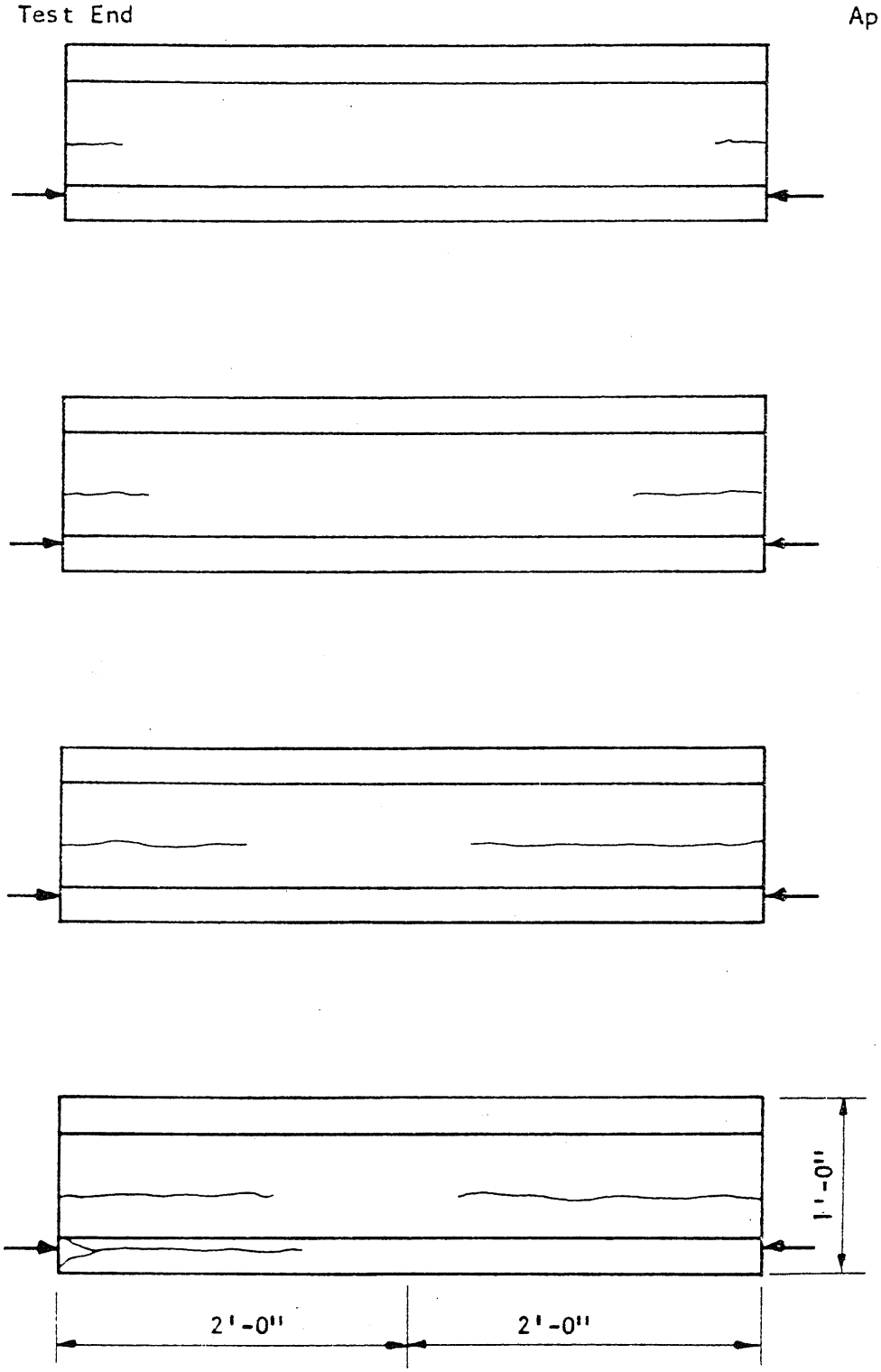

FIG. 3.11 DEVELOPMENT OF CRACKS IN I-BEAMS

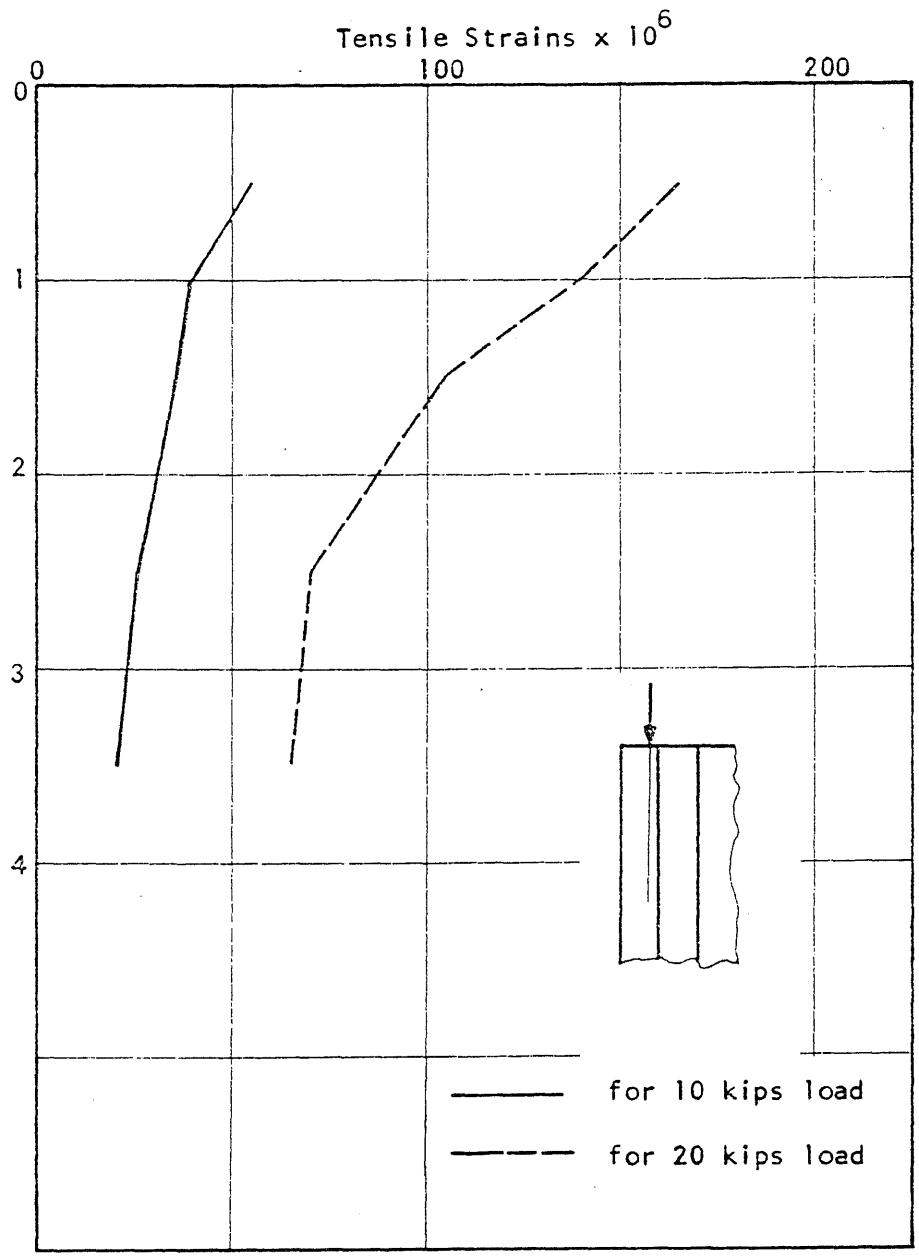

FIG. 3.12 TRANSVERSE STRAINS AT POINTS ALONG THE LINE OF LOAD FOR SPECIMEN T7

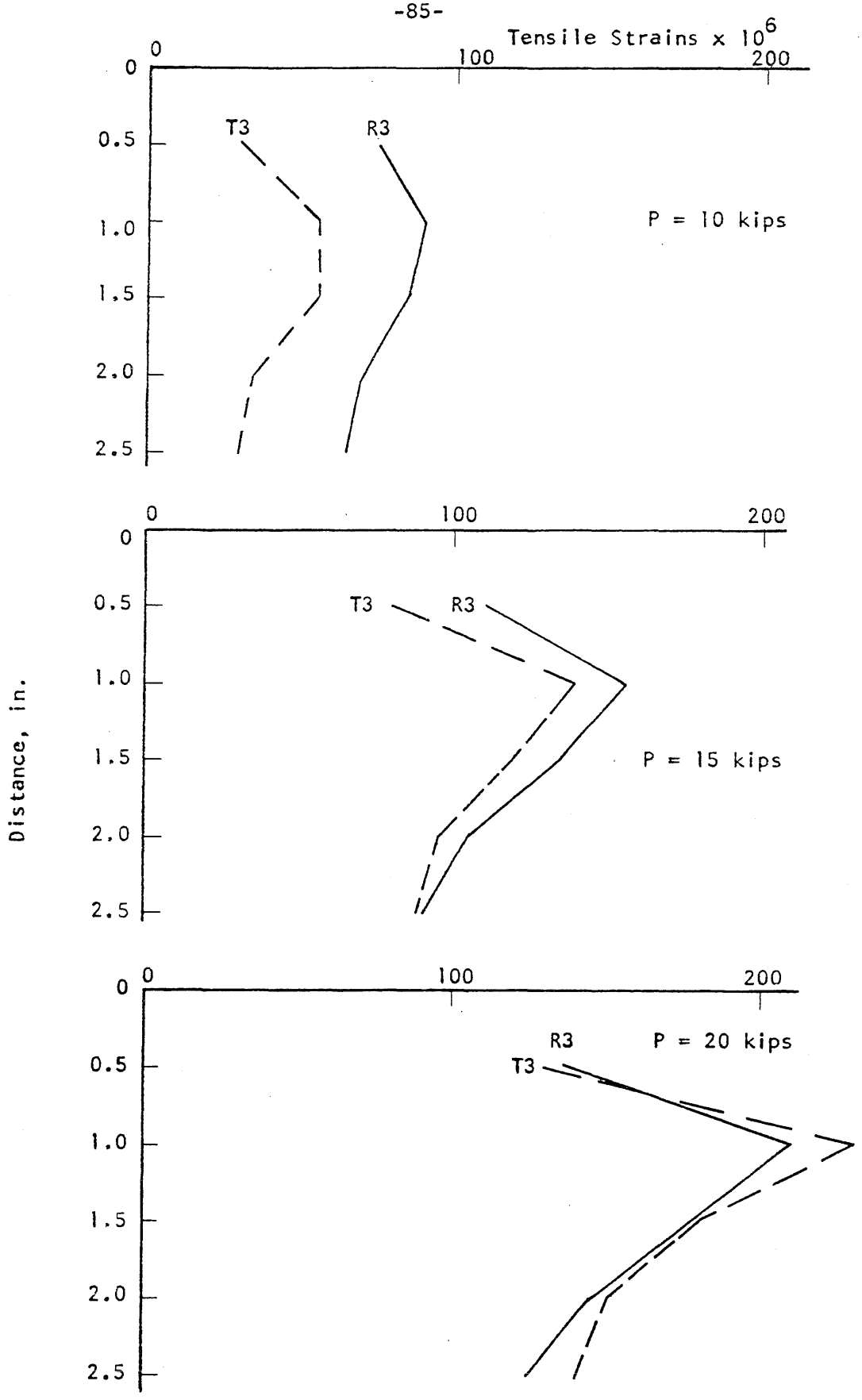

FIG. 3.13 MEASURED TRANSVERSE STRAINS ALONG LINE OF LOAD FOR SPECIMENS R3 and T3

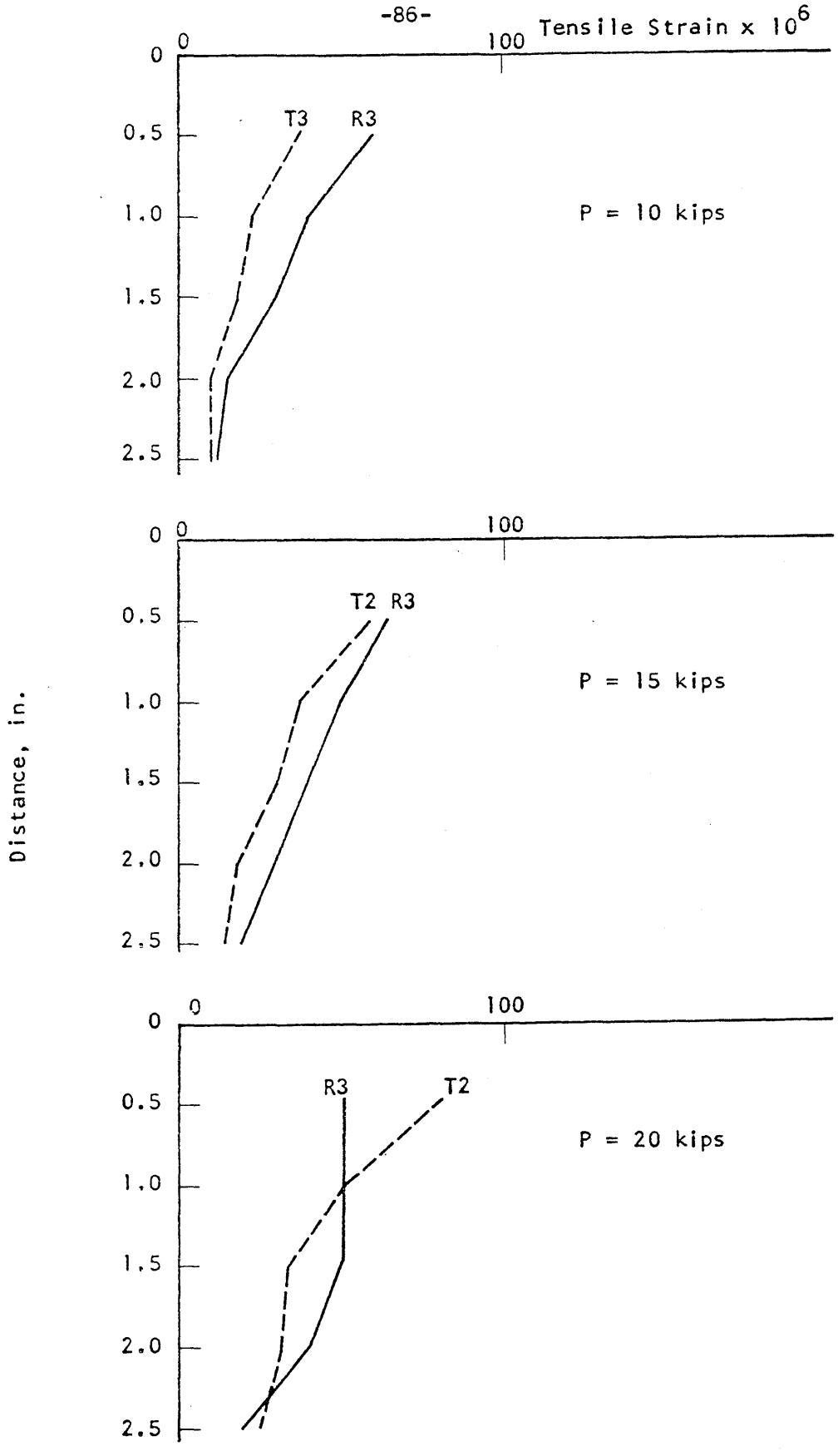

FIG. 3.14 MEASURED TRANSVERSE STRAINS ALONG THE CENTER LINE FOR SPECIMENS R3 and T2

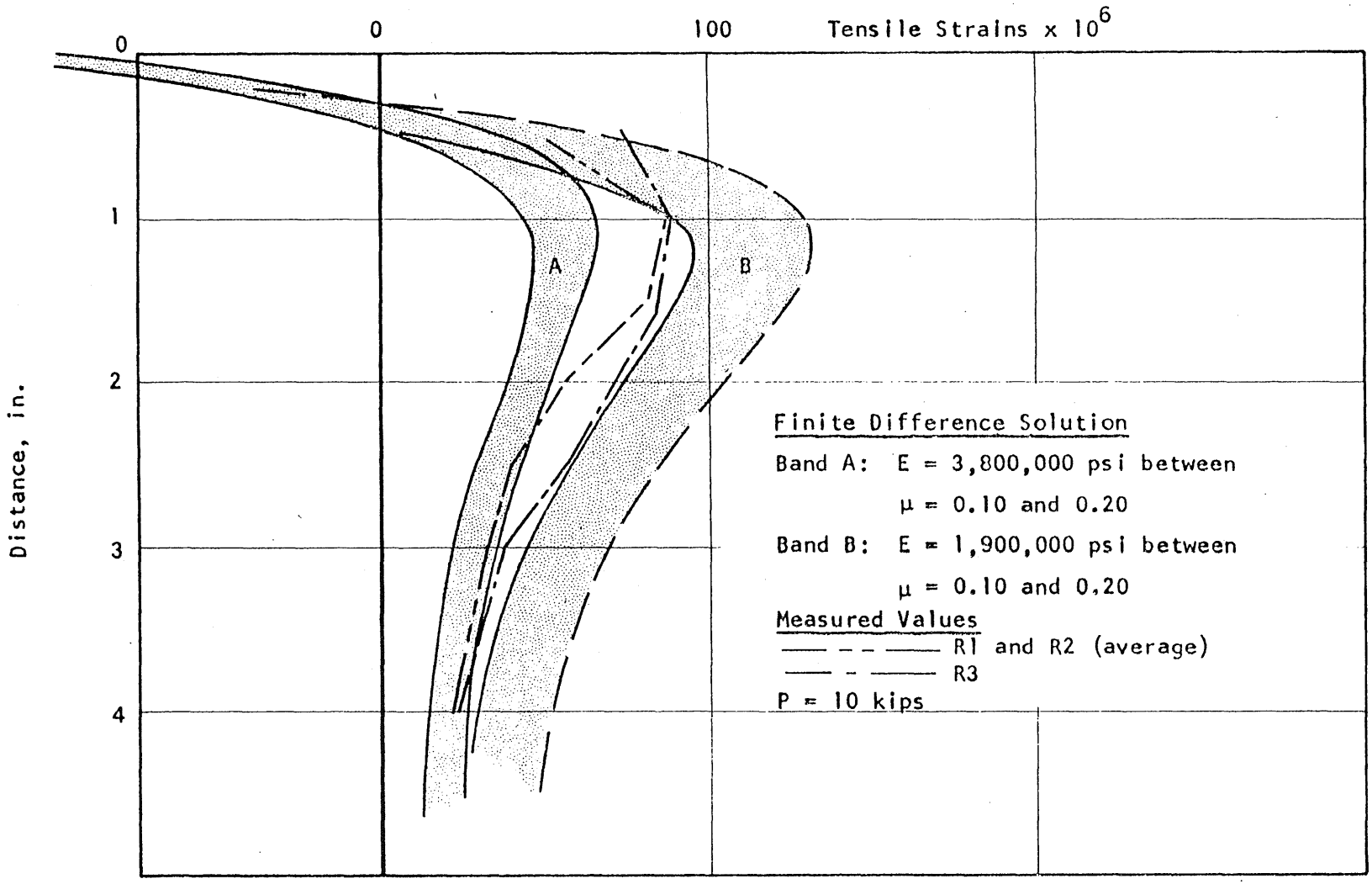

FIG. 3.15 COMPARISON OF MEASURED TRANSVERSE STRAINS ALONG THE LINE OF THE LOAD WITH THE FINITE DIFFERENCE SOLUTION

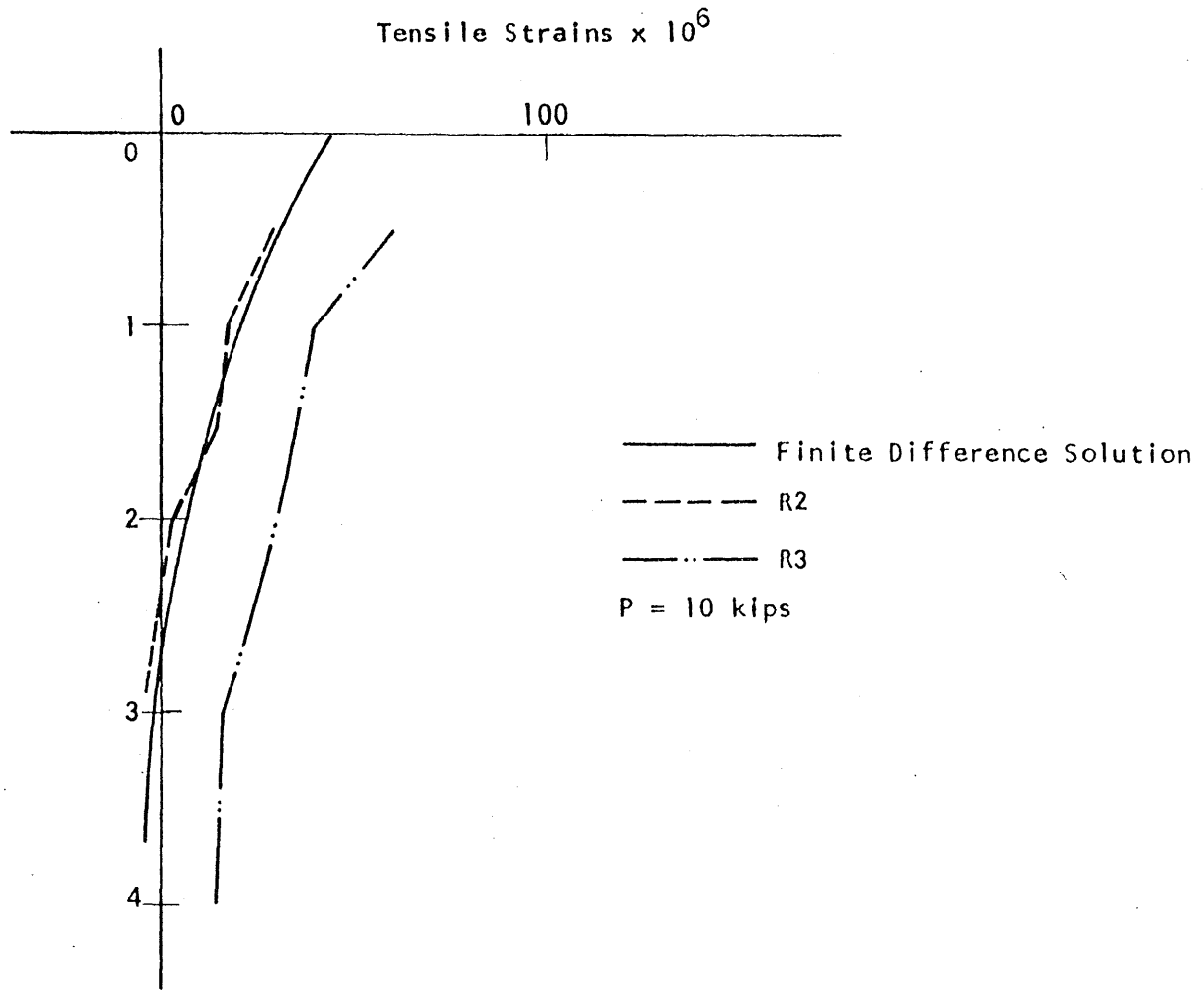

FIG. 3.16 COMPARISON OF MEASURED TRANSVERSE STRAINS ALONG CENTER LINE WITH THE FINITE DIFFERENCE SOLUTION

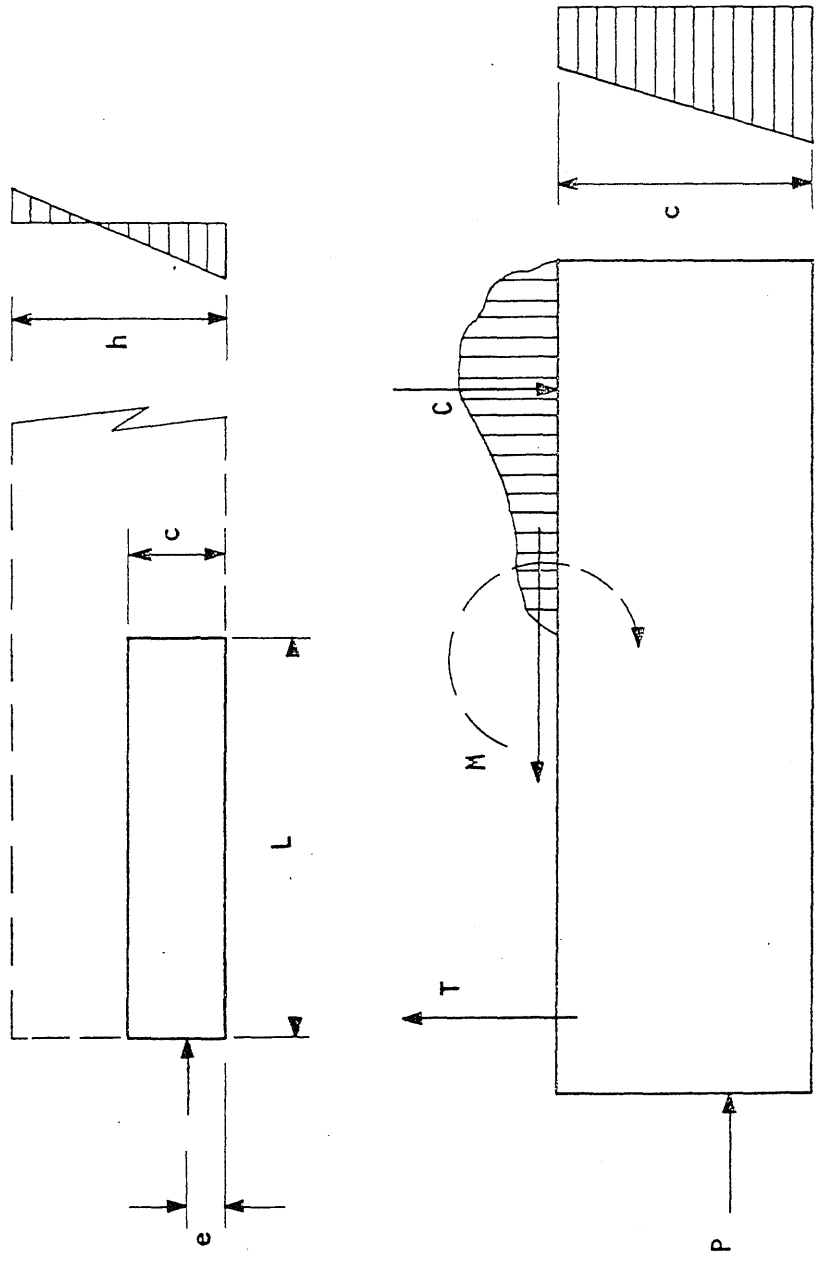

FIG. 4.1 FORCES ON FREE BODY

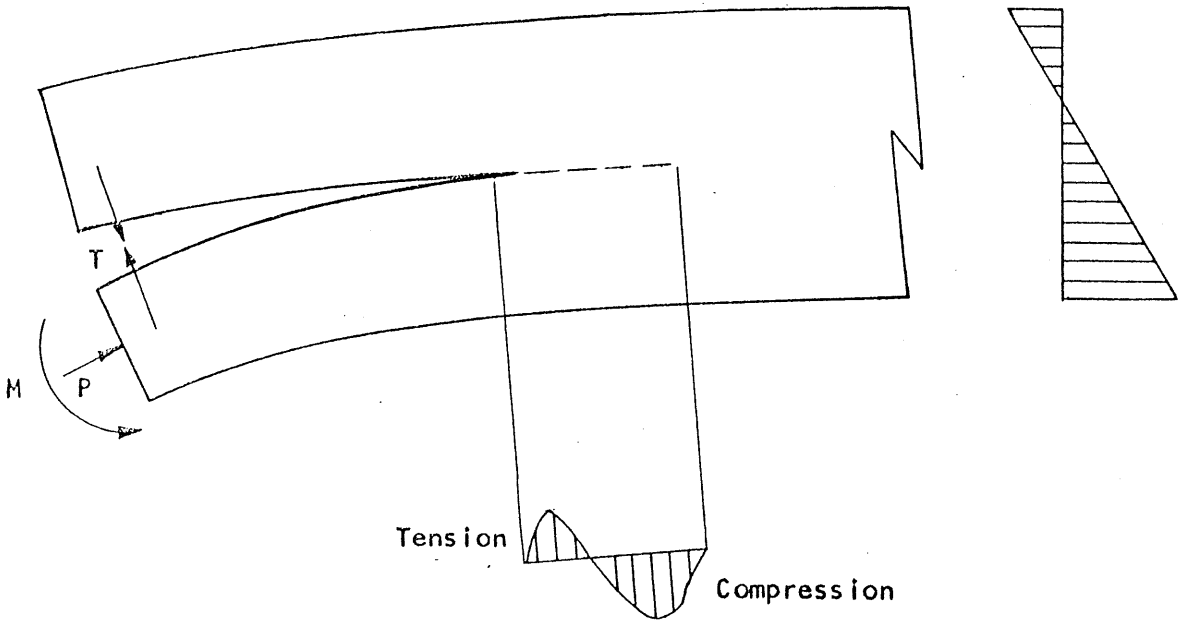

FIG. 4.2 CONDITIONS OF FORCES AND STRESSES IN THE CRACKED BEAM

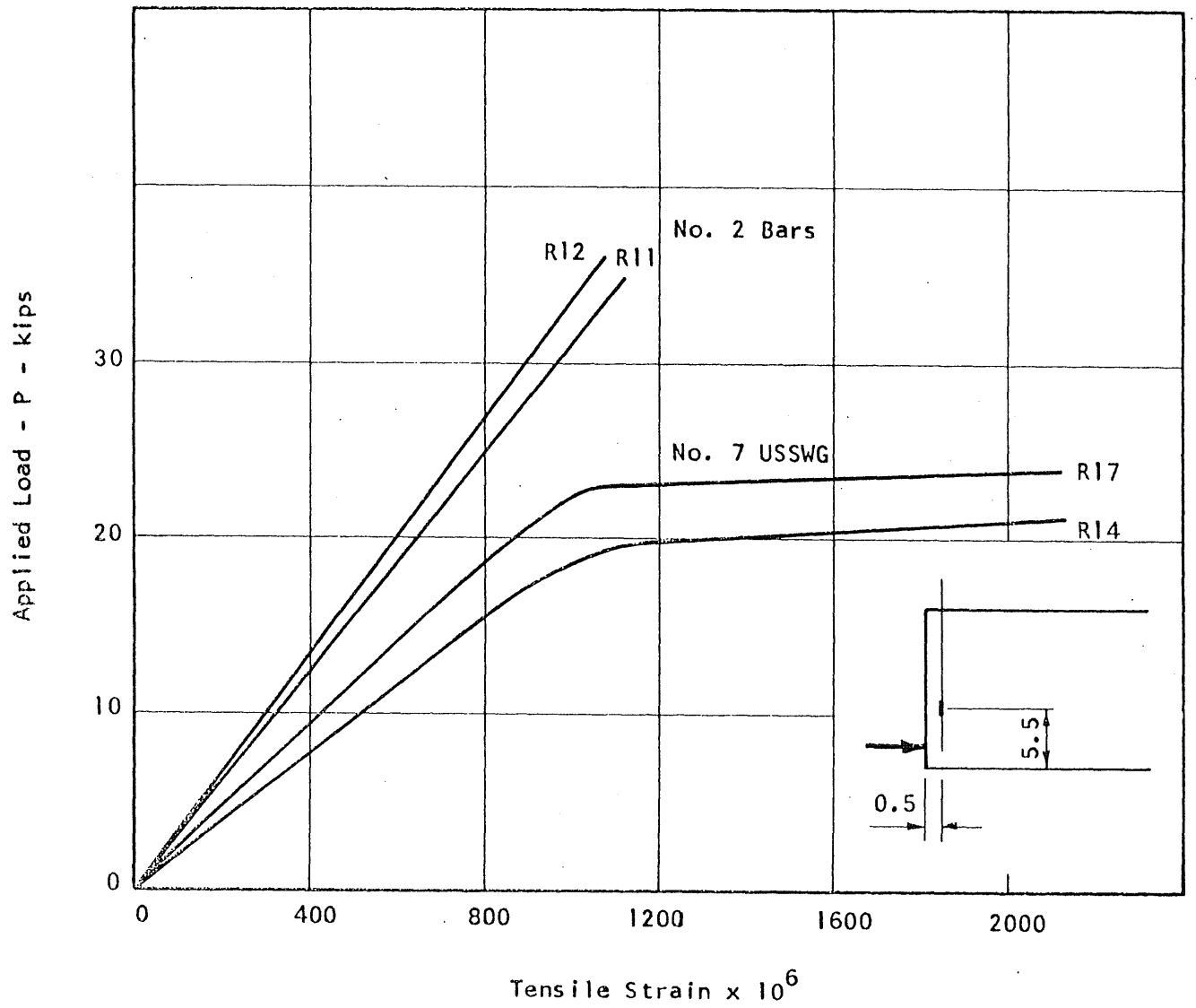

FIG. 5.1 MEASURED RELATIONSHIPS BETWEEN LOAD AND STIRRUP STRAIN FOR SPECIMENS R11, R12, R14 and R17

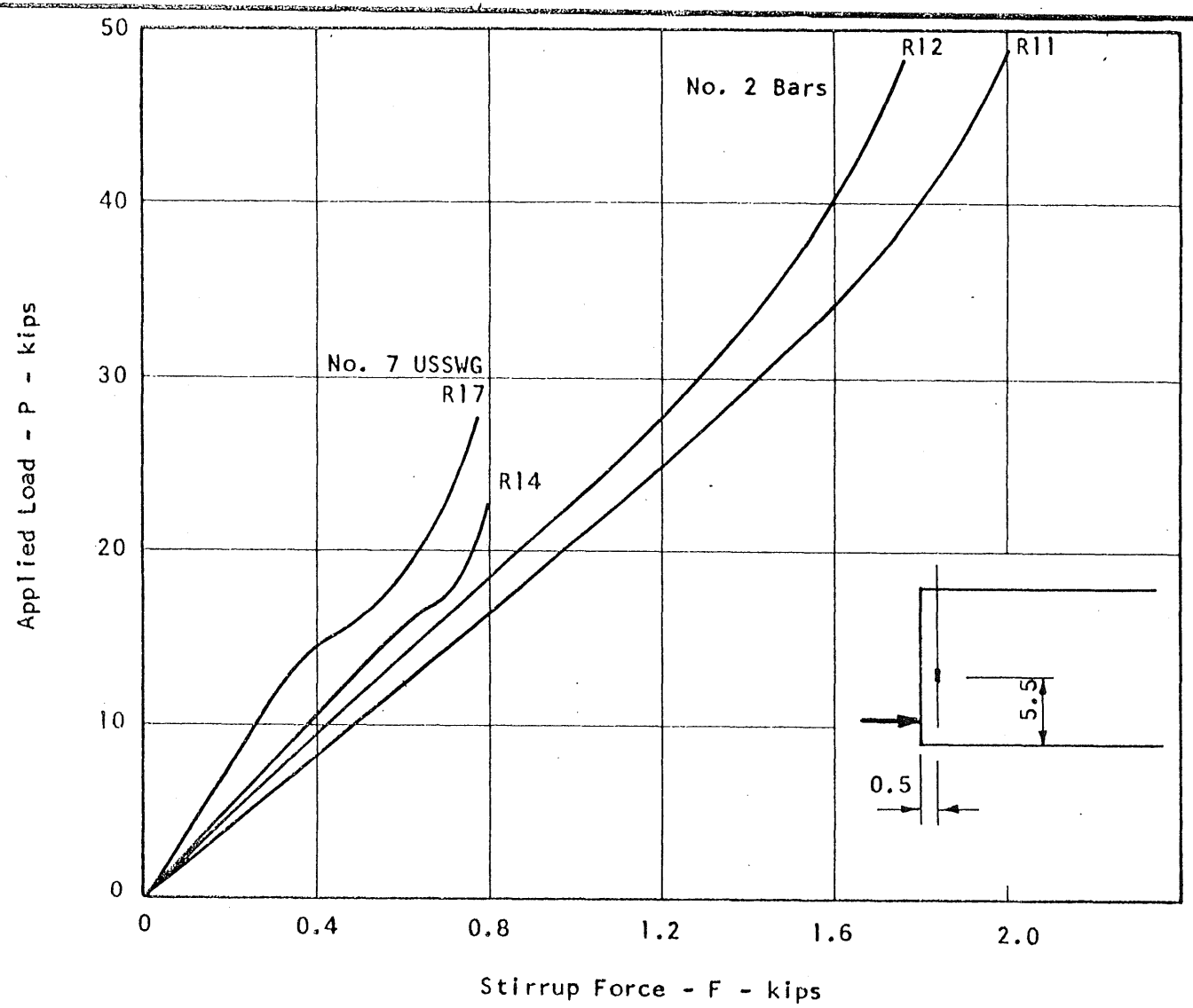

FIG. 5.2 MEASURED RELATIONSHIPS BETWEEN LOAD AND STIRRUP FORCE FOR SPECIMENS R11, R12, R14 and R17

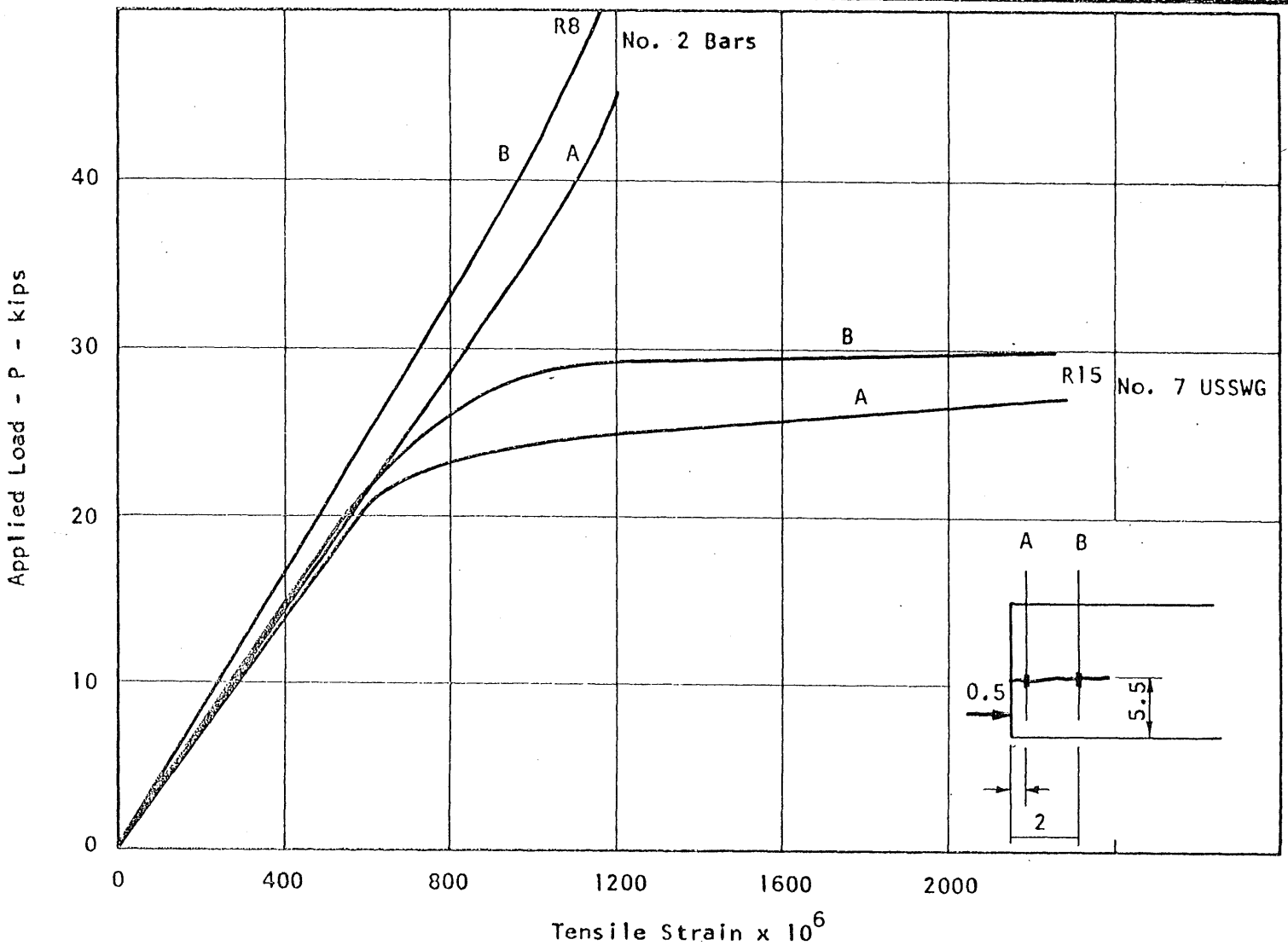

FIG. 5.3 MEASURED RELATIONSHIPS BETWEEN LOAD AND STIRRUP STRAIN FOR SPECIMENS R8 and R15

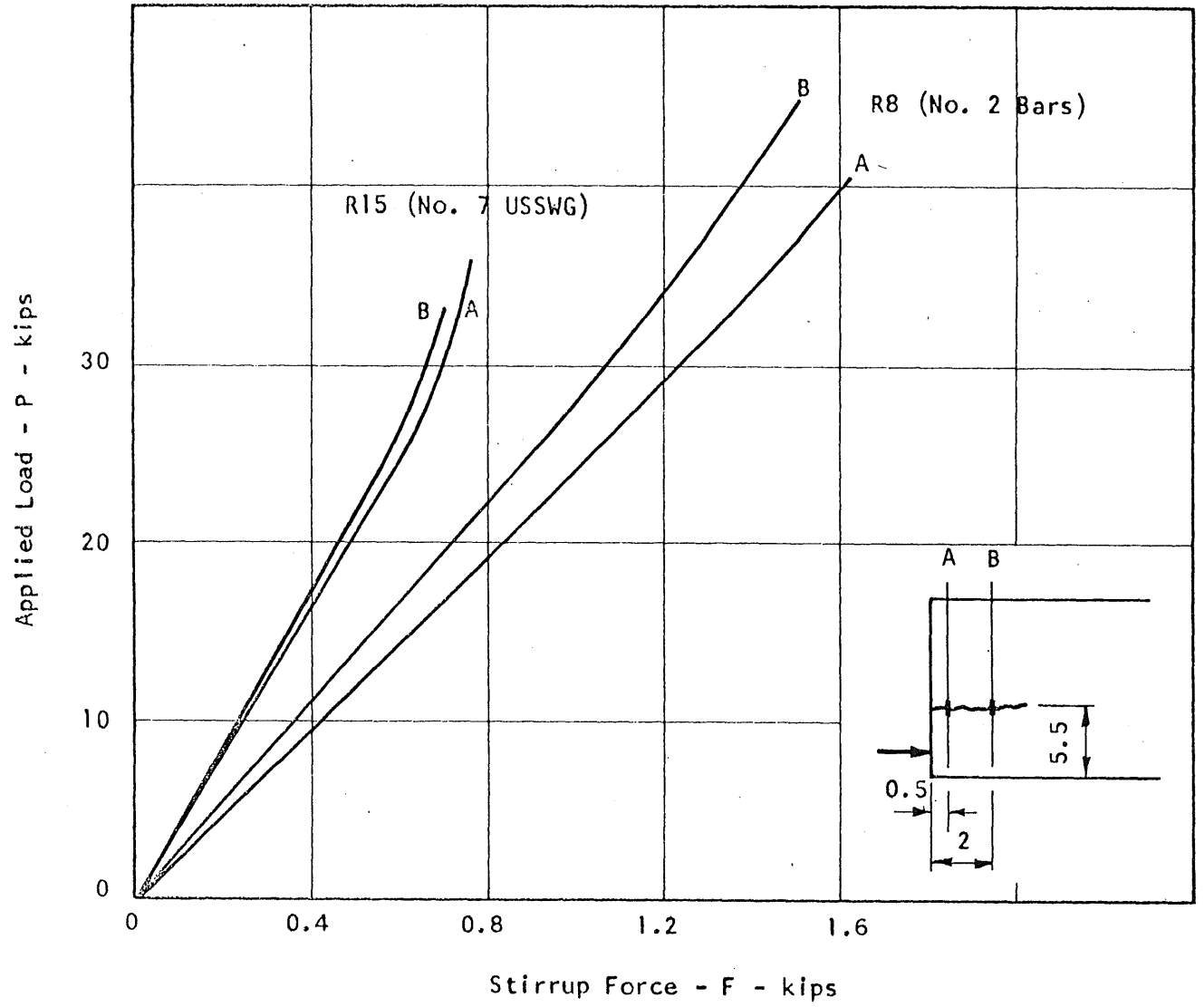

FIG. 5.4 MEASURED RELATIONSHIPS BETWEEN LOAD AND STIRRUP FORCE FOR SPECIMENS R8 and R15

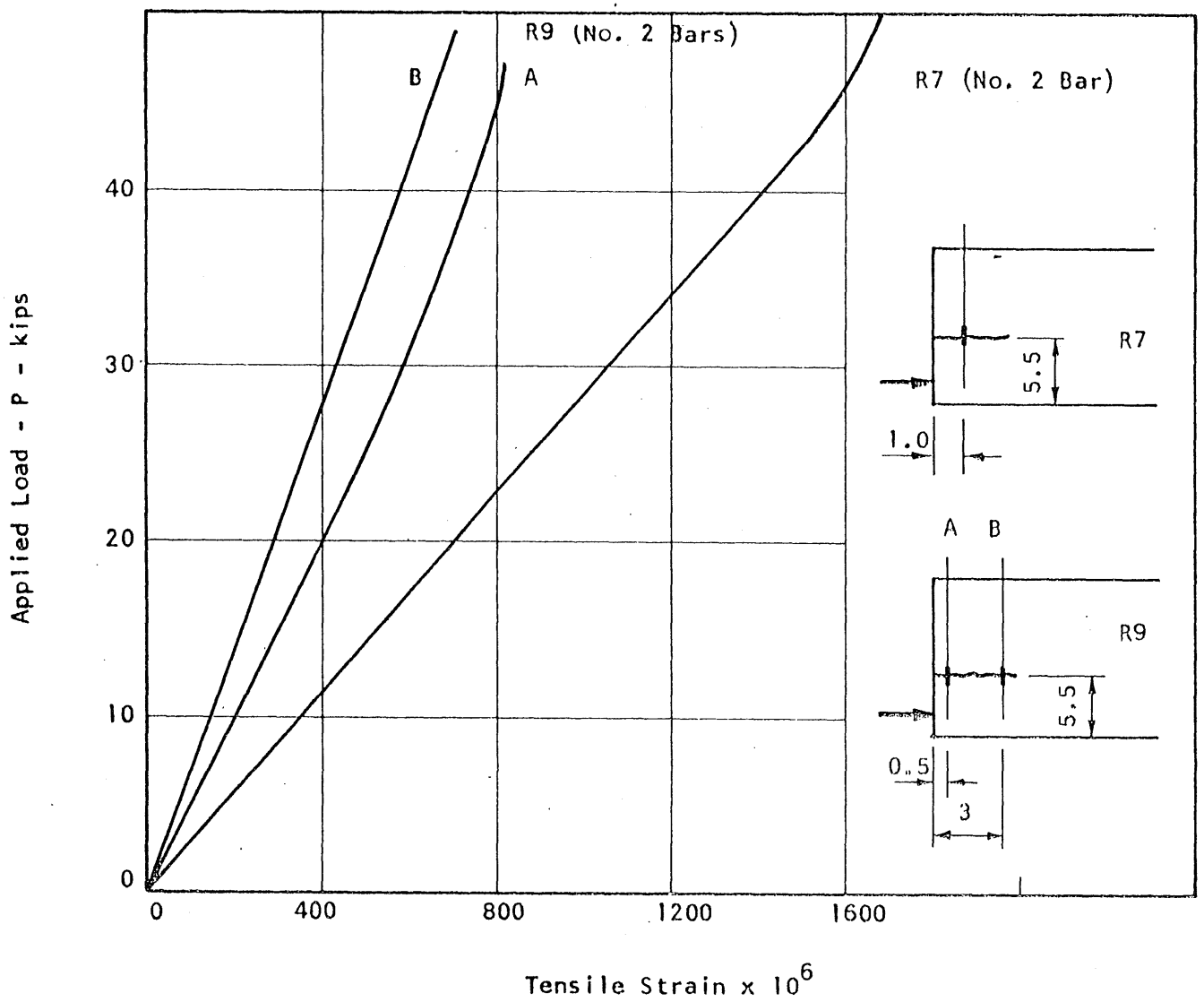

FIG. 5.5 MEASURED RELATIONSHIPS BETWEEN LOAD AND STIRRUP STRAIN FOR SPECIMENS R7 and R9

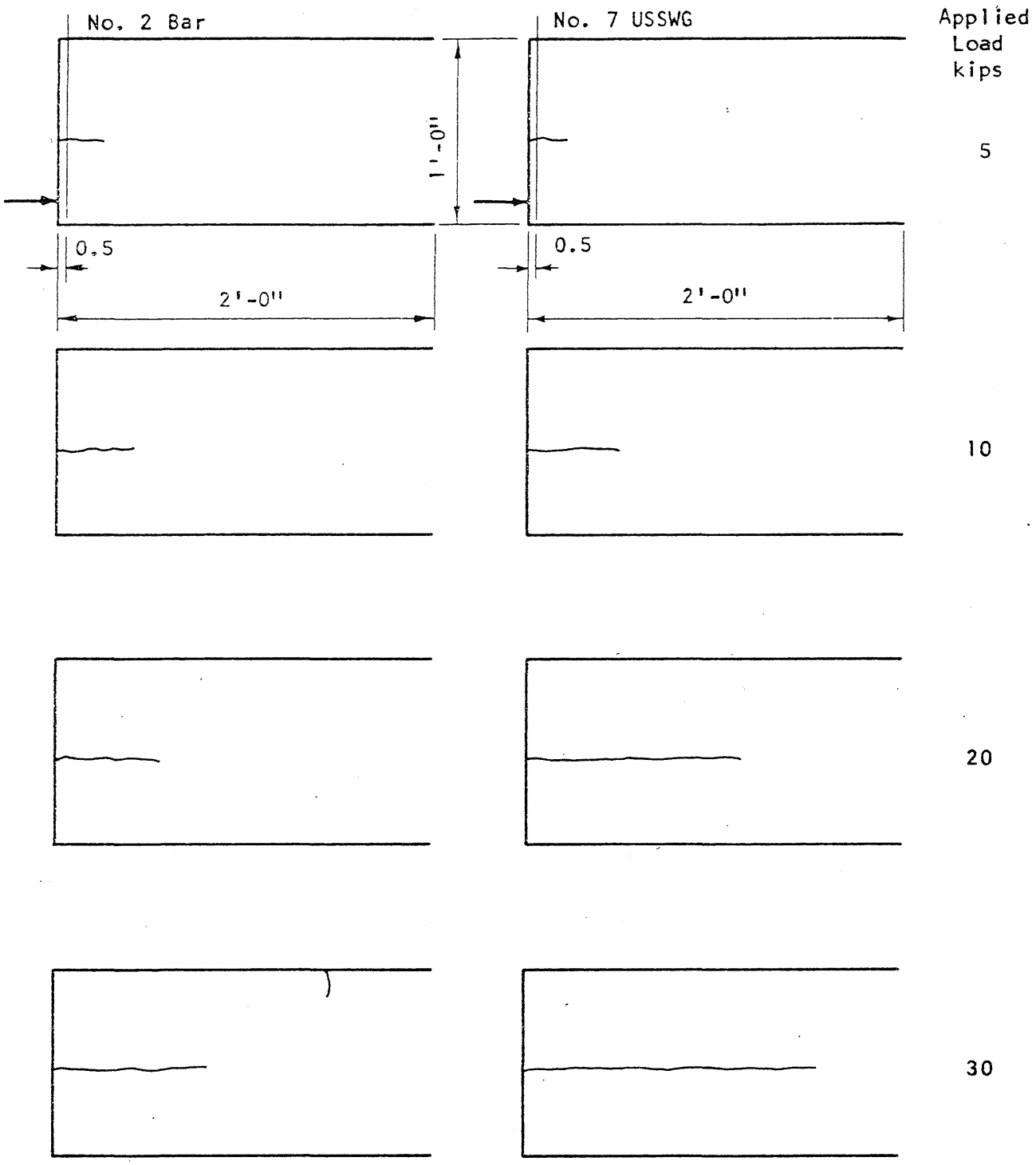

FIG. 5.6 DEVELOPMENT OF CRACKS IN SPECIMENS R11, R12, R14 and R17

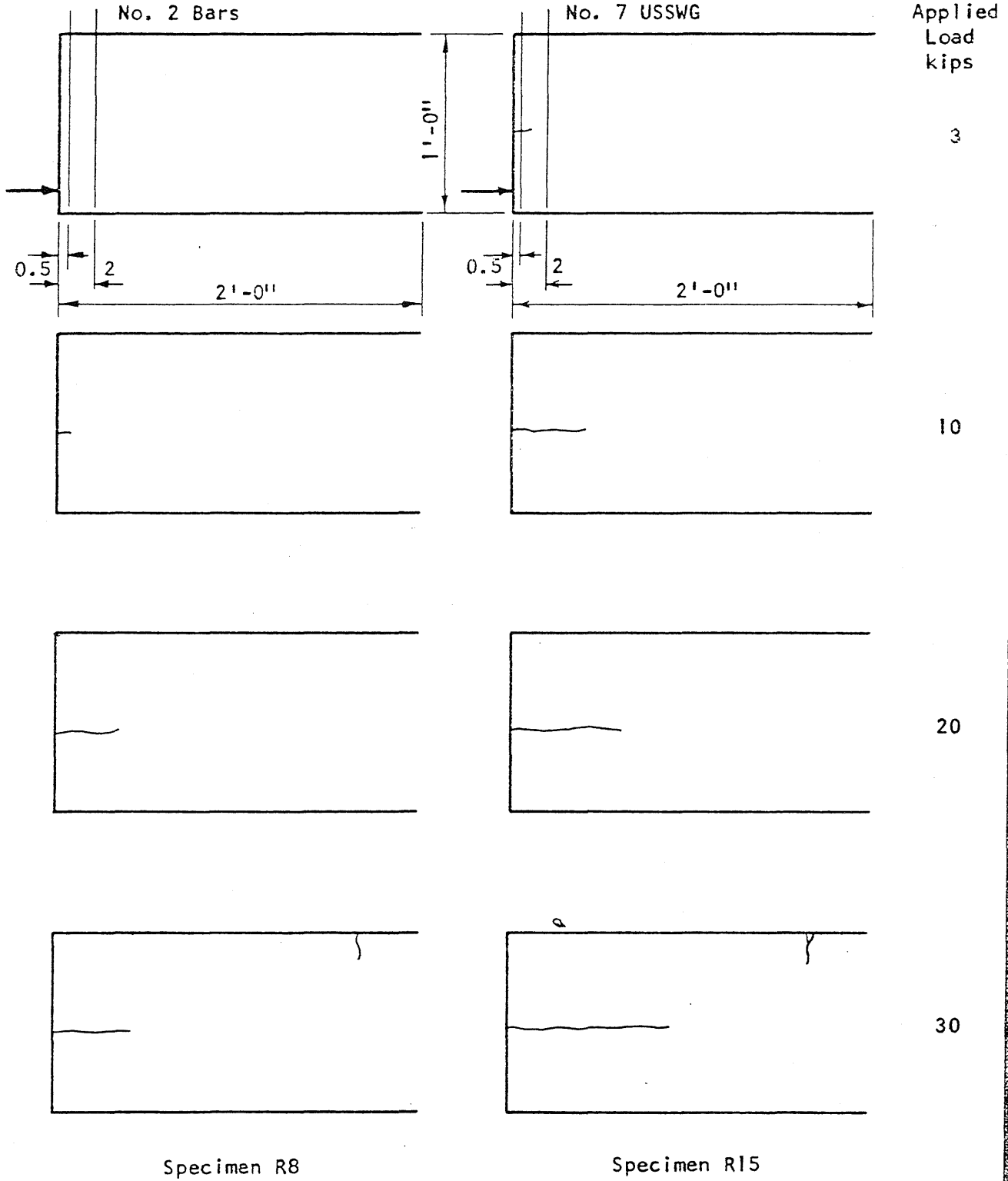

FIG. 5.7 DEVELOPMENT OF CRACKS IN SPECIMENS R8 and R15

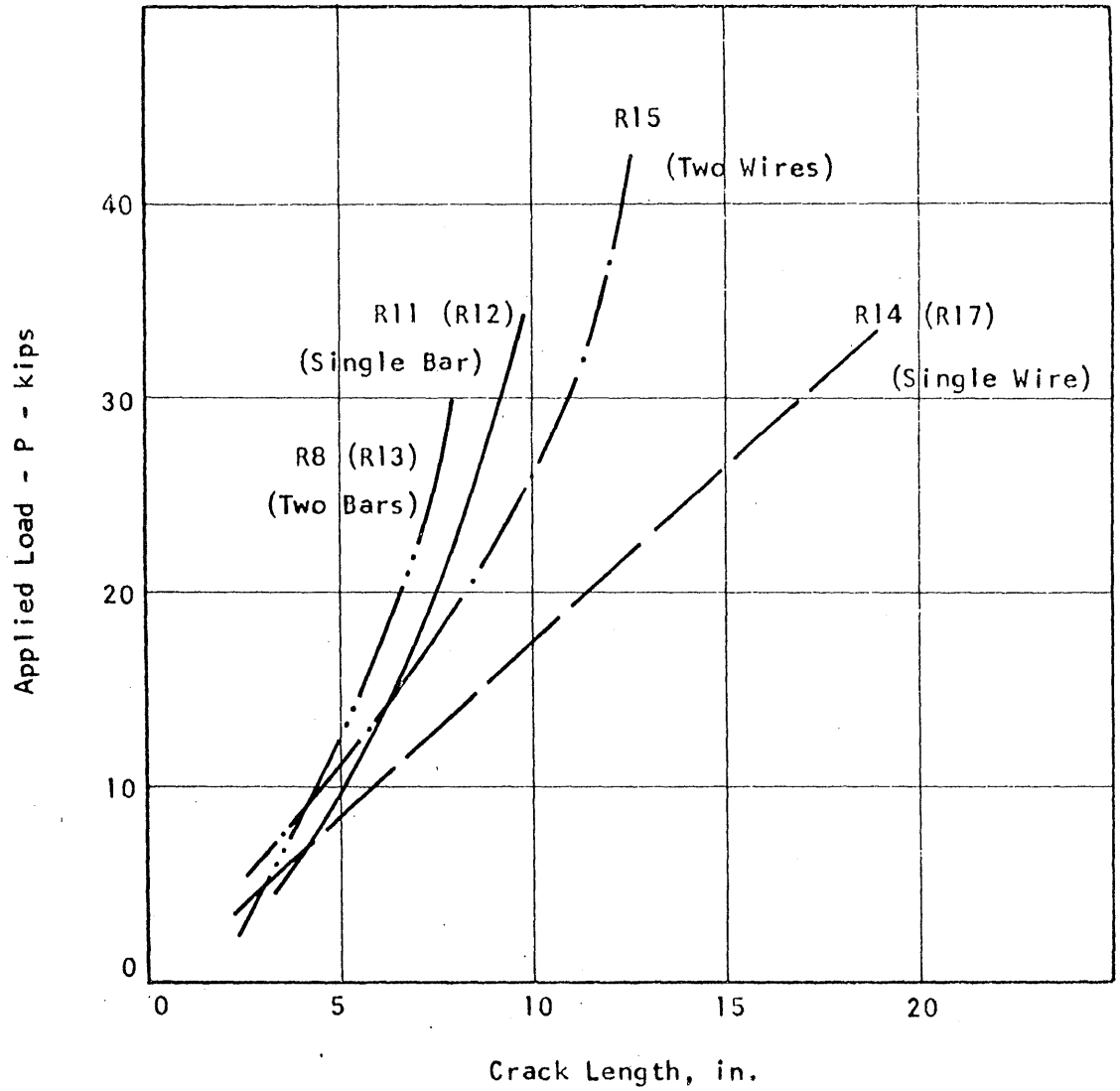

FIG. 5.8 MEASURED RELATIONSHIPS BETWEEN LOAD AND CRACK LENGTH FOR RECTANGULAR SPECIMENS

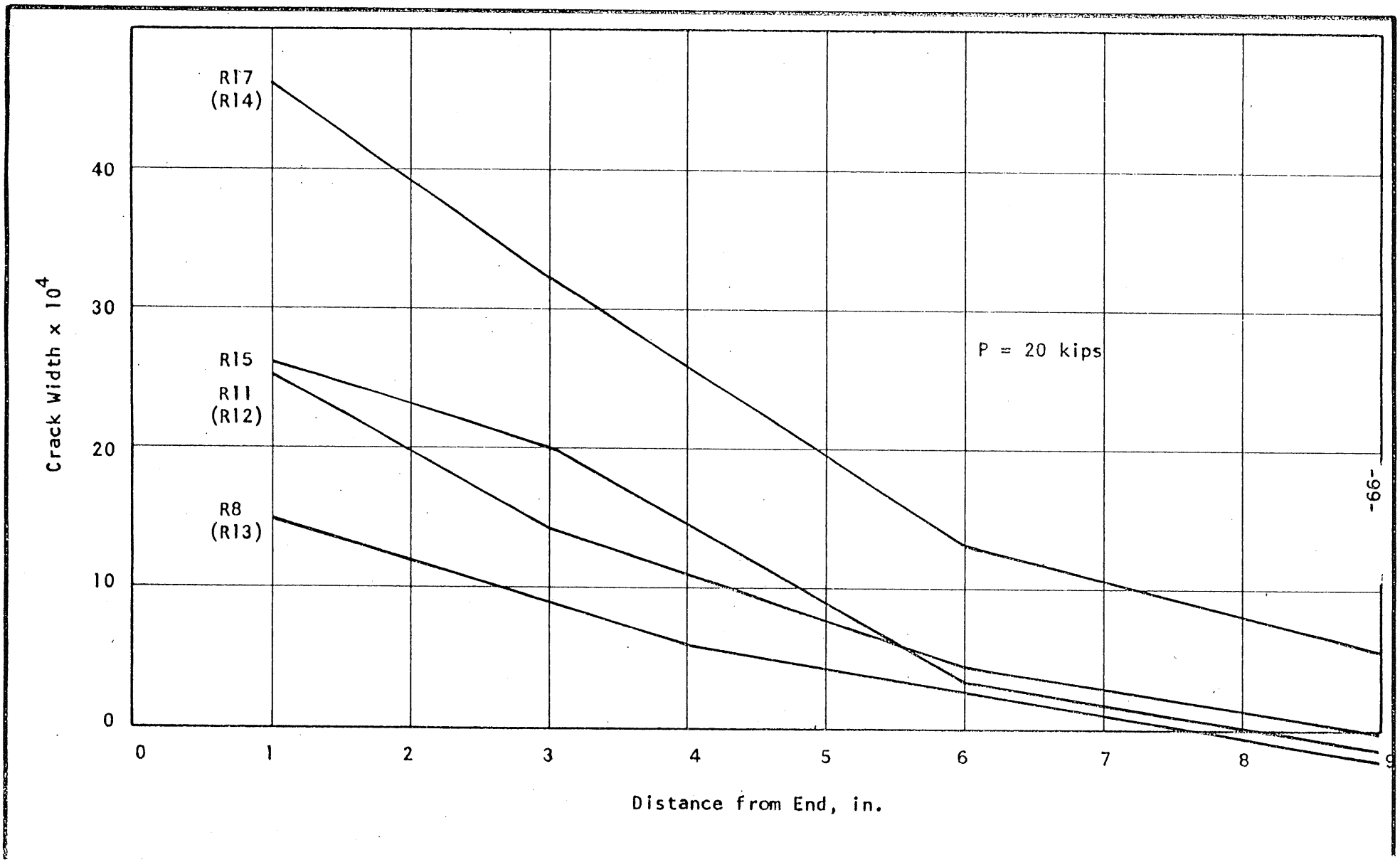
R17
(R14)
R15
R11
(R12)
R8
(R13)
P = 20 kips
Crack Width x 10^4
0
10
20
30
40
0
1
2
3
4
5
6
7
8
9
Distance from End, in.

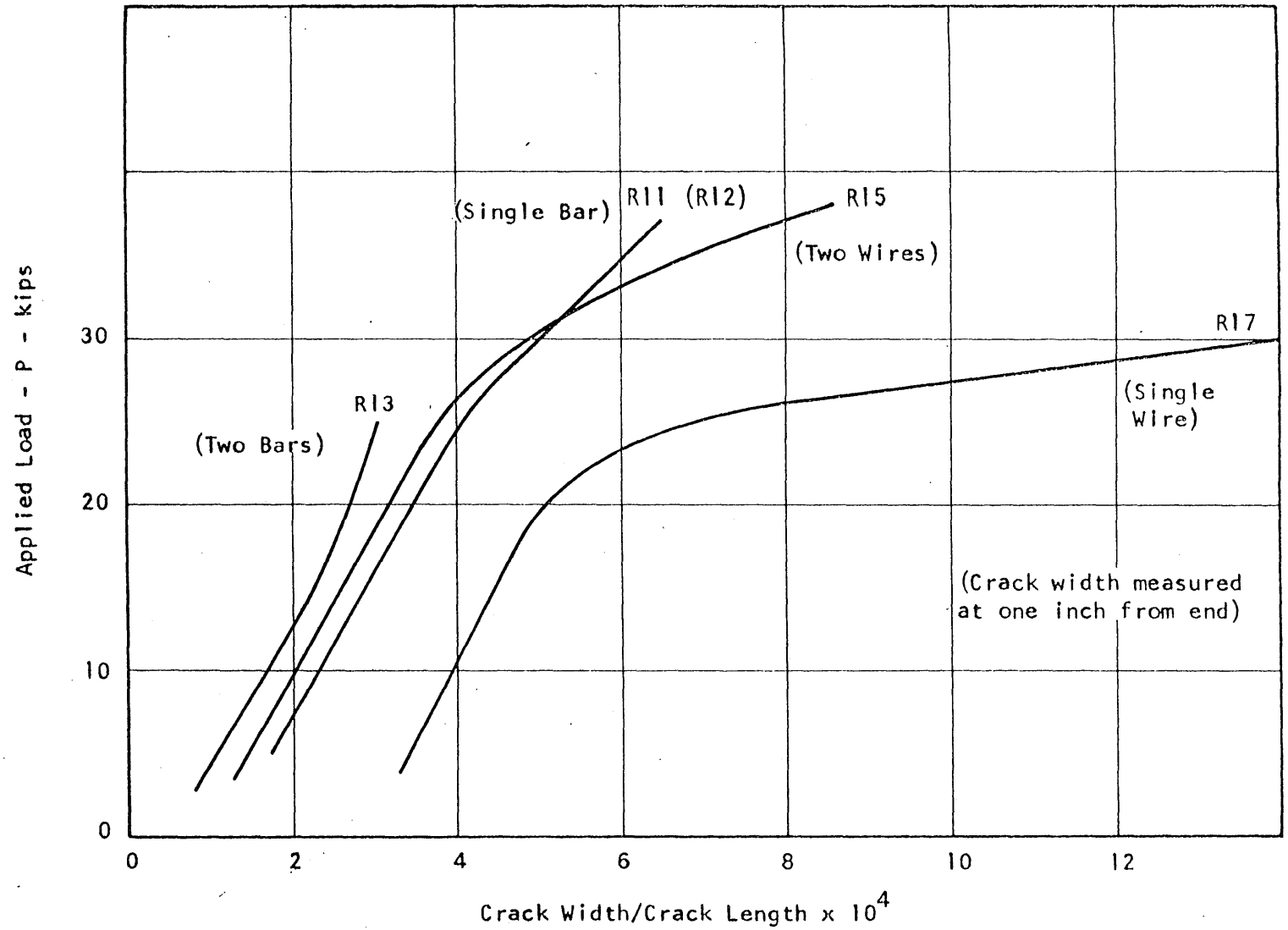

FIG. 5.10 VARIATION OF THE RATIO OF MEASURED CRACK WIDTH TO MEASURED CRACK LENGTH WITH THE APPLIED LOAD IN RECTANGULAR SPECIMENS

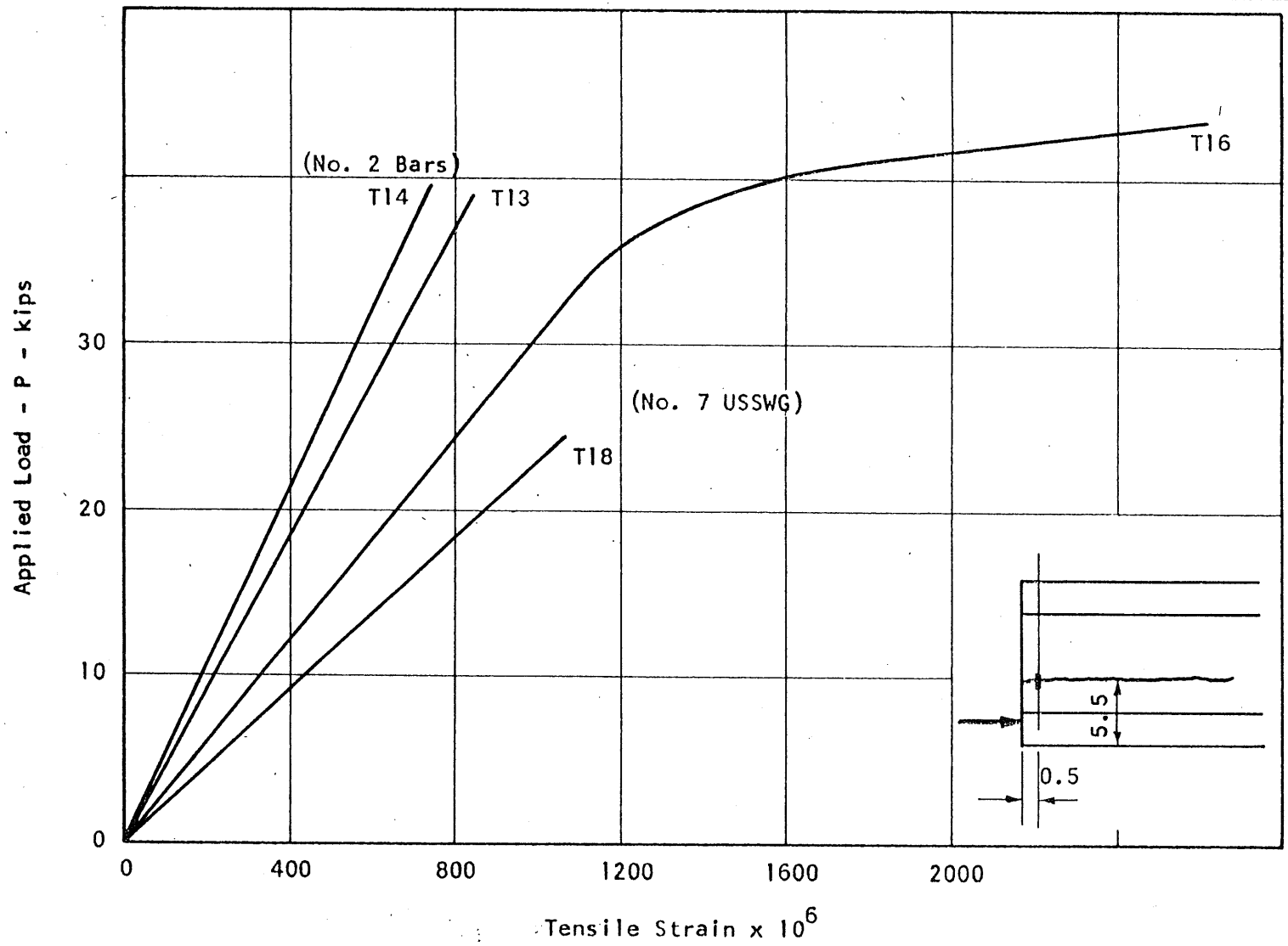

FIG. 5.11 MEASURED RELATIONSHIPS BETWEEN LOAD AND STIRRUP STRAIN FOR SPECIMENS T13, T14, T16 and T18

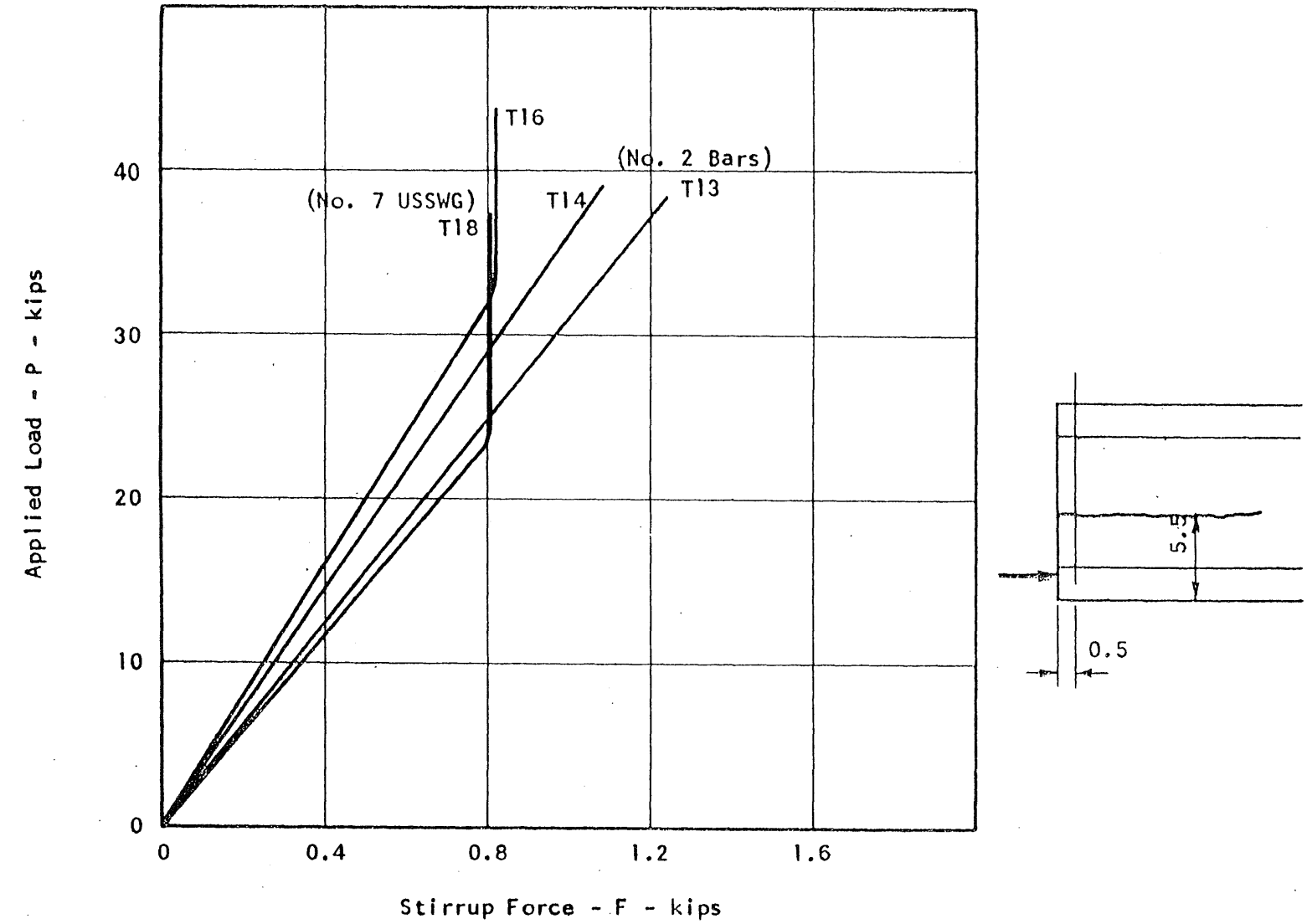

FIG. 5.12 MEASURED RELATIONSHIPS BETWEEN LOAD AND STIRRUP FORCE FOR SPECIMENS T13, T14, T16 AND T18

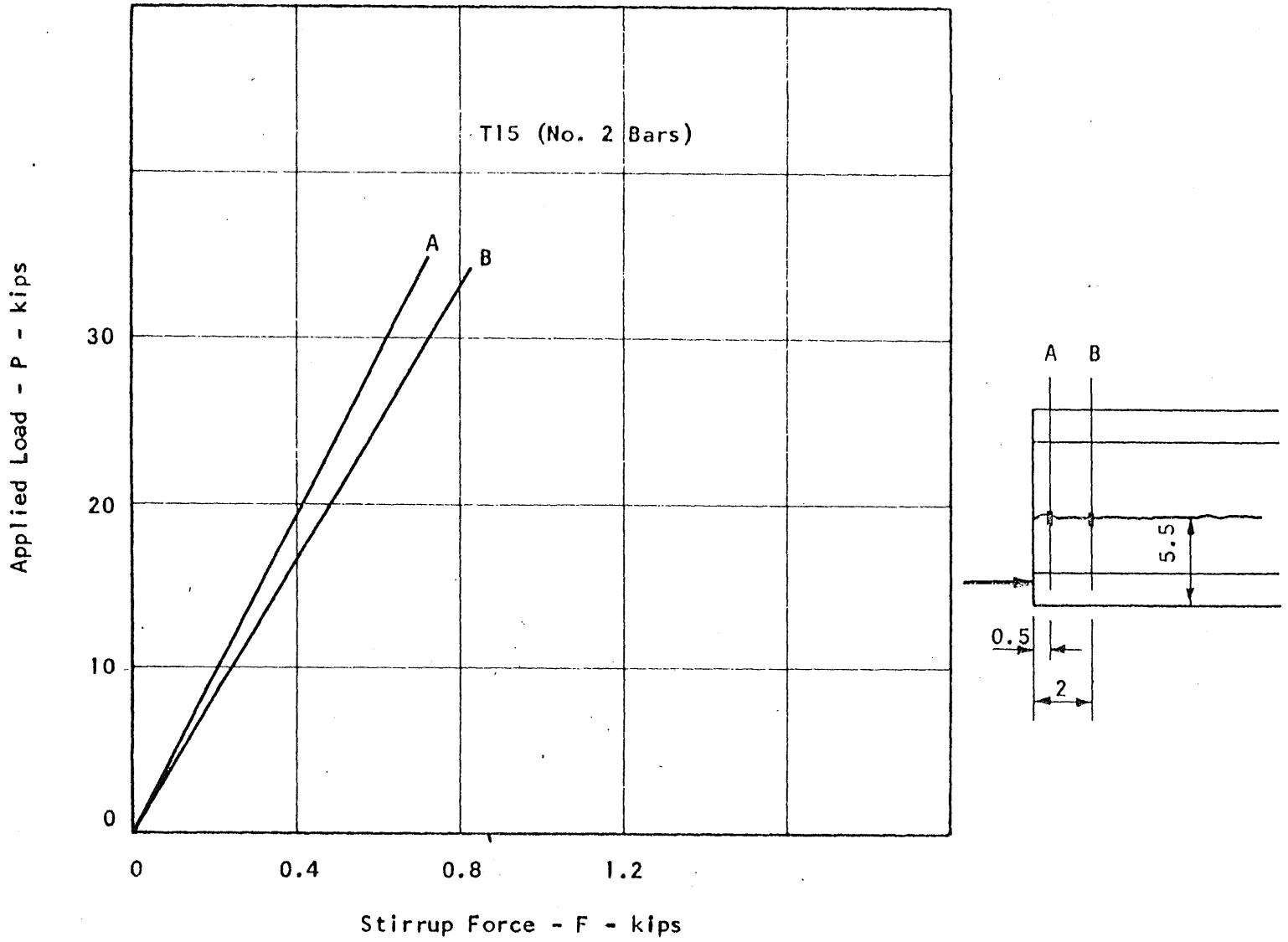

FIG. 5.13 MEASURED RELATIONSHIPS BETWEEN LOAD AND STIRRUP FORCE FOR SPECIMEN T15

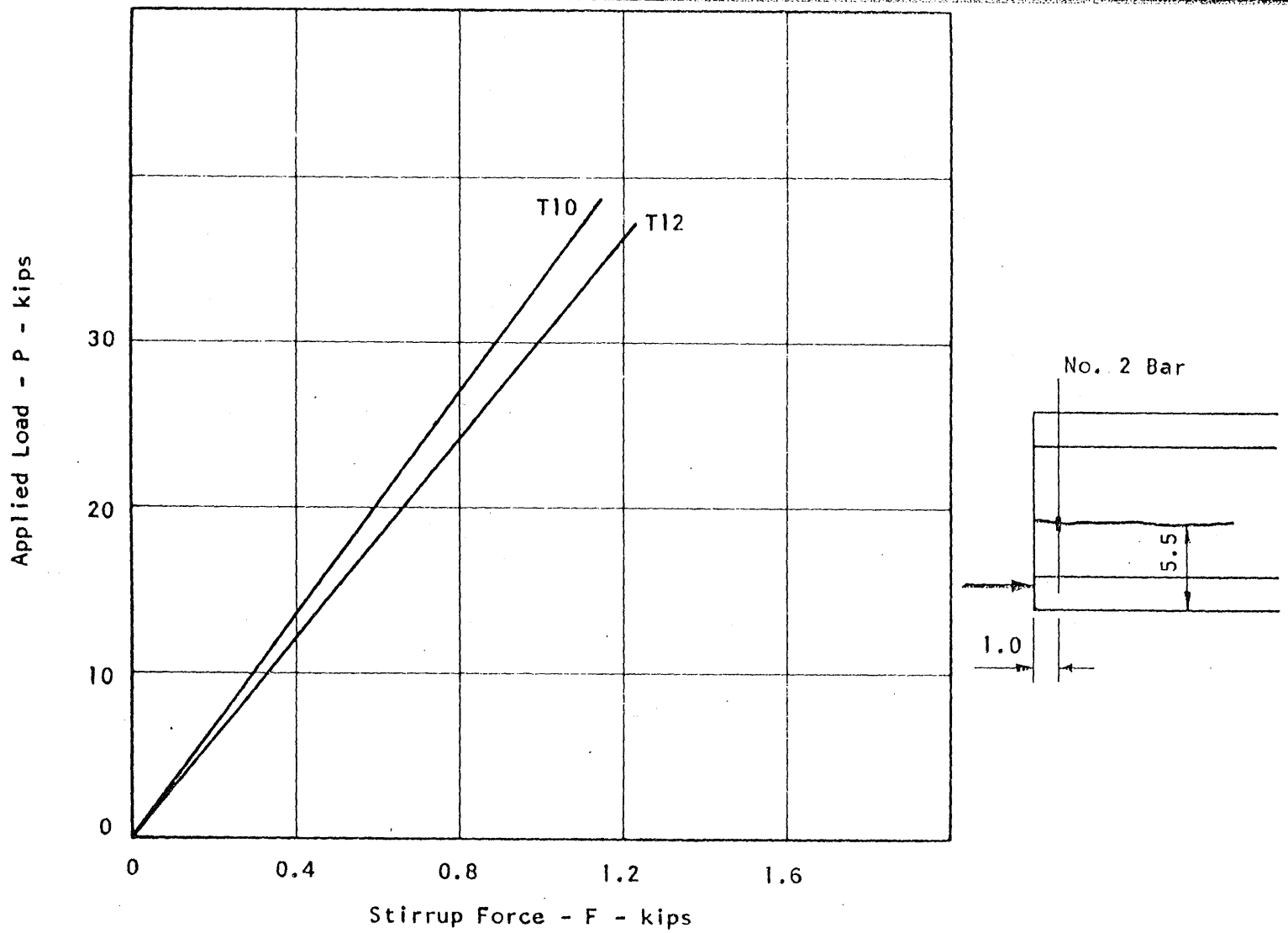

FIG. 5.14 MEASURED RELATIONSHIPS BETWEEN LOAD AND STIRRUP FORCE FOR SPECIMENS T10 and T12

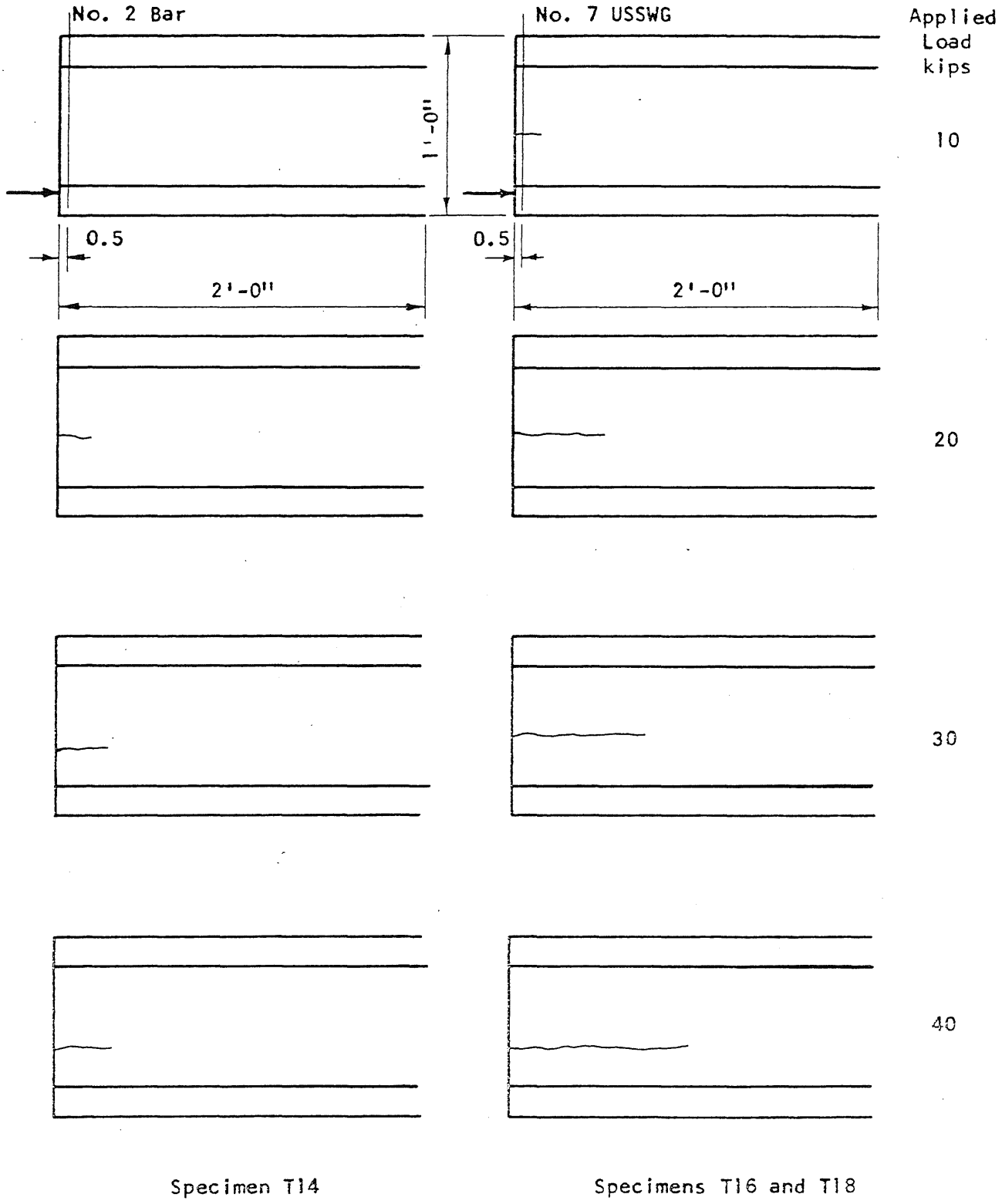

FIG. 5.15 DEVELOPMENT OF CRACKS IN SPECIMENS T14, T16 AND T18

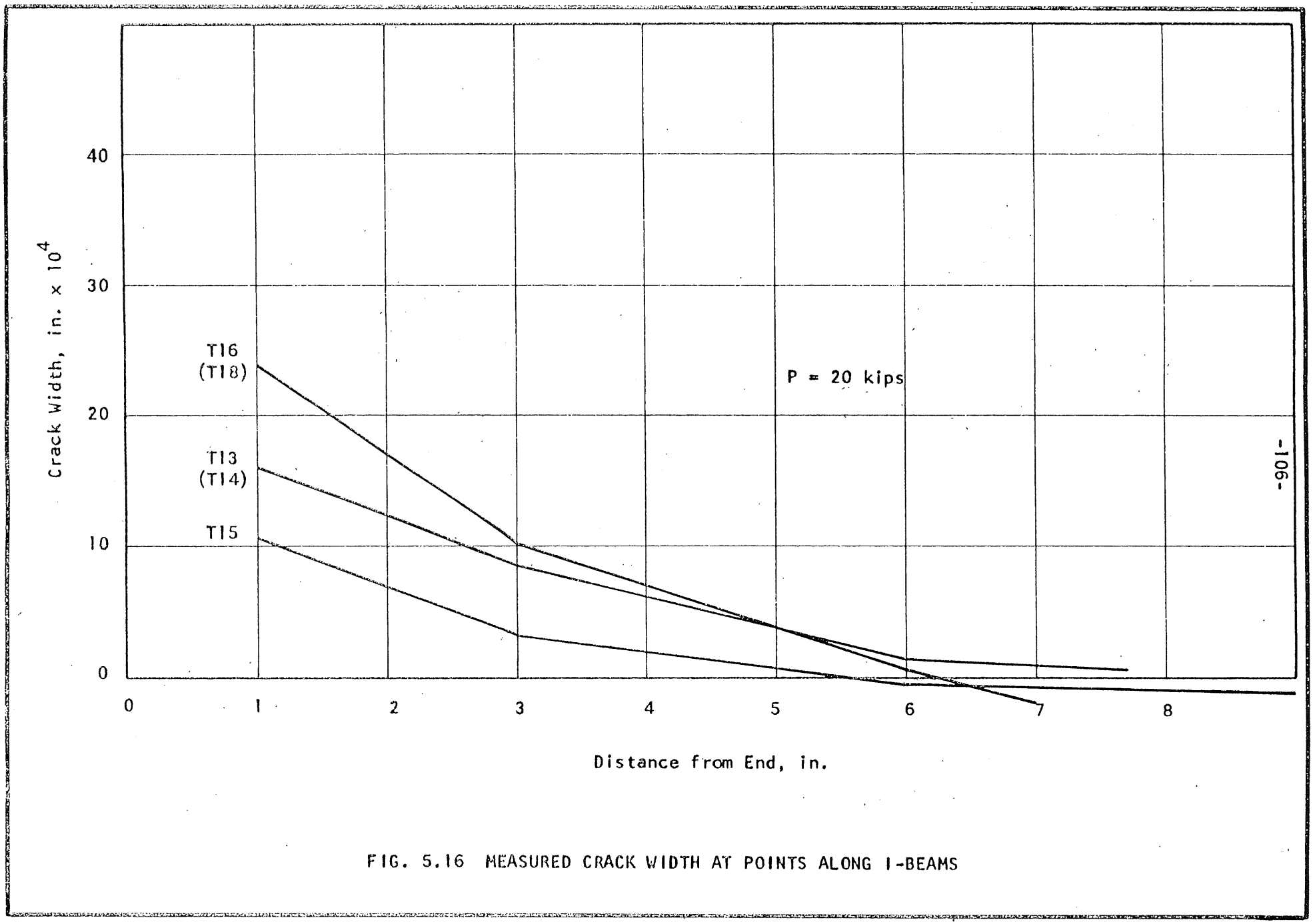

FIG. 5.16 MEASURED CRACK WIDTH AT POINTS ALONG I-BEAMS

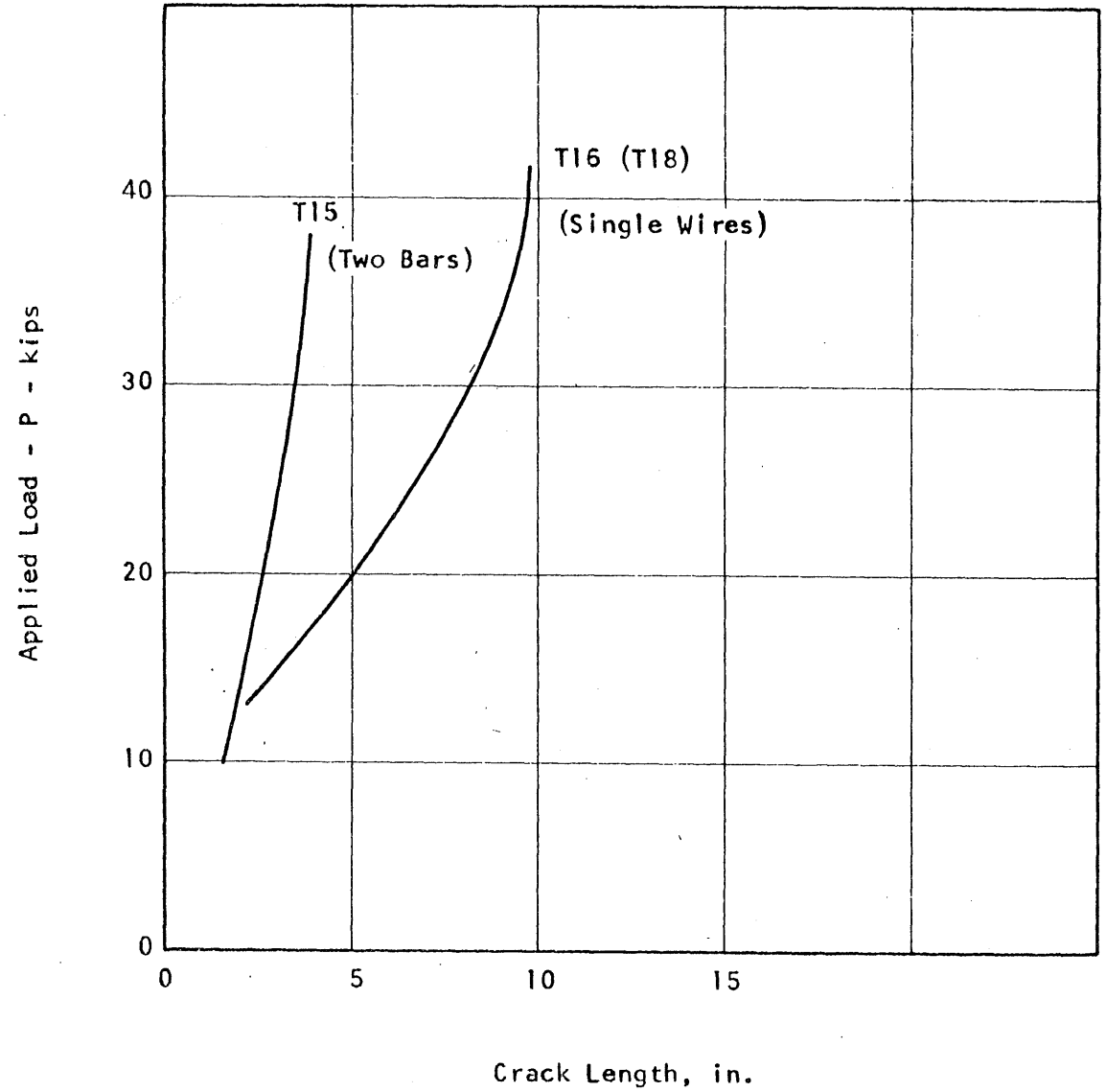

FIG. 5.17 MEASURED RELATIONSHIPS BETWEEN LOAD AND CRACK LENGTH FOR I-BEAMS

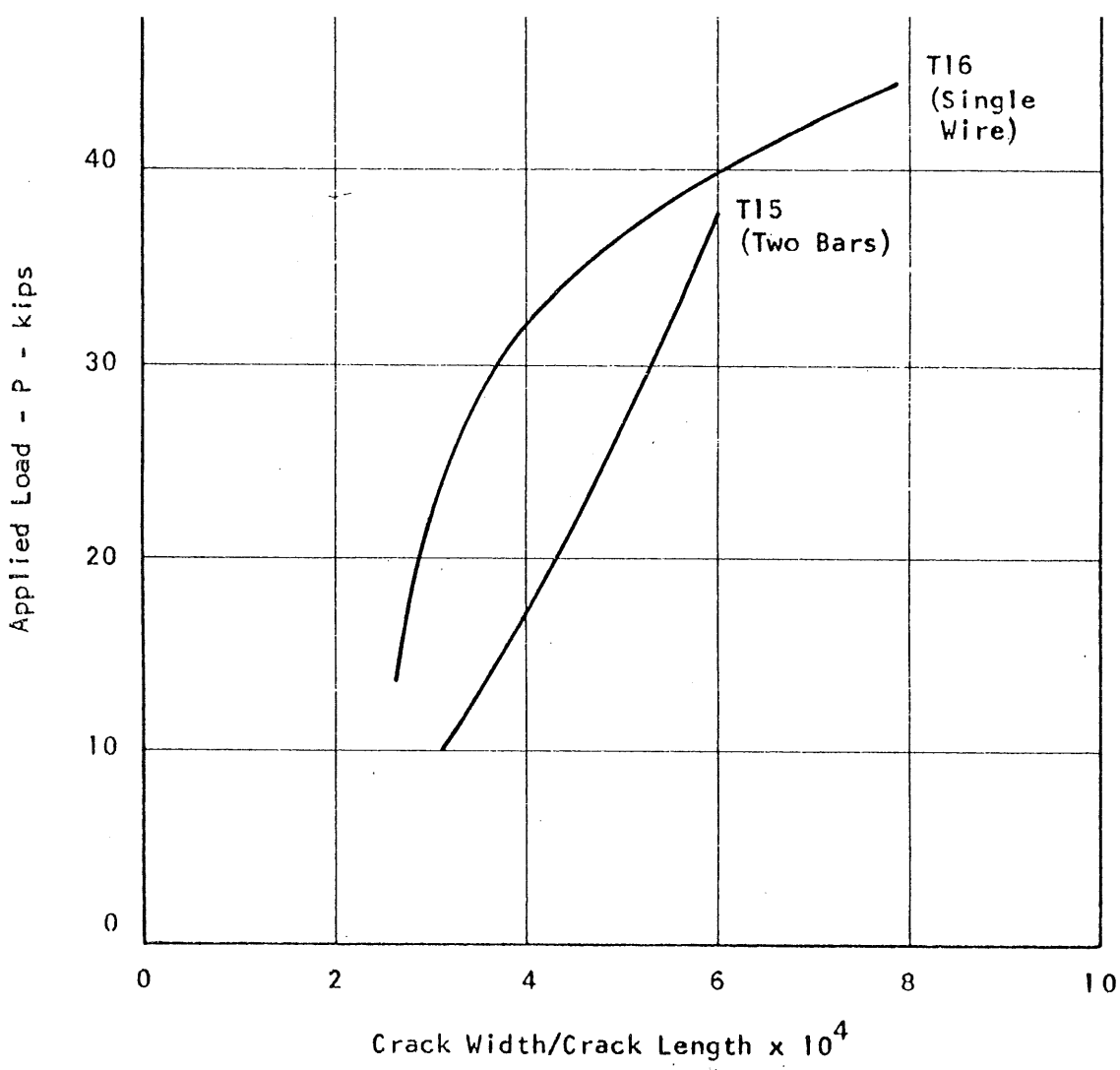

FIG. 5.18 VARIATION OF THE RATIO OF MEASURED CRACK WIDTH TO MEASURED CRACK LENGTH WITH THE APPLIED LOAD IN I-BEAMS

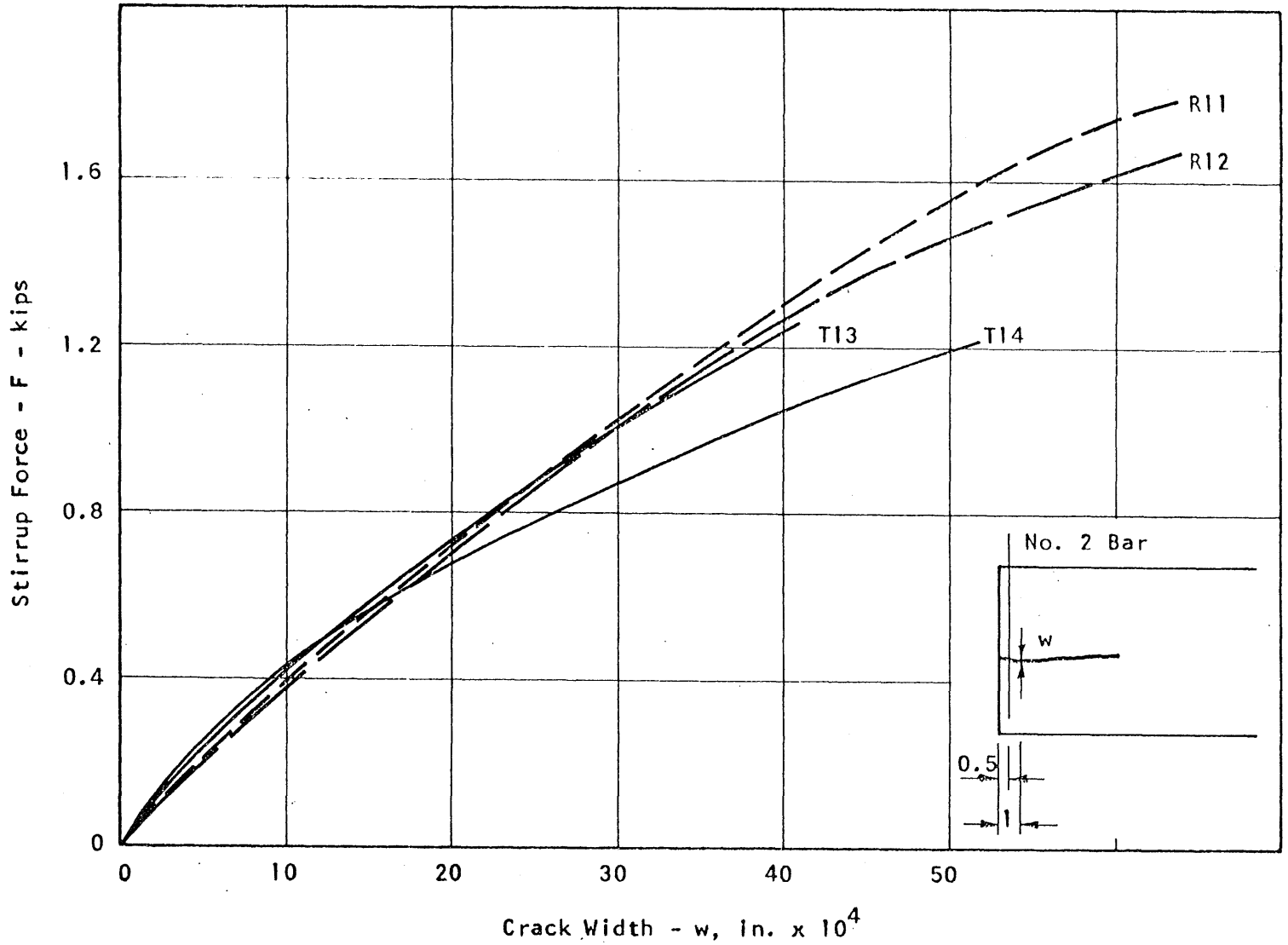

FIG. 5.19 MEASURED RELATIONSHIPS BETWEEN STIRRUP FORCE AND CRACK WIDTH FOR SPECIMENS REINFORCED WITH ONE No. 2 BAR

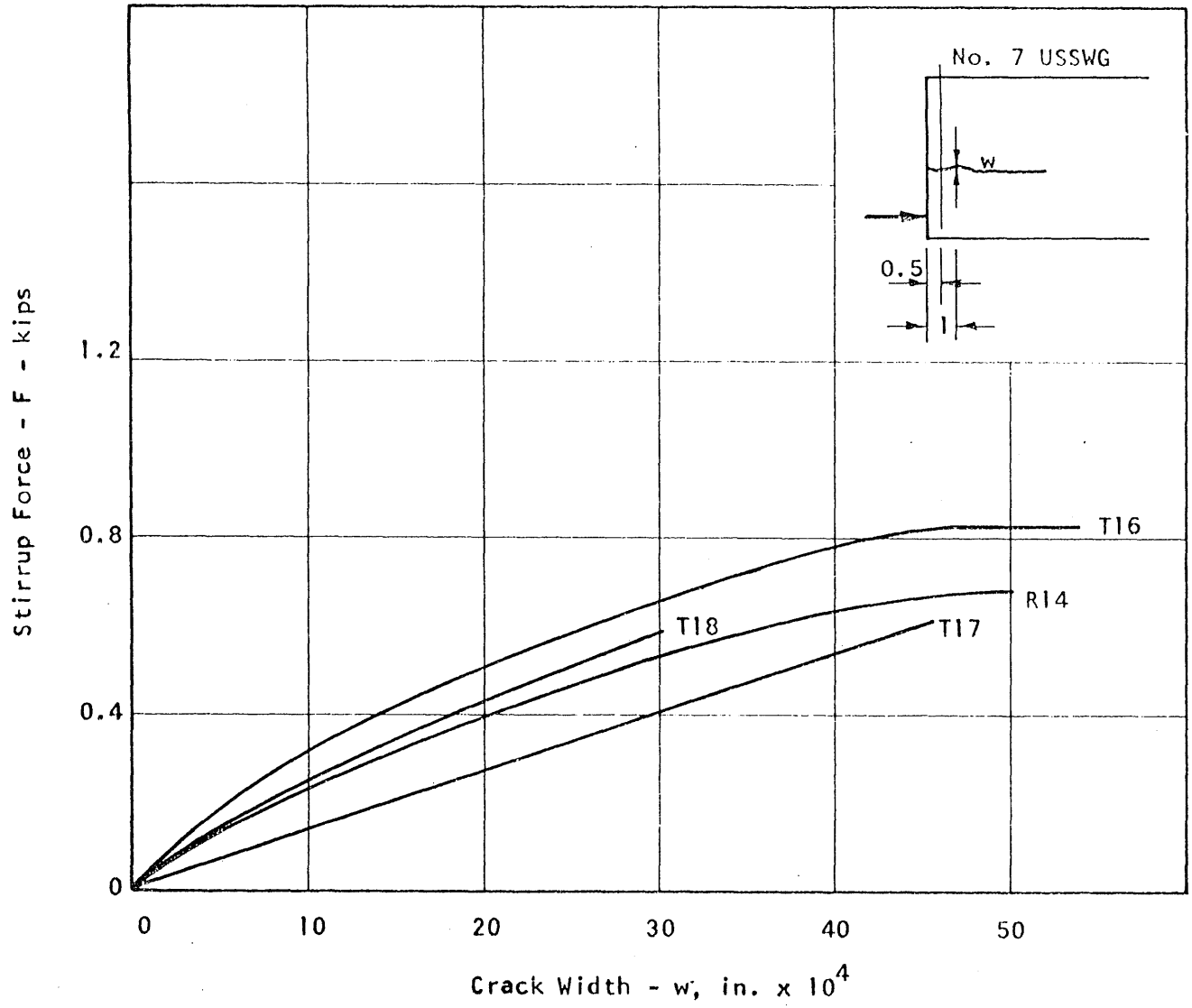

FIG. 5.20 MEASURED RELATIONSHIPS BETWEEN STIRRUP FORCE AND CRACK WIDTH FOR SPECIMENS REINFORCED WITH ONE NO. 7 USSWG

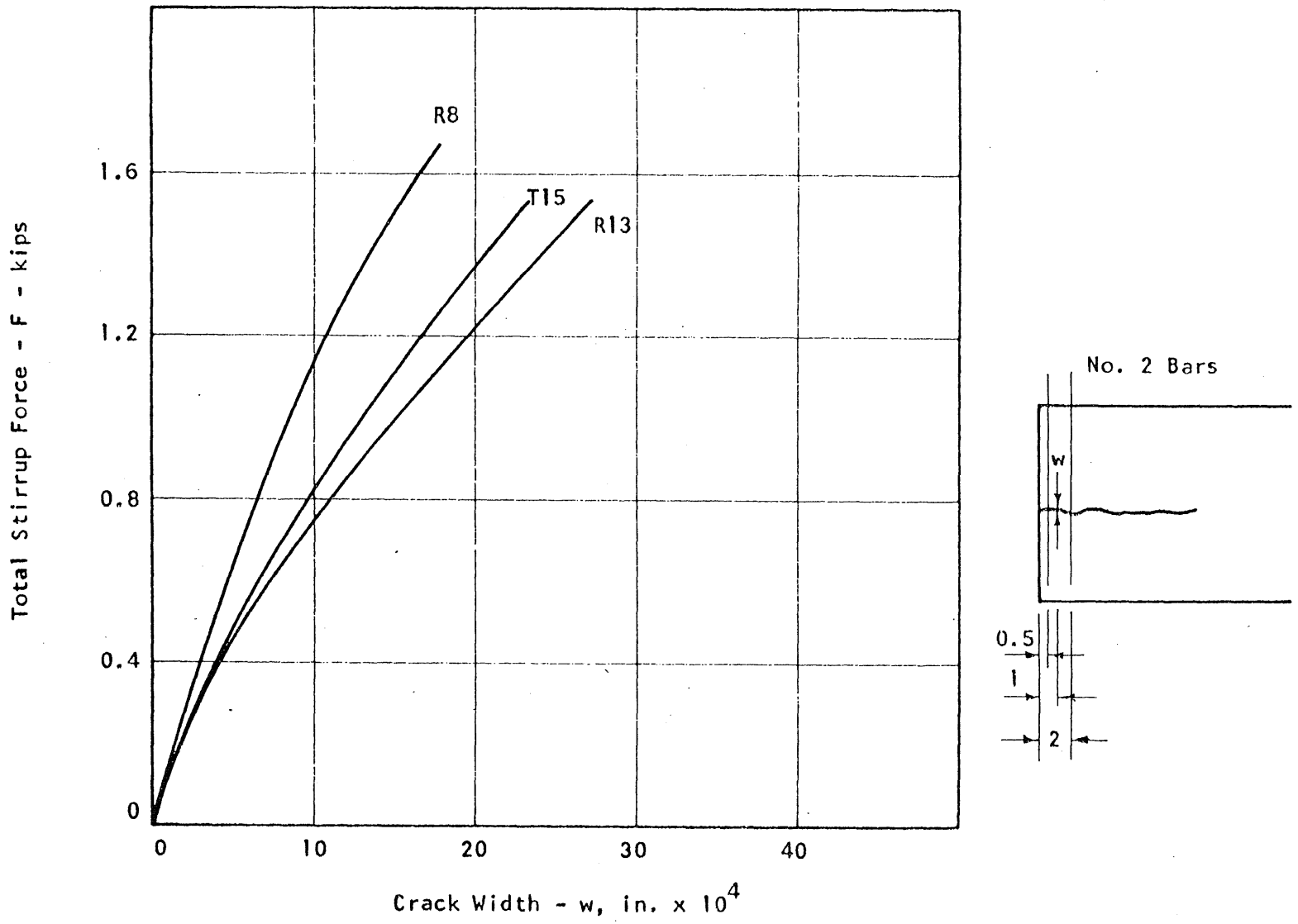

FIG. 5.21 MEASURED RELATIONSHIPS BETWEEN TOTAL STIRRUP FORCE AND CRACK WIDTH FOR SPECIMENS REINFORCED WITH TWO NO. 2 BARS

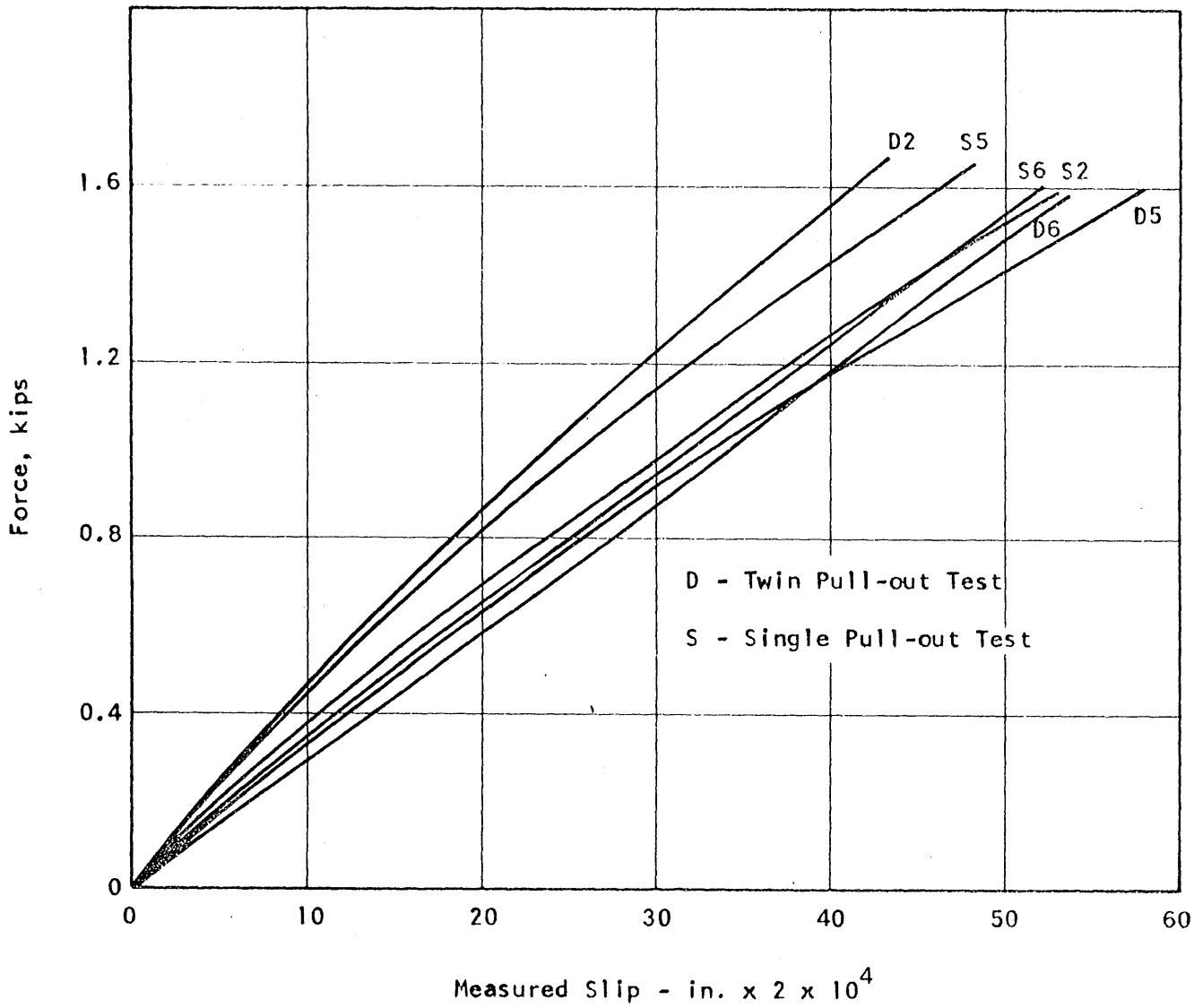

FIG. 5.22 MEASURED RELATIONSHIPS BETWEEN BAR FORCE AND SLIP IN BOND TESTS FOR NO. 2 BARS

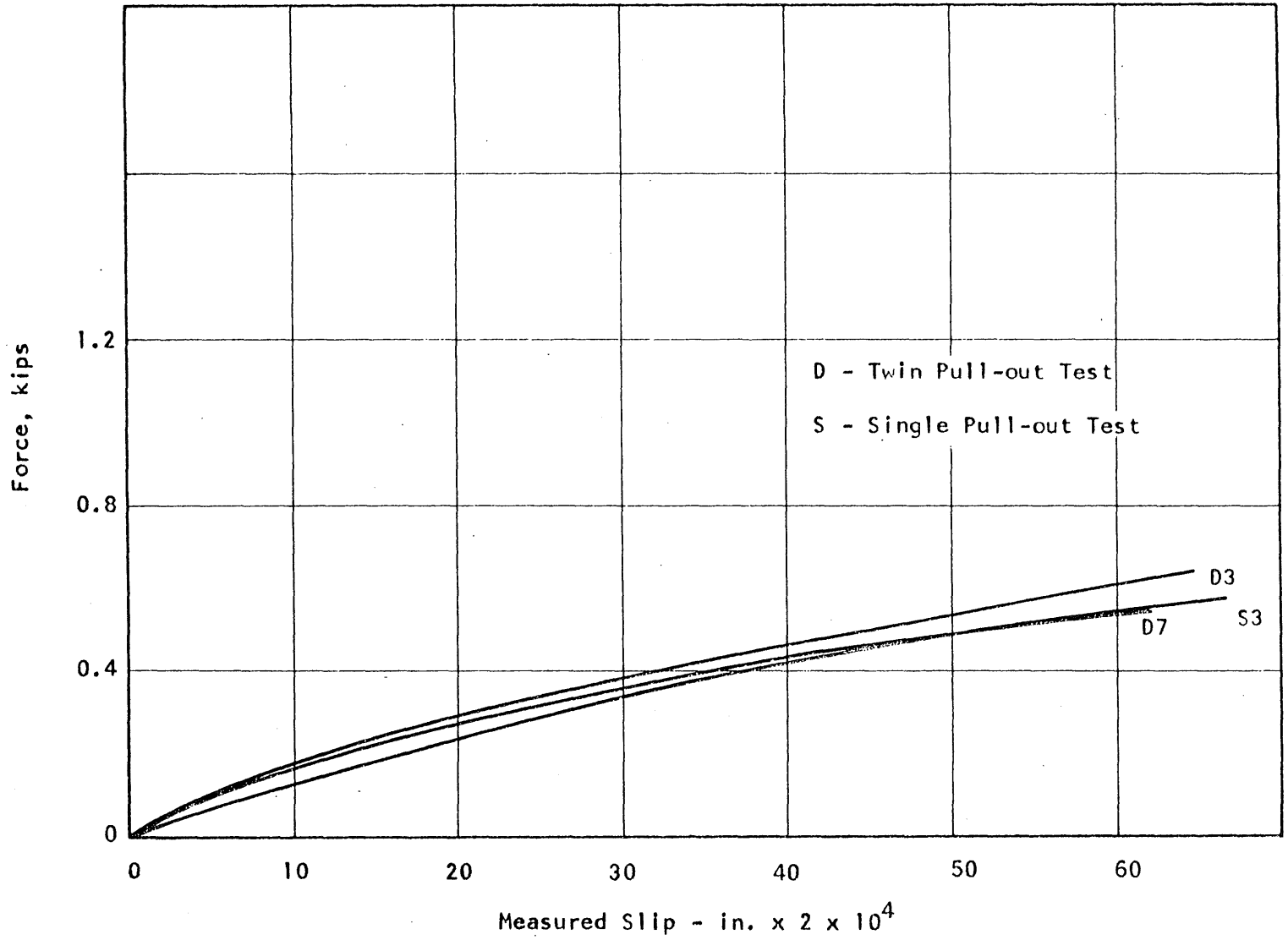

FIG. 5.23 MEASURED RELATIONSHIPS BETWEEN BAR FORCE AND SLIP IN BOND TESTS FOR No. 7 USSWG

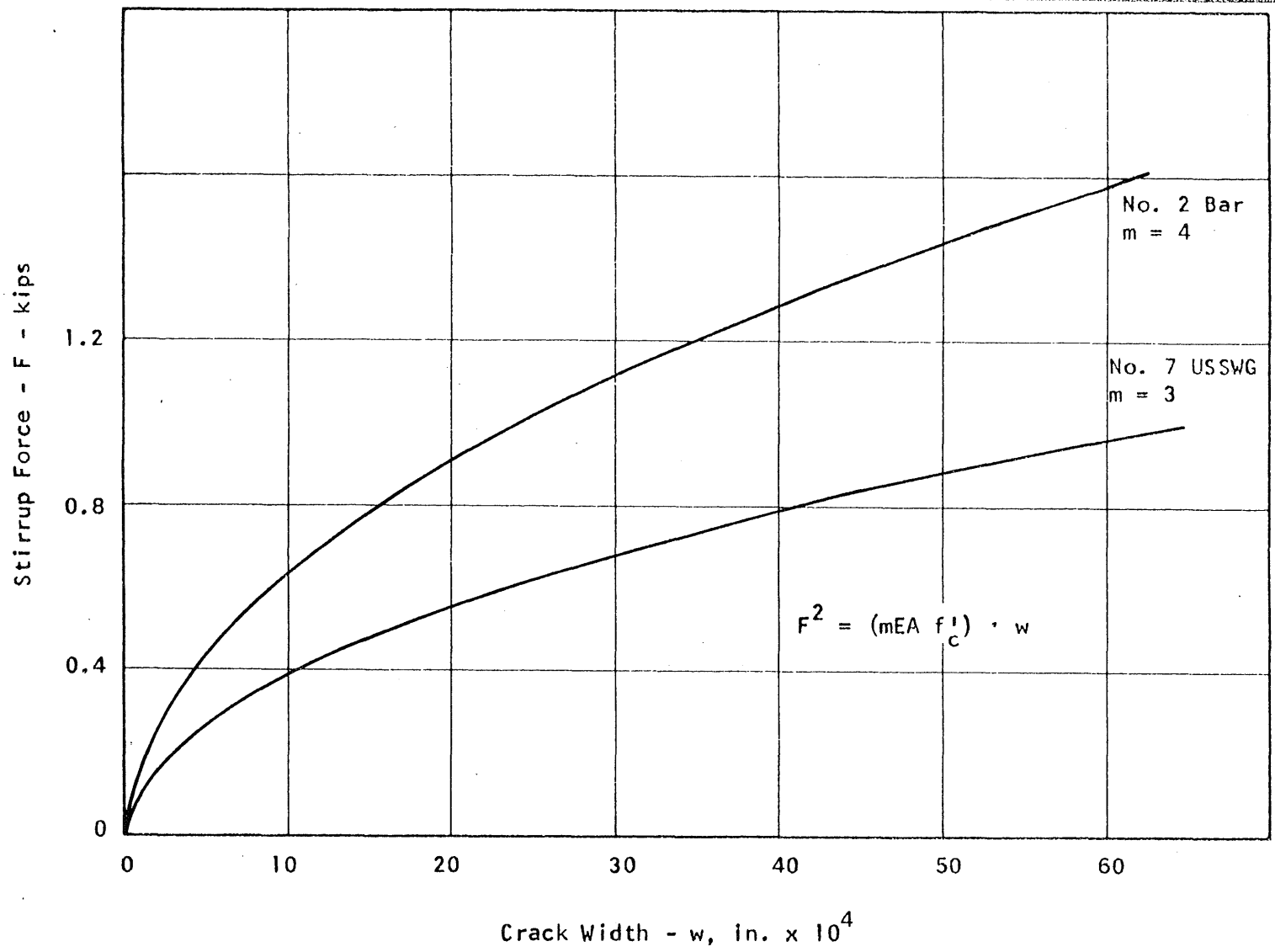

FIG. 5.24 RELATIONSHIPS BETWEEN STIRRUP FORCE AND CRACK WIDTH BASED ON UNIFORM UNIT BOND

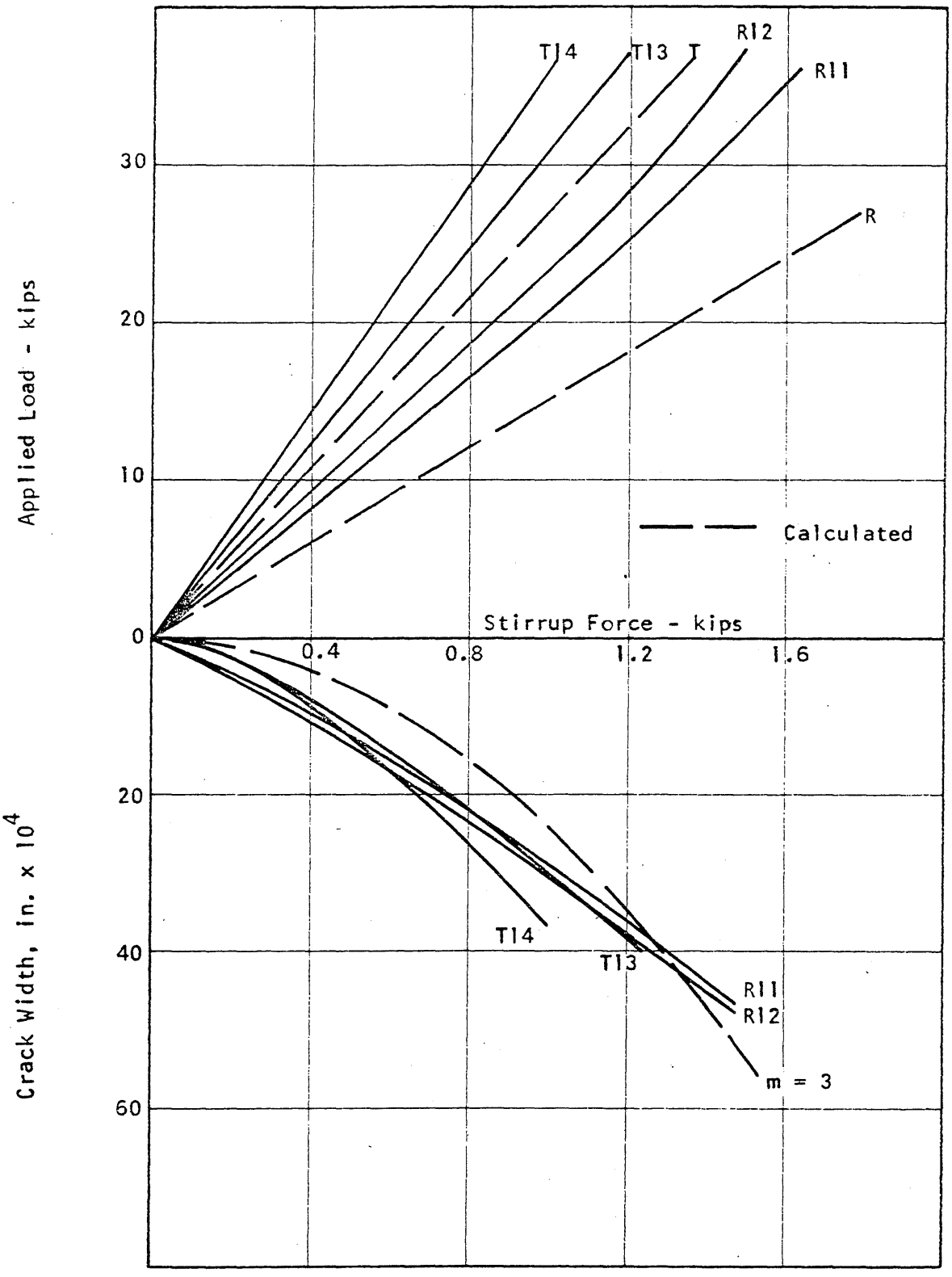

FIG. 5.25 COMPARISON OF THE MEASURED VS. CALCULATED VARIATION OF THE LOAD, STIRRUP FORCE AND CRACK WIDTH FOR SPECIMENS REINFORCED WITH BARS

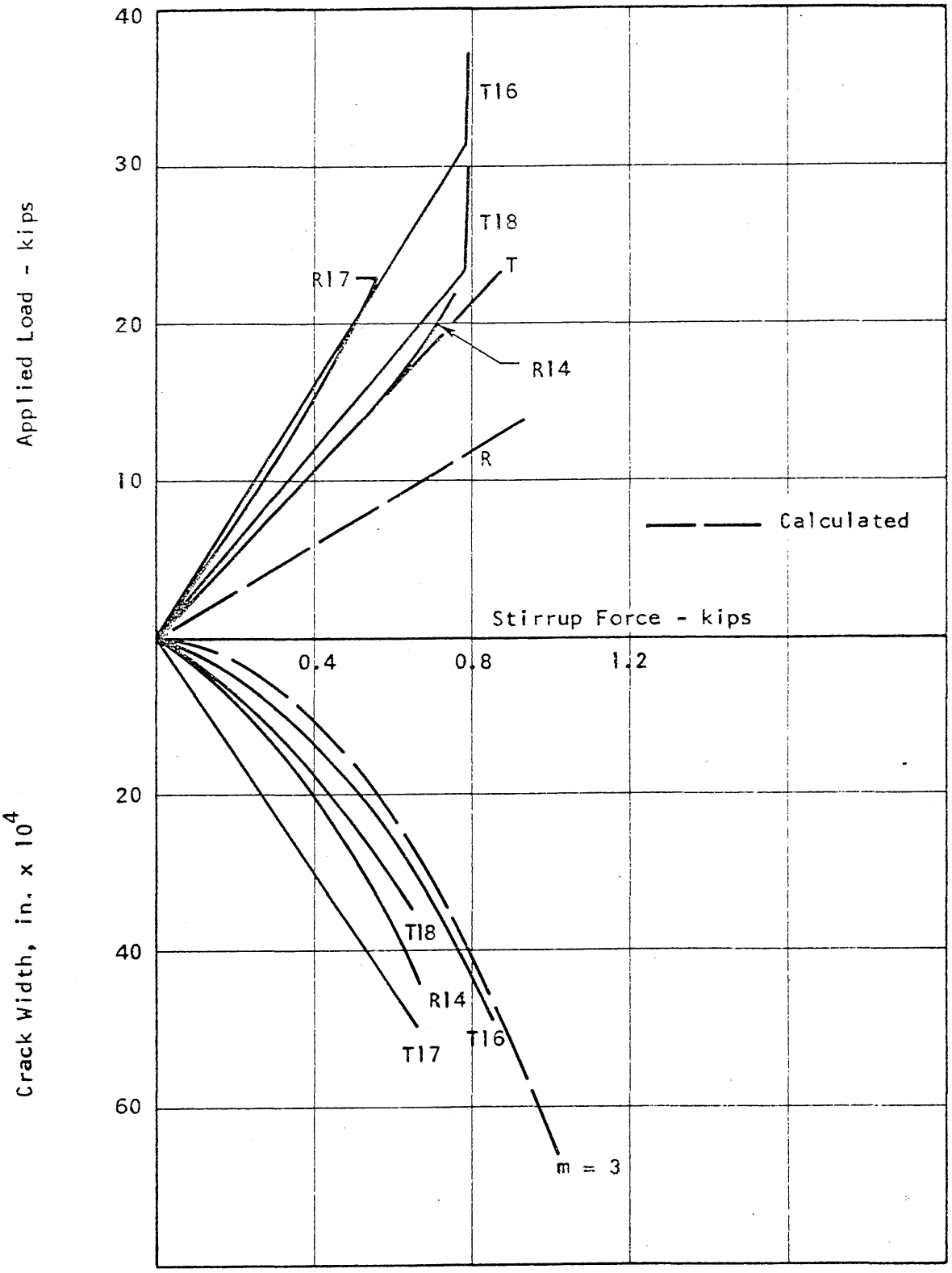

FIG. 5.26 COMPARISON OF THE MEASURED VS. CALCULATED VARIATION OF THE LOAD, STIRRUP FORCE AND CRACK WIDTH FOR SPECIMENS REINFORCED WITH WIRES

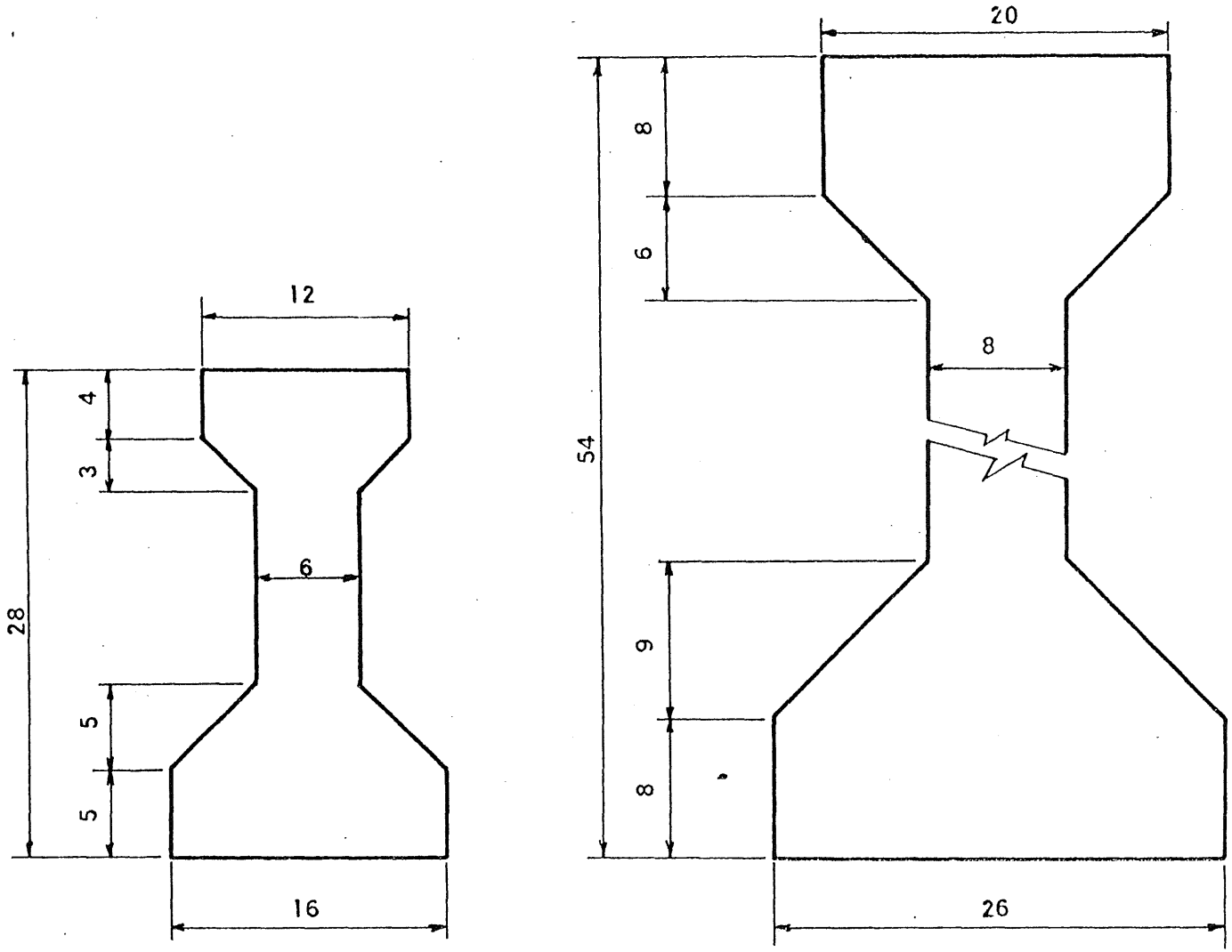

FIG. 6.1 CROSS SECTION OF BEAMS USED IN DESIGN EXAMPLES

APPENDIX A

REVIEW OF WORK RELATED TO ANCHORAGE ZONE STRESSES IN PRESTRESSED CONCRETE BEAMS

A.1 Methods of Investigation

One of the specific problems in the analysis of anchorage zone stresses is the stress distribution under concentrated loads. A wide variety of methods has been used to investigate this problem. All procedures utilized different assumptions and approximations that had to be confirmed.

The early relevant references treated the "concentrated load problem" as a question in elasticity: the solutions were not intended for use in prestressed concrete and were limited to two dimensions. In recent years, the larger part of the work has been experimental.

The mathematical solutions served as a good start in the early days of prestressed concrete. They were based on the mathematical theory of elasticity. Later some other methods were employed, a few of them directly for analyzing prestressed concrete end blocks. The analytical methods can be classified into three main groups:

(a) Most of the work done to date has utilized the two-dimensional Airy stress function. The results were derived either in terms of infinite series (6, 4, 2, 7) or were carried out using finite differences (8, 3 9).

(b) The second approach used a simple equilibrium analysis, here called the "beam method". This is a relatively recent approximate treatment (10, 11, 12, 13).

(c) Lattice analogies were used by the third group of investigators (14, 15). This method is considered to represent a check on other results in specific cases rather than a general approach. Lengthy numerical calculations are needed in every case.

Of the fifteen theoretical investigations considered, ten were strictly two-dimensional while the other five contained some kind of an extension to three-dimensional cases. Half of the references consulted were concerned only with axially symmetric problems.

The more detailed and popular analytical investigations belong to the first group. Some of the authors used high-speed computers to eliminate the use of assumptions made by previous investigators who did not have access to computers.

Ten references (out of 25) contained some experiments. Five of them were published since 1960 and all the important ones since 1955. This fact reflects the great interest in experimental analysis in recent years.

There have been two main types of tests: photoelastic experiments on models and tests on concrete specimens. Photoelastic investigations give the elastic stress distribution and, hence, are in certain respects, similar to the analytical methods using the theory of elasticity (8, 16, 17, 18, 19). The experiments with concrete models offer more useful results because they reveal the behavior and failure patterns (20, 21, 8, 22, 6, 19, 23). Unfortunately, most of the research was done on axially symmetric specimens only (21, 22, 16, 6, 17, 18).

Some of the experiments were done on concrete blocks, others on beams. The instrumentation and the way of observation of the failure is of importance. The instrumentation consisted of electric strain gages, mechanical gages and gages on steel reinforcements. The visual observation of the development of cracks (usually through hand magnifying glass) offered first rate indications of the failure mechanism. This has been realized in some recent investigations. However, the accuracy of these measurements (width and length of cracks) must be examined and the data handled with care.

The comparison of experimental and analytical investigations reflects an approach that is similar to the ones in other areas in concrete research. First theoretical solutions are attempted. Then tests are conducted to verify the assumptions and the theories. Usually these are then modified and a new theory is developed which is applied to cases with added variables. In some cases the experiments serve as controls, in others as guides. This relation of experimental and analytical methods is typical in reinforced concrete research. Neither can stand alone.

In the investigation of end blocks of prestressed concrete, analytical solutions were derived to determine the stress distribution. In some cases these results were taken over from calculations made for some other reasons. The results differed in certain areas and this controversy stimulated quest for further solutions. Some of the experimental investigations tried to settle the dispute and attempted to establish the "correct" stress distribution. In the meantime other analytical approaches were tried that endeavored to calculate the internal forces rather than the stress distribution. After a while (in about 1958) it became apparent to some researchers that the more pragmatical treatment was preferable. End blocks of different scales were tested with or without transverse reinforcement. With the findings of the present investigation, it has now been established that instead of treating the problem as a stress concentration problem in a homogeneous elastic body, it should be handled as an equilibrium problem of free bodies produced by the formation of cracks. The width and length of cracks became to be of concern. Therefore, the analytical and experimental methods are equally important. The question is not of distribution, extremes and averages of stresses under concentrated loads, but rather it is about the formation and extent of cracks. This also involves the study of bond

under special conditions. In addition, the bearing strength under complex stress conditions must also be investigated.

A.2 Major Variables

In the early mathematical investigations the only variable was the eccentricity of a line load on a semi-infinite body (7). Later, loads acting on a finite area were introduced. The major variable was the ratio of the loaded area to the width of the block (21, 6, 4, 2). An extension to three dimensions was presented by Sievers (10, 11) and by Douglas and Trahair (6), though the usefulness of their results is limited. In most cases the cross section was rectangular with the height to width ratio as a variable.

The stress distribution under a tangential load can be superposed on that due to normal loads to get the distribution under inclined loads (2).

In the experimental investigations, the major variables were the cross section and the eccentricity of the load. Some authors tested concrete blocks of various proportions to simulate the conditions in end blocks (21, 22, 6). In other instances different anchorages were employed (21, 6, 23). The amount and position of the transverse reinforcement was varied in some recent test programs (20, 21, 8, 22, 23).

The concrete strength and the value of Poisson's ratio were not considered to be major variables in any of the investigations. Only a few full-length beams were tested (20, 19, 9), the rest of the tests were done on shorter models.

A.3 Areas of Apparent Agreement in Analytical Studies

As it was mentioned in Section A.1, the early investigations were analytical. There was not much agreement among the results. It was one of the principal findings of later (mainly experimental) research that some

of the analytical work was concerned with problems that were too idealized. The shortcomings of analytical investigations will be discussed in Section A.5.

It has been found by most investigators that St. Venant's principle holds. The desired linear stress distribution is reached at a distance equal to, or in some cases (15, 24) somewhat less than, the depth of the section. At the same distance the transverse stresses become zero. In some cases, however, this fact was assumed a priori (8, 14, 10, 11, 12, 13).

Nearly all investigators treated the two-dimensional case only. No detailed three-dimensional analysis would be practical, hence this approximation is generally accepted. The photoelastic tests of Mahajan (24) showed that the stresses in the third principal plane were small and occurred only near the anchorages.

The most significant contribution of the analytical solutions was the confirmation of Guyon's principle of partitioning (2). This approximate procedure was described in Section 2.4. Zielinski and Rowe (21, 23) agree with this method and recommend its use. It is a very easy procedure and a set of curves gives the transverse stresses for various a/h values. Iyengar (4) also agrees with Guyon. The limitation of the symmetrical prism method is presented in Section A.5.

(a) Magnitude and Position of the Maximum Transverse Stress

There is some variation in the magnitude and position of the maximum transverse stresses reported by various authors. An important conclusion is that these stresses increase as the eccentricity of the load increases (7, 2). They decrease as the size of the loading plate increases (see later in this section). Guyon gives 0.5p for the maximum transverse

stress due to an axial load. It occurs at about 0.17 h (2). This agrees with Ross (15). The corresponding values reported by Ramaswamy and Goel are 0.60p and about 0.50h (14). The latter value is too high. Siever's maximum stress and zero stress are always at 0.4h and 0.2h, respectively. Goodier gave 0.58p as the maximum stress under concentrated load on a block with length to width ratio of two (25). For a square plate this value is 0.42p. A comparison of the position and magnitude of the maximum stresses calculated by Iyengar, Guyon, Bleich, Sievers and Morsch is presented by Iyengar (4). It is reproduced here in Fig. A.1. These quantities are plotted against the a/h ratio and are all valid for the axial case. Iyengar also published the total tensile force given by the above authors. It assumes a value of 0.3p for a concentrated force and decreases approximately linearly to zero for a/h = 1. It can be seen from his figure that the position of maximum transverse stress is between about 0.2h and 0.3h for most loading plate sizes used in practice. The curves of Iyengar and Guyon are to be taken as the basis for comparison. The approximate linear decrease of the maximum stress (from 0.5p under point load) offers an easy way to estimate its size for increasing a/h ratios. The accuracy of the method of superposition used by Bleich and Guyon has been studied. Guyon's results have been confirmed by Gerstner and Zienkiewicz (3), though they also used the superposition but employed finite differences instead of Fourier series. The basic ideas were the same. Only the calculation methods differed. With the availability of very high speed computers, all corrections for boundary conditions could be bypassed and finer grids could be applied for the finite difference solution that was part of the present investigation.

Considerable attention has been paid to the relative importance of the bursting and spalling stresses. A number of authors did not find

high spalling stresses. This will be explained in the section that follows. Both Guyon (2) and Bleich (7) substantiated the important result that at small eccentricities the maximum tensile stress is in the bursting zone while at large eccentricities it shifts into the spalling zone. Their results also show that the spalling stresses always act on a smaller area, hence the corresponding force remains small. But they (with most other authors) did not realize the importance of the localized spalling stresses. The bursting stresses become compressive in the immediate vicinity of the load. This was not confirmed by all authors.

(b) Size of Loaded Area

The effect of the size of the loaded area has been emphasized by most authors. According to Zielinski and Rowe (21, 23), it is one of the dominant factors affecting design. The a/h ratio influences the magnitude of the transverse stresses but does not alter the position of the maximum and zero stress. Ban, et al. (22) also found that the cracking and ultimate loads increased with the loading area. Hence the calculations for concentrated loads are conservative. Goodier reported that the ratio of maximum transverse tensile stresses for a = 0.1h and for a = 0.2h is 1.3 (25). For axial loads the same ratio is about 1.2 according to Guyon (2). But he gives a shift of the position of the maximum stress from 0.25h to 0.32h. There is a similar change in the location of zero stress. The distribution of transverse stresses as a function of the a/h ratio is shown on Fig. A.2, together with Bleich's curves. This figure was taken from Reference 22. A similar set of curves is given by Iyengar for the symmetric case (4). Experimental investigations resulted in similar plots. They will be discussed in the next section.

The distribution of the applied load affects the transverse stresses. The pressure under the loading plate may be parabolic (convex or concave) or uniform, depending on the stiffness of the plate. Goodier has published some calculations about this question (25). A comparison of representative results are shown on Fig. A.3 for a region with length to width ratio of two (L/h = 2). It can be seen that there is a large reduction of stresses when the applied load is uniform. The parabolic load causes stresses that are closer to the point load case. This variable influences all experimental results.

(c) Beam Reaction

Sargious investigated the effects of a reaction close to the end of the beam (8). There are tensile stresses near and perpendicular to the reaction. The maximum of these stresses was about 0.6p for a reaction that was one fifth in magnitude of a slightly inclined central prestressing force. This was comparable to the tensile stresses caused by prestress transfer, but acted on a small area only.

(d) Difference between Principal and Transverse Tensile Stresses

From the distribution of the transverse, longitudinal and shear stresses, the principal stresses can be computed. It was found that these stresses have about the same maximum values as the transverse stresses, though the former act on somewhat larger area (2, 8). Therefore it seems sufficient to be concerned with transverse stresses only.

A.4 Areas of Apparent Agreement in Experimental Studies

Numerous experimental investigations have been conducted in recent years. They have resulted in a large amount of information directly

applicable to the understanding of the behavior of end blocks. Some experiments were made to measure the stress distribution, others to shed light on the modes of failure of concrete end blocks. Investigations of the latter kind seem to offer more valuable information than the ones that are merely checks on elastic analyses. In this section the most important conclusions and factors are presented.

(a) Spalling Stresses

Some tests showed the existence of spalling stresses that were not predicted by analytical methods. Sargious found spalling stresses in concrete specimens that were up to 30 per cent higher than in the corresponding photoelastic analyses (8). For an applied force at an inclination of 2.6 degrees from the horizontal and acting at h/3 from the bottom, the ratio of the maximum spalling stress to the maximum bursting stress was 1.3. This ratio ranged from about 0.75 to about 1.69. Absence of the reaction and large eccentricity gave the highest spalling stresses. Huang measured small bursting stresses (0.1p) and large spalling stresses (0.8p) in a concrete beam (9). In the case of two symmetrical loads, Christodoulides obtained tensile stresses between the line of symmetry and either one of the loads (18). These stresses were compressive at the end of the specimen and changed to tension with a maximum value of about 0.6p. This compares well with some analytical studies. When a single axial load was applied, he found the maximum tensile stress to be located on the center-line.

Zielinski and Rowe have measured transverse strains under two eccentric loads (23). The strains under the loads were similar to those under a single eccentric load. Between the loads the transverse strains increased toward the end of the beam, indicating spalling as shown on

Fig. A.4. It is to be noted that there is a relatively large compression zone just off the line of the load. It is unfortunate that the strains were not measured along the load acting in the flange.

(b) Bursting Stresses

Zielinski and Rowe checked the validity of Guyon's method of partitioning (23). They compared the performance of symmetrical prisms with loads on cubes and found that the surrounding concrete has some restraining effect on the symmetric prism. When there were several loads acting in the flange, tension occurred between these forces, similar to spalling stresses. For the stresses along the load the principle of partitioning applied approximately. When the loads acted close, tensile stresses did not develop between them. They also tested I-beams with rectangular end blocks. In three tests single eccentric load acted (at 0.224h) in the web. The measured transverse stresses are shown in Fig. A.5. The strains were larger for smaller anchorage plates. This agrees with the findings of other authors. The so-called "lower" tensile stress zone at the junction of the web and the end block can also be seen. It will be discussed later.

Zielinski and Rowe have also tested concrete blocks under axial loads (21). The measured transverse strains were generally higher than what all the theories they used to predict those strains (Magnel, modified Magnel, Bleich, Bleich-Sievers, Guyon). For some a/h values the Bleich-Sievers distribution came close to the experimental curves and in a few cases exceeded them. Marshall and Mattock also concluded that analysis underestimates the maximum stresses (20). For large eccentricities (or when most strands are concentrated), the difference is quite large. Other authors also inferred that Guyon's values are low (22, 19) and that Magnel

also underestimated the stresses (9). Ban, et al. (22) preferred Bleich's values, but this preference is not considered to be conclusive or convincing. Only Huang measured stresses that were smaller than Guyon's values but were higher than those by Magnel (9).

For axial loads the resulting stress distribution is easily obtained by two sets of curves. One shows the effect of a/h on the stress distribution along the axial load (Fig. A.6), the other gives the variation of these stresses across a section normal to the axis as shown on Fig. A.7 (21).

(c) Tensile Forces

From the measured strain distribution the stresses and the resultant forces were calculated by most authors. Sargious found in his photoelastic tests that the tensile force has an inclination of about 5 degrees from the vertical (8). This justifies the use of the transverse rather than principal stresses. The magnitude of the force ranged between 0.15P and 0.24P depending on the inclination of the applied load and the size of the reaction. Similar values were calculated by Zielinski and Rowe from measured strains on axially loaded blocks for a/h ratios ranging between 0.67 and 0.31 (21). They also list the corresponding values given by other theories as listed below:

	Tensile Force/Applied Force	
	a/h = 0.31	a/h = 0.67
Zielinski-Rowe (measured)	0.36	0.19
Magnel	0.19	0.10
Bleich	0.19	0.09
Bleich-Sievers	0.27	0.11
Guyon	0.17	0.08
Morsch	0.17	0.10

There is relatively small scatter among the calculated values. The averages are 0.105P and 0.215P for the two cases considered. The values calculated by Iyengar are 0.075P and 0.17P (4). Sargious proposed a linear approximation based on Guyon's results and on his photoelastic studies. According to this method, the tensile force diminishes, from 0.30P for a/h = 0, in proportion to the ratio of the loaded area and the area of the end face of the block (8). This assumed linear relation would give 0.12P and 0.22P for the above values of a/h.

The values measured by Zielinski and Rowe are considerably larger than those based on theory. This disagreement was also observed between the experimental and analytical results presented in this report as discussed in Section 3.3.

So far in this section the experimental stress distributions (spalling and bursting) have been examined and compared with some of the theories. In the remainder of this section some of the important influencing factors (concrete properties, loading plate, anchorage, shape of cross section, reaction) will be discussed, followed by some comments on crack formation, action of reinforcement and design procedure.

(d) Concrete Quality

Most researchers have agreed that reinforcement is the most effective way of strengthening end blocks. A few of them (namely Abeles) emphasized the need for better concrete and the importance of careful mixing and casting (26). Due to the complex stress conditions existing in an end block, the stress-strain relation of the concrete differs considerably from that in a standard cylinder. The strain capacity prior to cracking is increased (23). Zielinski and Rowe found that in a prism loaded over a

small area the tensile strength may be 28 per cent higher than in the splitting test for a/h = 0.3. This margin goes up to 47 per cent for a/h = 0.7 (23). They suggest an increase in the maximum permissible strain for strip loading.

Only a few authors registered some dependence of the ultimate load on concrete strength (22, 6). Good compaction is thought to be more important.

(e) Loading Plate

There is a large amount of data on the effect of the size of the loading plate. Most authors consider it to be the most important variable. Perhaps only eccentricity is more influential. Zielinski and Rowe obtained maximum transverse stresses of 0.40p for a/h = 0.7 and 0.73 p for a/h = 0.3 (21). These are 2 and 2.8 times larger than the corresponding values based on Guyon's method. Hiltscher and Florin made photoelastic tests to study this question (16). For h/a = 1 the tensile force is zero and the force increases as h/a increases. For $h/a > 30$, the force is close to the limit, about 90 per cent of the case for $h/a = \infty$. The upper limit of the tensile force is 0.3P. Hiltscher and Florin tested blocks that were fixed on one side and loaded on the opposite side. The dimensions of the sections normal to the force were not small compared with the length in the direction of the loads. The results were given as a set of curves that show the position and magnitude of the resultant transverse tensile forces for various h/L ratios. These values are of no direct interest in prestressed concrete where this ratio is small. For a value of L = 23a the stress distribution is shown as a function of h/a (Fig. A.8). All his results for long blocks (including the position of the tensile force) agree with Iyengar's results.

Sargious proposed a linear correction for the size of the loading plate. This simple procedure was discussed above.

The thickness (rigidity) of the bearing plate also has influence on the behavior of end blocks. For stiffer plates the cracking and ultimate loads increase (22). The variation in the rigidity of the loading plate affects the pressure distribution over the bearing area. Hiltscher and Florin found that the effect of this variation is usually less than 10 per cent. When the stiffness of the plate is large, the pressure under the center of the plate is smaller than under the edges and the transverse stresses are smaller than in the case of uniform pressure (16). Conical action increases the stresses and decreases the cracking load by 5 to 15 per cent (21). The method of embedment and the material of the anchorage has no appreciable effect on the stresses.

The bearing capacity of the concrete is increased due to the confinement under the loading plate. Zielinski and Rowe obtained contact stresses that were more than three times the cube strength (21). The reinforcement has significant effect on the bearing capacity up to about 2 to 3 times the cube strength. The above mentioned authors obtained higher bearing stresses in end blocks than in similar small cubes and hence concluded that the remainder of the end block imposes some restraint. Also, the bearing capacity is larger under strip loading than under more individual loads. Parabolic pressure distribution must be assumed for larger (less stiff) plates to yield the higher measured stresses (22). The difference between the effects of cone and plate loading is small, usually less than 12 per cent (21).

(f) End Blocks

One of the major results of recent experimental investigations is that rectangular end blocks can be omitted on I-beams. Relatively few

tests were made on this kind of specimen. There are two tension areas present: one is the usual spalling and bursting zones and the other is at the change of the cross section. Huang found the latter zone at the center-line near the junction of the end block and the I-beam web. The tensile stresses in the second area are of the same order of magnitude as the regular spalling stresses but act on a larger domain, hence are more critical (9). He concluded that for the distribution of the force h is sufficient as the length of an end block. Zielinski and Rowe observed cracks at the junction of the web and the end block. With eccentric loads, these cracks first occurred due to maximum stresses at the inner edge of the end block (23).

There is a different stress flow (spreading of forces) in I-beams without rectangular end blocks than in beams with them. This was explained in Section 3.2. Zielinski and Rowe measured failure loads of I-beams about 17 per cent higher without end blocks than with end blocks.

(g) Beam Reaction

The effect of reactions is generally considered to be beneficial. Only Sargious made tests to substantiate this supposition. He found (in concrete beams and photoelastic tests) that the spalling stresses were smaller when reaction was present (8). However, the reaction induced high horizontal spalling stresses in the bottom fiber near the reaction. Fortunately, they act on a small area and hence nominal reinforcement should take care of them. The reaction decreases the transverse tensile stresses and shift the resultant tensile force farther from the end. For a reaction of 0.2P at h/6 from the end, the maximum spalling stresses are reduced by 40 per cent and the maximum bursting stresses by 37 per cent. This reduction can not be utilized in practice, where the reaction is due to dead load only when the prestress is applied.

(h) Cracking

Information on the development of cracks is insufficient. Marshall and Mattock observed the cracks in the lower part of the web close to the centroidal axis. The width of the cracks were from 0.001 to 0.004 in. (20). Zielinski and Rowe noticed the first crack under an axial load at 0.15h to 0.25h from the end (21). In some cases there was a splitting in the flange parallel to the axis of the beam.

(i) Reinforcement

The action of the web reinforcement has been investigated in recent years only. The need for reinforcement is advanced by all authors. It is generally accepted that some reinforcement should be placed close to the end face to take care of the spalling stresses. Guyon prescribes reinforcement to provide for a nominal spalling force of 0.03P which is enough for the cases considered by some authors but insufficient in certain cases of large eccentricity. The problem is often three-dimensional and reinforcement must be provided in the two principal directions normal to the axis of the loads.

Reinforcement restricted the width of the cracks in bridges to 0.01 in. and limited their length to a few inches (20). More stirrups take a larger total force for a certain applied load. The variation of stirrup strains along a pretensioned beam is shown on Fig. A.9 (taken from Reference 20). Zielinski and Rowe remarked that the amount of useful reinforcement is limited because of the contact stresses under the anchorage or bearing plate will control the strength. The increase in bearing capacity due to reinforcement is less than 40 per cent.

According to Siever's analysis, the reinforcement should be distributed over an area where $x < 0.2h$ (11). Zielinski and Rowe agreed

with other authors that helical reinforcement is more efficient than mat reinforcement, especially in the case of axial loads.

Some references contain recommendations for design and describe how to predict an approximate stress distribution and how to proportion the reinforcement to take care of the tensile forces. Zielinski and Rowe recommend the use of the symmetrical prism method (21, 23). They note that the successive resultants approach may be used, but maximum stresses are confined to lines along actual loads and do not include lines of resultants where there is no load acting. They use two figures to simplify the calculations. It is advised to continue the steel from top to bottom to take care of the spalling stresses. When a rectangular end block is used on an I-beam, there is deep beam action and the lower tensile zone yields a tensile force that is about 70 per cent of the force near the end face. This is valid for an end block whose length is equal to the height of the beam, since only this case was investigated by the authors.

Other authors follow similar procedures to design the reinforcement. They all start with picturing the resulting elastic stress distribution and then give a few additional hints.

A substantial amount of information was gathered in this section. It resulted from experimental investigations conducted in recent years. The disagreement found in the references will be discussed in Section A.6.

A.5 Areas of Apparent Disagreement in Analytical Studies

There are a few limitations common to all analytical investigations. These will be mentioned in this section together with the discussion of some points of disagreement among some of the analytical methods.

Practically all investigations (with the notable exception of that of Sievers) limited their work to two dimensions. A three-dimensional

analytical investigation would be very complicated even with a few variables. The two-dimensional approximation is considered to be good if the loading plate is wide (or if the individual loads are close to each other on a horizontal line). However, this approximation is not good when the loads are separated across the cross section and in the case of I-beams without rectangular end blocks. In these cases experimental methods are more convenient. The equilibrium method advanced in Section 4.2 gives some information also in the three-dimensional case.

As it was already discussed in Chapter 4, the analytical solutions that treat elastic stress distributions reflect actual conditions only at very low loads. Measured strains indicated that at some highly stressed points inelastic action begins at low loads. Also, as soon as the first crack forms, the elastic stress distribution changes suddenly. Forces calculated from the elastic stress distribution can serve as a first estimate only.

Some of the theories are based on assumptions that are not valid, others hold in certain cases only. Thus, Magnel assumed that the transverse stresses are distributed along a third degree parabola on longitudinal sections (13). This is quite good along the line of a load, but is completely wrong off this line. Morsch's analysis gives forces that do not agree with the results of other solutions and the positions of these forces are wrong (12). Iyengar criticizes the solution of some authors (for example, Guyon, Bleich, Sievers) on the grounds that either they give stresses that do not satisfy the equilibrium equations and the conditions of compatibility of the mathematical theory of elasticity, or that they do not give all three kinds of stresses and, hence, such checks can not be made(4).

For a long time only Bleich's solution was known. With Guyon's work published in 1951, some controversy developed. Numerous investigators

have tried to resolve the differences (3, 4) in the stresses calculated according to Bleich's and Guyon's methods. The lack of conclusive evidence precluded confidence in either solution for a number of years. An account of this was given in Chapter 2. It is now established that Guyon's solution is better than Bleich's (3, 4).

Guyon published tables of coefficients for the stresses for certain positions of the load. However, the stress gradient near the load is quite large and interpolation does not yield reliable values between points. The maximum stresses could have twice the values listed in the tables (27).

Many authors treated axial loads only and most of them (notably the symmetrical prism method) did not predict spalling stresses. Some other methods also neglected these stresses (10, 13, 28).

Available analytical methods do not take the problem as a whole. The possible failure mechanisms are complex and may be due to multiple causes. Cracking, bearing, high shear and inelastic action are all present.

The successive resultants method of Guyon gives the stresses on resultants of groups of loads. If there is no load acting along the line of the resultant, then the method is not reliable (23).

There is considerable disagreement between the analytical and experimental results. This may be due to numerous causes. The conditions are, as mentioned above, complex under the loads. There is inelastic action and the failure may be the result of a number of contributing factors. Douglas and Trahair questioned the adequacy of failure theories for these conditions (6). They have measured strains that were much larger than the values given by the split cylinder tests. Zielinski and Rowe also noted that the stress-strain relationship for the concrete under the complex

stress conditions was quite different from the one measured in standard specimens (23). Thus, the applicability of the calculated maximum stresses is questioned.

The strains measured by Zielinski and Rowe were generally higher than predicted by any of the theories (21). This was found in other comparisons too. They have also observed that the position of the measured maximum stresses agrees with the one given by theories, while the position of zero transverse stress is closer to the end face in the former case. Neither Siever's approximation, nor Sargious' finite difference solution gives the compression zone under the load.

The bursting stresses based on measured strains were generally higher than those calculated. This was found by Zielinski and Rowe (21) and by Ban et al. (22) and also in the present investigation.

Sargious attributed the differences between calculated and measured stresses to various causes (inelasticity, microcracks, etc.). Also he found that the inaccuracy of the finite difference solution accounts for some of the discrepancy between his predicted and measured values. He obtained tensile stresses and forces by the photoelastic tests that were up to 30 per cent higher than the calculated ones. He could modify this number by changing the grid spacing. Aside from the improvement in the mathematical representation of the equations, a finer grid would reflect the loads under the loading plate much better. Better results could be obtained when grid points coincided with the edges of the loading plate.

There is even larger discrepancy between the results of analytical methods and tests in the case of spalling stresses. This indicates that the spalling stresses might be higher than the theories would indicate. Large difference was noted by Sargious as mentioned above. Similar

differences between measured and calculated spalling stresses were found in the present investigation (Chapter 3).

A.6 Areas of Apparent Disagreement in Experimental Studies

The number of experimental investigations has greatly increased in recent years. It became apparent that measurements give more trustworthy results under the complex conditions that exist in the end block. The agreement among the results is good, especially qualitatively.

The photoelastic tests can be classified with the analytical methods in the sense that they yield elastic stresses. Sargious measured spalling stresses in concrete specimens that were 30 per cent higher than the corresponding values in the photoelastic tests (8). He explained the difference by the inelastic action of the highly stressed concrete, and by the presence of microcracks.

In most experiments the strain gages were not close enough to the end face to detect the compression zone (20). Also there is no good instrumentation that would measure the action in the third dimension (across the section).

When axial loads were applied, especially if spread over a relatively large area, the spalling zone is small and can not be measured (6).

While most experimental results agreed with those of Guyon's theory, the tests of Ban, et al. tended to follow Bleich's and Siever's values, that were higher than Guyon's results (22). They also found that the size of the loading plate does not influence the cracking load appreciably. They also disagree with other authors by finding a linear relationship between the concrete strength and the cracking and ultimate loads.

The three-dimensional nature of the problem is illustrated by some test of Zielinski and Rowe (23). When there is more than one load

acting across the section, vertical cracks may occur between the loads. This is especially important in the case of I-beams with loads acting in the flange.

To interpret experimental results correctly, more basic research is needed to obtain information on the behavior and failure of concrete under complex combination of stresses.

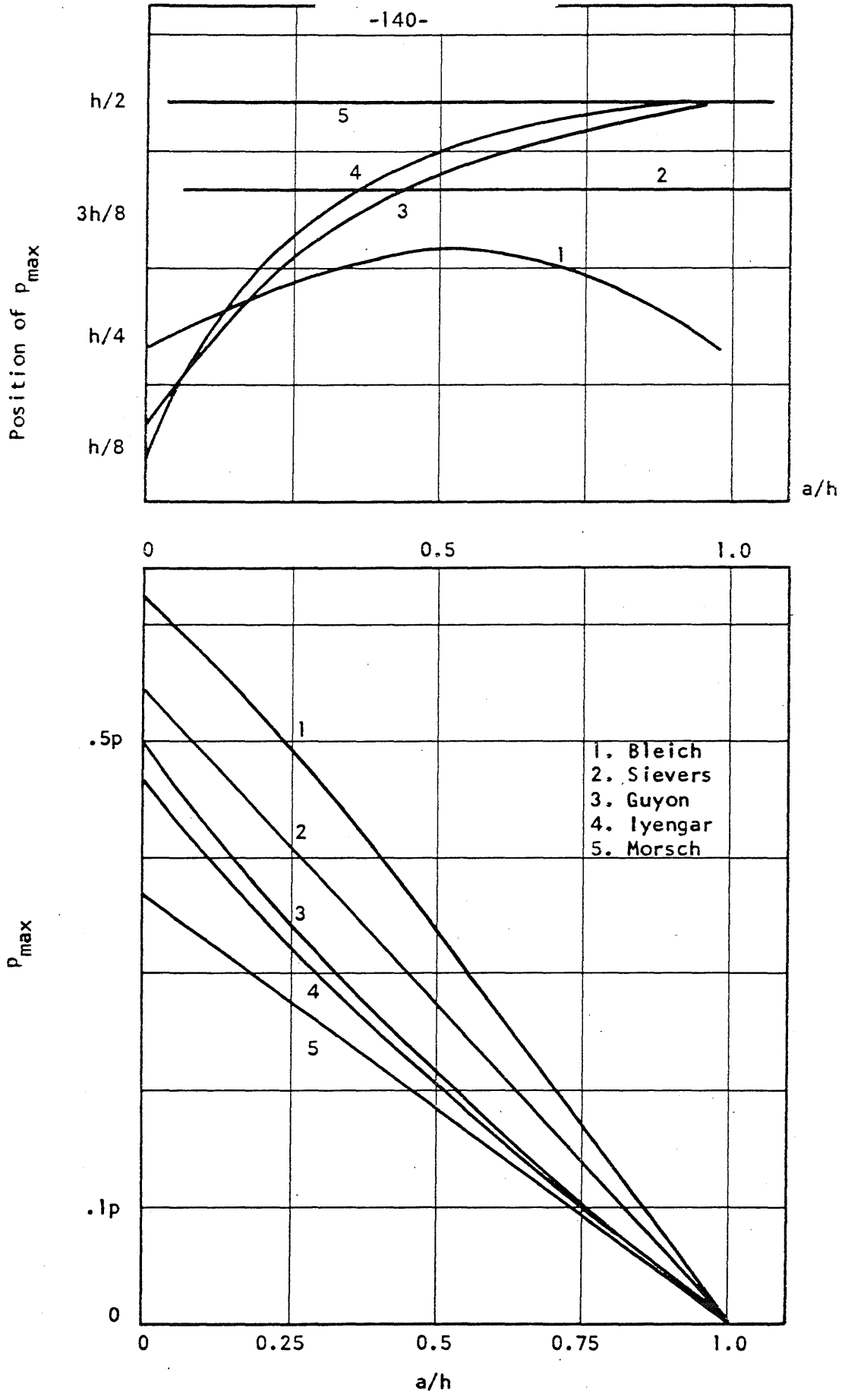

FIG. A.1 MAXIMUM TRANSVERSE STRESS

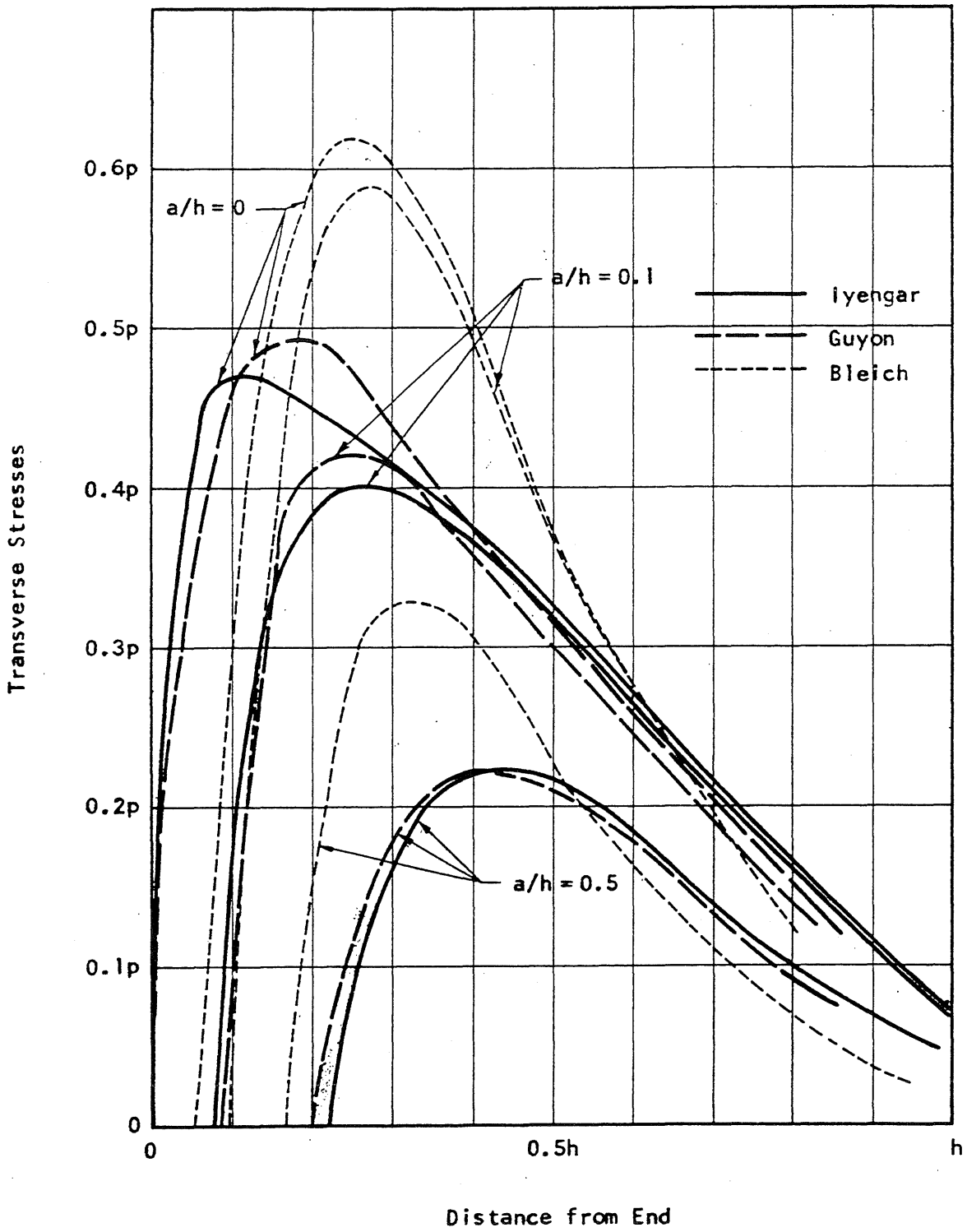

FIG. A.2 COMPARISON OF TRANSVERSE STRESS DISTRIBUTION BY IYENGAR, GUYON AND BLEICH

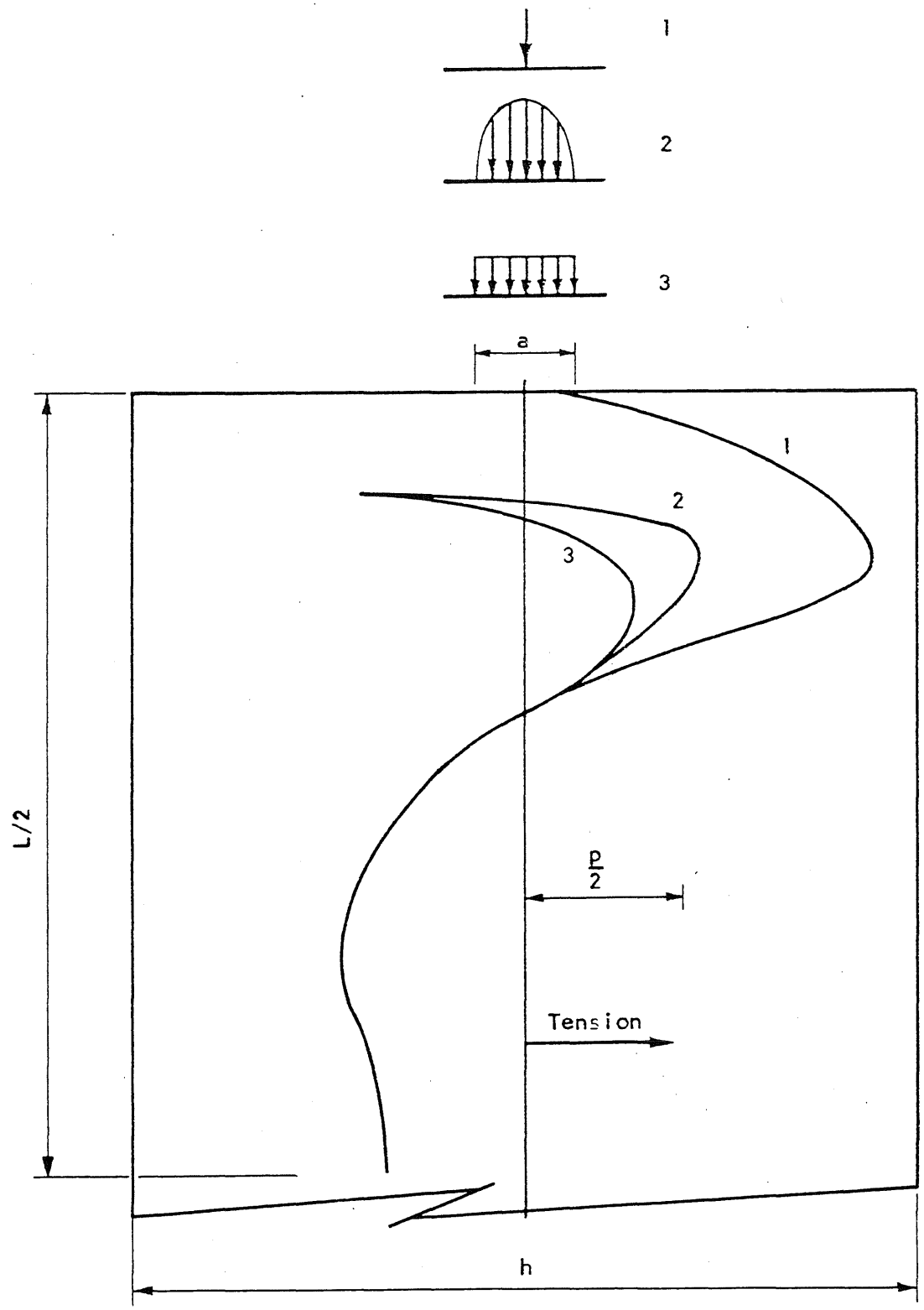

FIG. A.3 EFFECT OF LOAD DISTRIBUTION - GOODIER

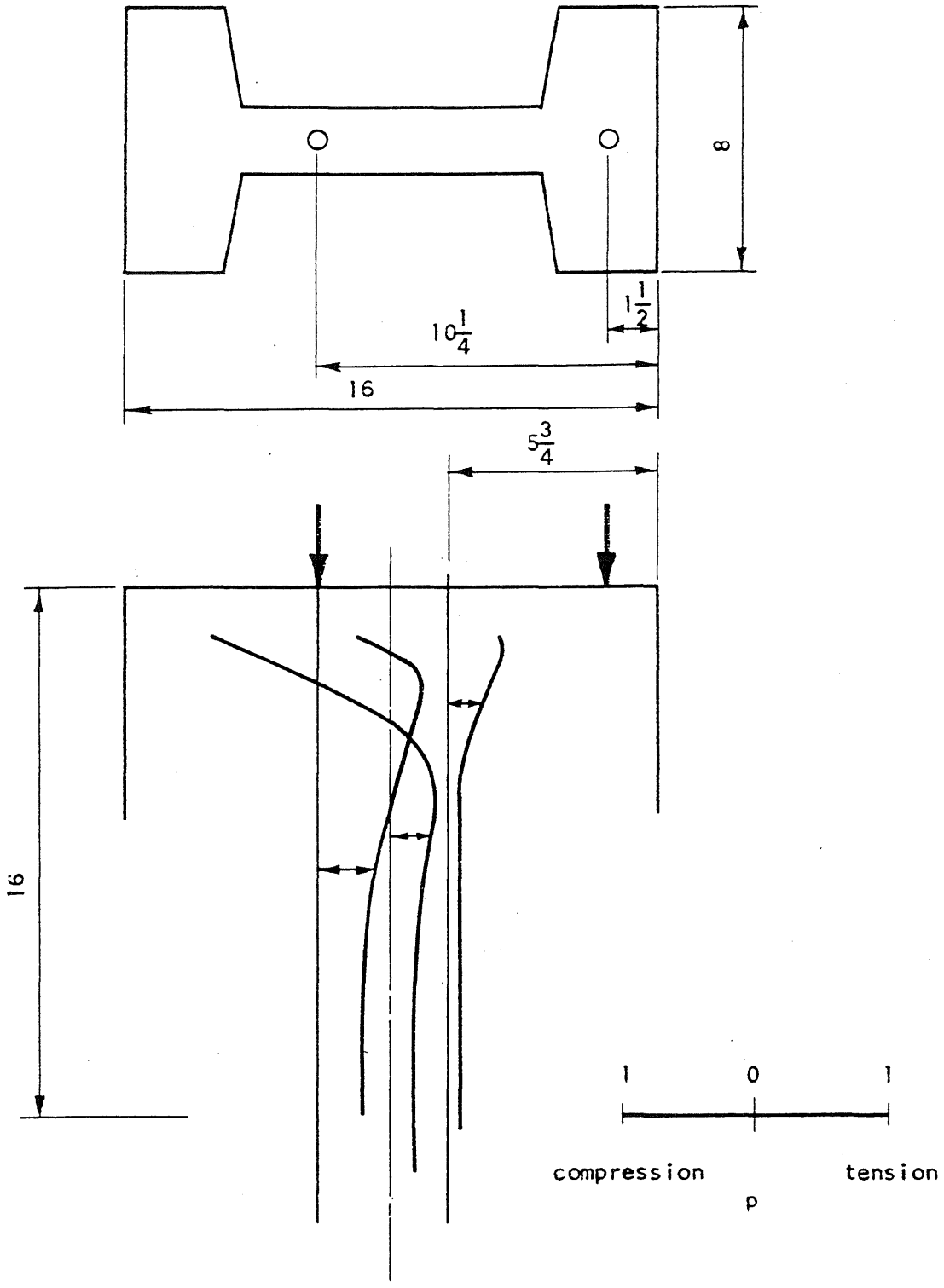

FIG. A.4 TRANSVERSE STRESSES BY ZIELINSKI AND ROWE

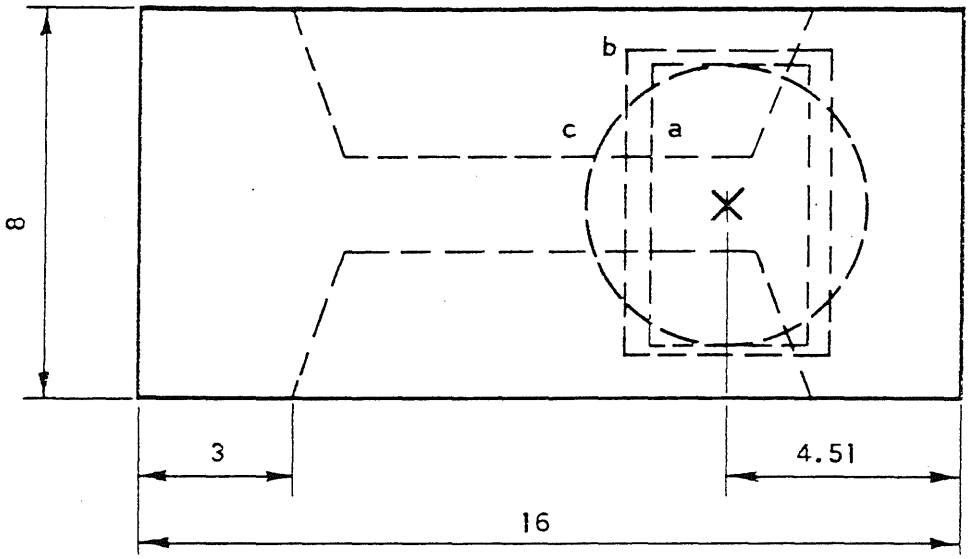

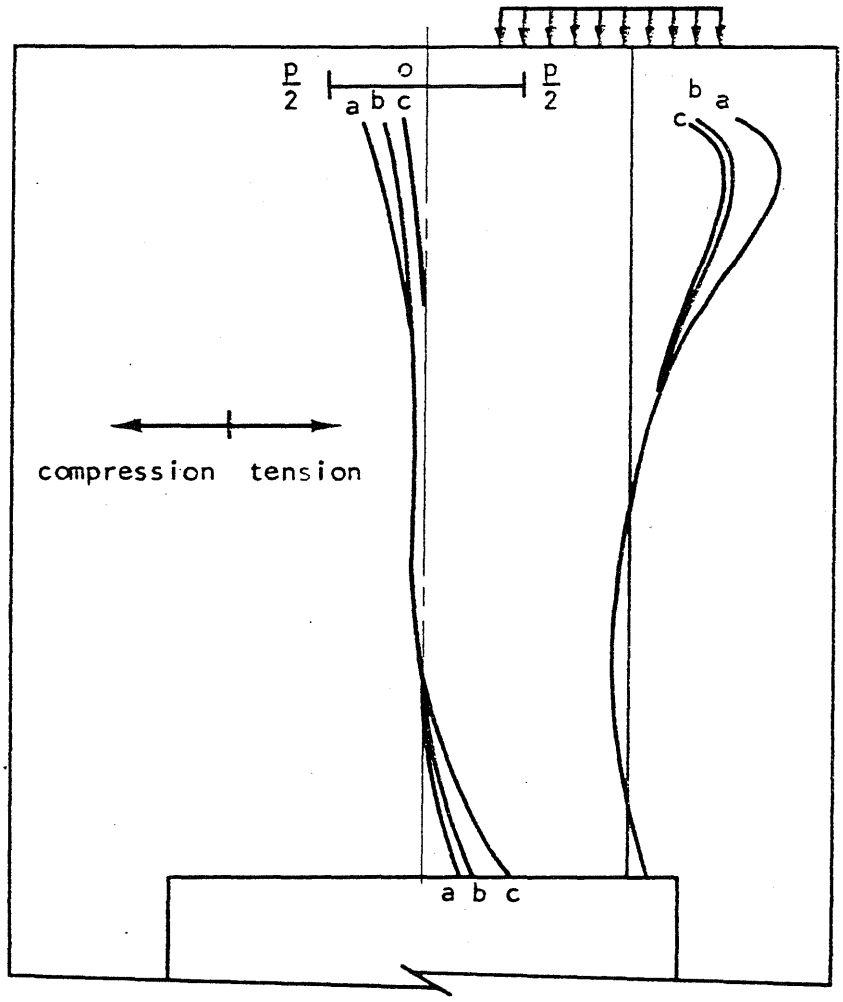

FIG. A.5 EFFECT OF LOADING PLATE ON TRANSVERSE STRESSES (ZIELINSKI AND ROWE)

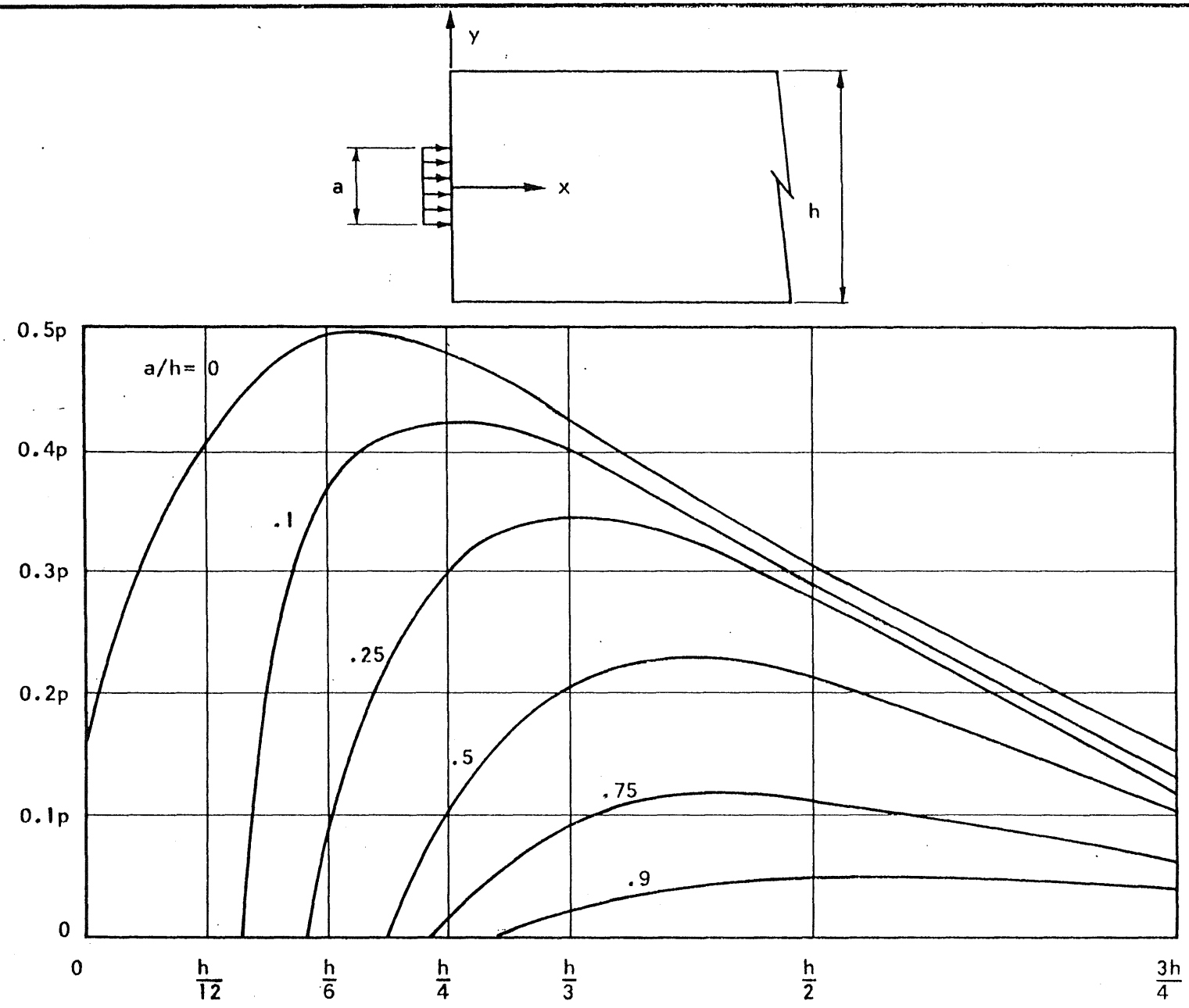

FIG. A.6 INFLUENCE OF THE SIZE OF THE LOADING PLATE - GUYON

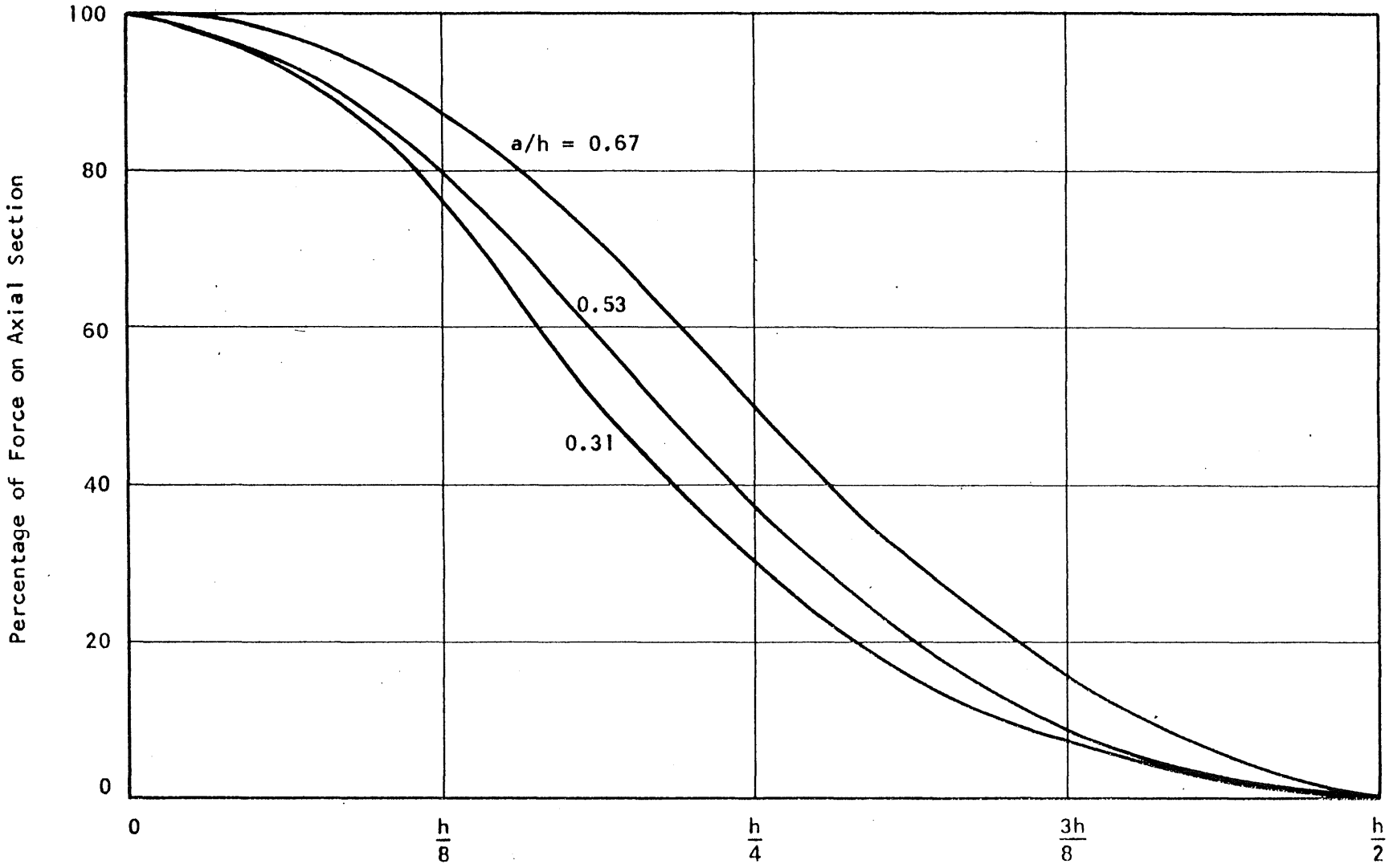

FIG. A.7 FORCE ON SECTIONS PARALLEL TO AXIAL SECTION

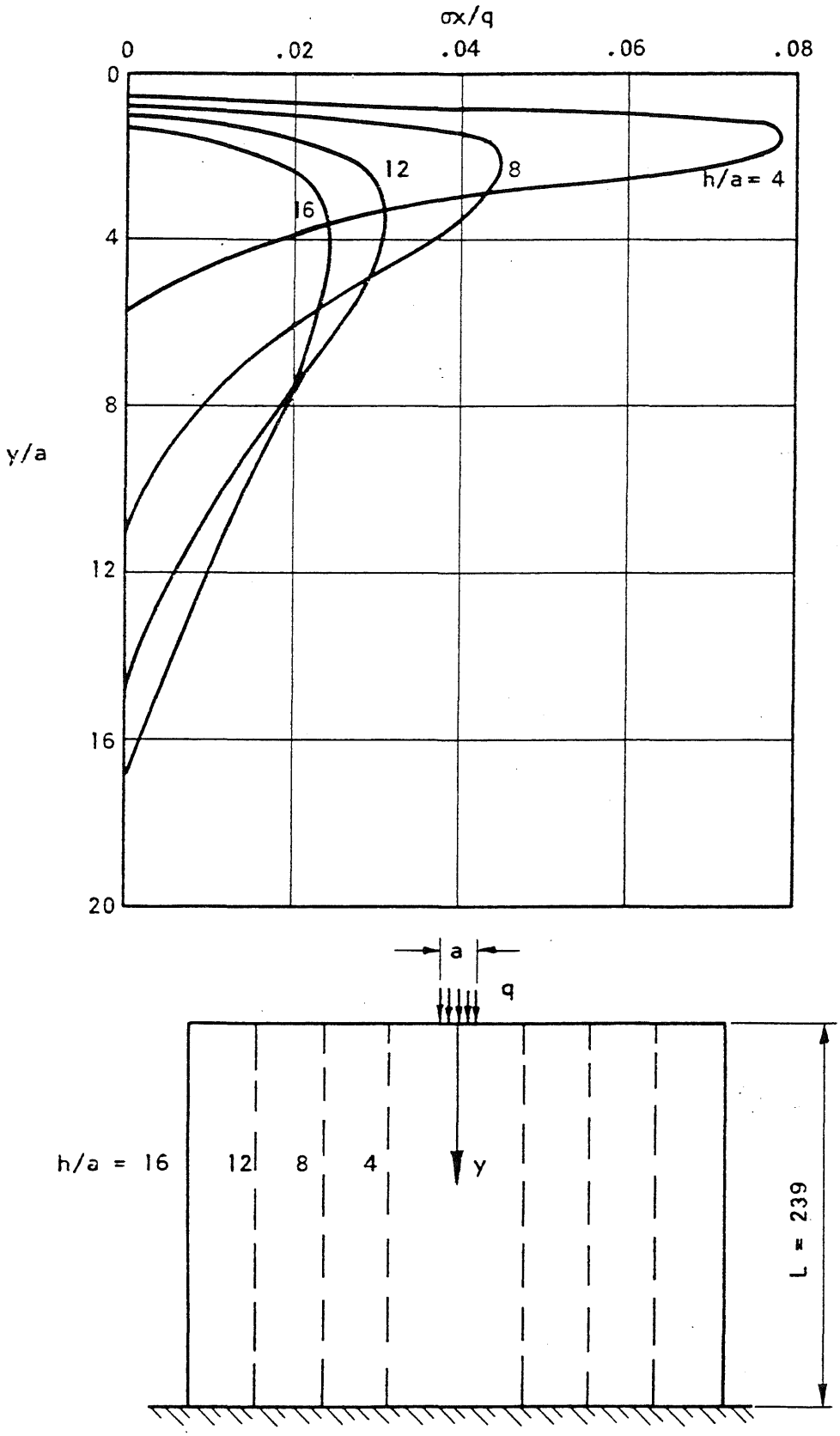

FIG. A.8 TRANSVERSE STRESSES BY HILTSCHER AND FLORIN

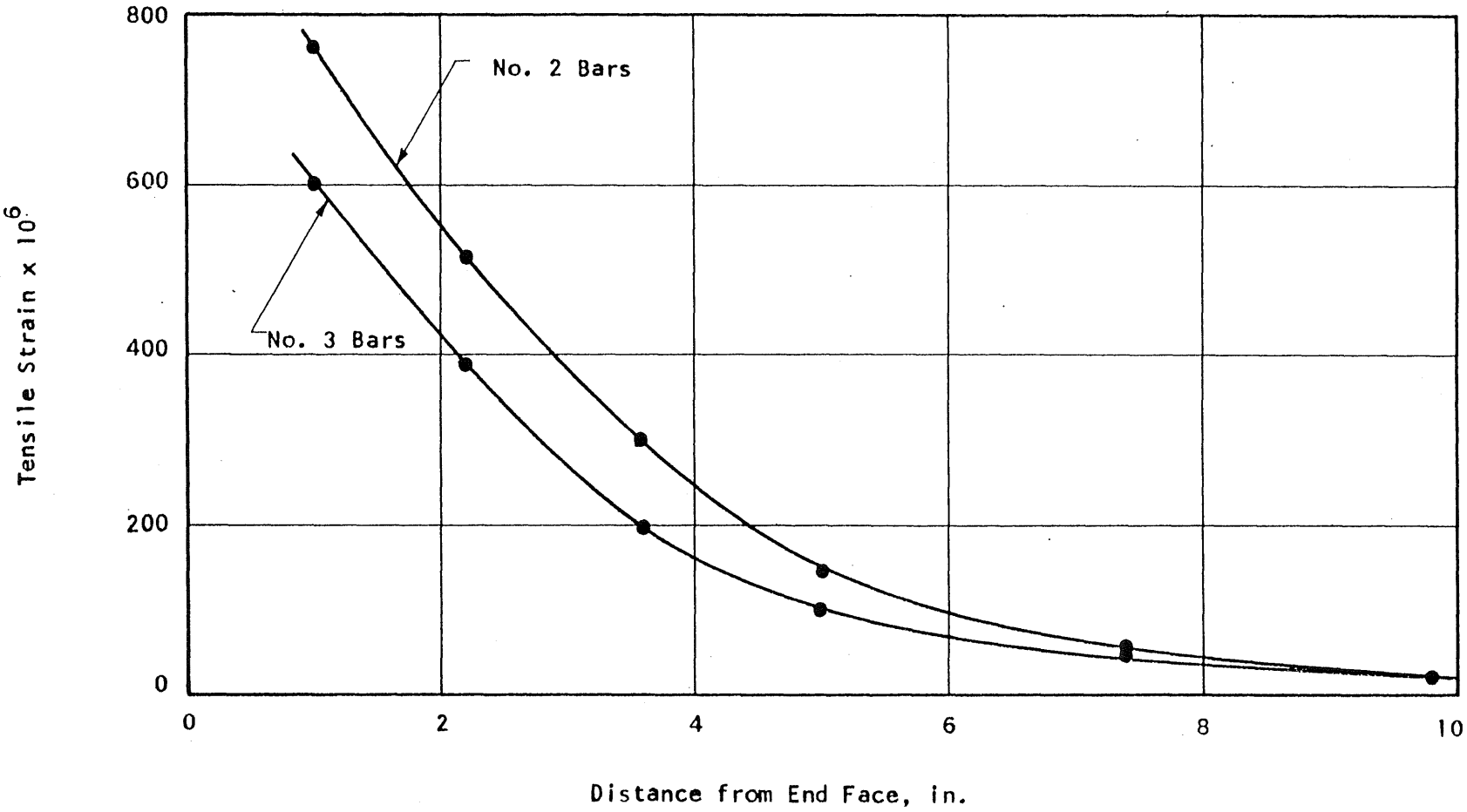

FIG. A.9 TYPICAL VARIATION OF STIRRUP STRAINS ALONG BEAM BY MARSHALL AND MATTOCK

APPENDIX B

MATERIALS, FABRICATION, AND TESTING

B.1 Materials

(a) Cement

Marquette brand Type III portland cement was used in all specimens.

(b) Aggregates

Wabash River sand and gravel were used for all specimens. The coarse aggregate had a 3/8 in. maximum size. These materials have been used in this laboratory for a number of years.

The origin of these aggregates is an outwash of the Wisconsin glaciation. The major gravel constituents were limestone and dolomite. The sand was made up largely of quartz.

(c) Concrete

The design of the concrete mix was based on the trial-batch method. The concrete strength ranged from 4500 psi to 5900 psi with most of the test results grouping around 4700 psi, 5200 psi and 5700 psi. The proportion by weight of the aggregates was about 1:3.1:3.4. The amount of water was adjusted according to the moisture content of the aggregates.

Cylinders for compression strength tests and for splitting tests were cast, as well as beams for the determination of the modulus of rupture in some cases. Table B.1 gives the properties of the concrete in the specimens. The values are averages of two or three tests.

The split cylinder tests were done on 6 by 6-in. concrete cylinders. Two strips of 1/8-in. fiber board were used to apply given loads on diametrically opposite generators. The tensile splitting strength f_b is given by the following formula:

$$f_b = \frac{2P}{\pi dL}$$

where P is the load at splitting and d and L are the diameter and the length of the cylinder, respectively.

There was not enough spread in the concrete strength to procure a usable relation between the splitting strength and the compressive strength. The length of the cylinders varied between 5.6 and 6.7 in. The speed of testing was 6 kips.per minute.

(d) Reinforcement

Two kinds of reinforcing steel was used as web reinforcement: No. 2 deformed bars and No. 7 USSWG wires. The bars had a nominal cross-sectional area of 0.05 $in.^2$ and a measured yield point of 50,000 psi. The cross-sectional area of the wires was 0.025 $in.^2$ with a measured yield stress of 32,000 psi. The nominal yield force for the bars and the wires were 2.5 kips and 0.8 kips, respectively.

(e) Tensioning Rod

One inch diameter STRESSTEEL rods were used to apply the external force. They had a yield stress of 137,000 psi and a modulus of elasticity of 25,800,000 psi. There were four of them in use to expedite the program. Ordinary lubricant was applied on the rod to prevent bond. The ends of the rods were threaded.

B.2 Description of Specimens

The principal part of the investigation involved tests on so-called beams. A complementary program was also carried out to determine the load-slip characteristics of the transverse reinforcement.

The beam specimens had two kinds of cross section: 6 by 12 in. rectangular and 6 by 12 in. I-sections with 2 in. webs. The specimen length was 4 ft. These dimensions are shown on Fig. B.1. None of the I-beams had rectangular end blocks.

The one-inch diameter tensioning rod was cast 1.5 in. from the bottom of the specimens. In addition to the lubricant, household wax paper was wound around the bar for the first four specimens, but later the paper was omitted and the lubrication was found to be sufficient to prevent bond.

The specimens with the "pre-crack" were cast in two parts. The first part was vibrated and a thin plastic strip was laid on it. The top half was then cast. The period between the casting of the two layers varied from 20 minutes to 3 hours. The plastic strip covered the whole horizontal section in most cases. In some of the beams the strip was somewhat narrower than the width of the rectangular section or the web thickness of the I-section. This was done to facilitate the observation of the progress of cracking.

The web reinforcement consisted of single stirrups looped around the tension rod with the circling end welded to the bar above the rod. One stirrup was placed at 1/2 or 1 inch from the end. When two stirrups were used, one was always placed at 1/2 in. and the second at 2 or sometimes at 3 inches. Identical stirrup arrangements were used at both ends of the specimen (see Fig. B.2).

Two kinds of bond tests were performed. The single pull-out specimens were 6 in. cubes with a single bar or wire protruding at the center of one face. These served for simple pull-out tests. To simulate the conditions in the end block, twin pull-out specimens were also made. Here there was no pressure on the concrete around the bar that would produce

confinement. Two symmetrically placed bars were pulled at the same time. The dimensions of both blocks were 6 by 7 by 24 in. as shown on Fig. B.3. A No. 3 bar was placed as indicated in these blocks as well as in the beams to prevent failure due to bending stresses.

B.3 Casting and Curing

All beams were cast in steel forms. The tensioning rod was lubricated and, in some cases, wrapped in wax paper.

The concrete was mixed in a drum type mixer of 6 cu. ft capacity. Usually two batches of concrete were required in each beam. When a pre-crack was desired, the concrete from the first batch was placed in a layer to the height where the crack was to be had and a thin strip of plastic was placed on it just before the casting on the top half. The top part was placed usually 2 to 3 hours after the casting of the bottom half, although in a few cases this period was only 20 minutes. Three compression cylinders and three 6 in. long split cylinders were cast from each batch.

A few hours after casting, the top surface of the beam was trowelled smooth and the cylinders were capped with neat cement. On the following day, the specimens and the cylinders were removed from the forms and were placed under wet burlap for about five days. Then they were set up for instrumentation and testing. The specimens were usually seven to nine days old at the time of testing.

B.4 Instrumentation

(a) Gages on Concrete

Various methods were tried to measure the strain distribution on the surface of the end blocks. Electric strain gages proved to be the best suited.

Type A3 SR-4 gages were placed along lines on which the strain distribution was to be determined. A typical pattern is shown on Fig. B.4. The gages have a nominal length of 3/4 in. and a minimum trim of 3/16 in. A base layer of duco cement was applied on the concrete that had already been smoothed with sand paper. A second layer of cement was used to attach the gages about ten minutes later. The lead wires were soldered one day later.

(b) Mechanical Strain Gages

On some of the end blocks mechanical gages (plugs) were glued in order to measure the strain distribution. This was mainly done in order to obtain an approximate idea of the extent of the lead-in zone and of the beam action. Readings were taken with a Whittemore gage that had a gage length of ten inches. The sensitivity of the measurement was about 0.0002 in.

(d) Dials

Ames dials were used to measure the crack width in most reinforced specimens and also to determine the amount of slip of the stirrups in the beams and of the bars in the bond tests. The dials had a sensitivity of about 0.00002 in.

The gages were mounted on the concrete above the line where the crack was expected at 1, 3, 6 and 10 in. from the end. Aluminum angles were glued on the concrete below the line. This can be seen on Fig. B.5a.

In some cases similar dials were fastened to the protruding end of the transverse reinforcement. The plunger of the dial rested against the top of the beam.

In the bond tests one dial was fastened to the end face of the concrete block. The tip of the dial rested on the end of the bar that came flush to the concrete surface.

(d) Strain Gages on Reinforcement

The strain was measured in the transverse reinforcement at the crack. Type A7 SR-4 electric strain gages were put on the bars and wires. The pre-crack was made at the center of the gages. After the beam was tested, it was broken to check if the crack passed through the gage. This was true in most cases. The gages were applied in the prescribed manner. The bar was filed smooth and sanded with emery cloth. The gage was trimmed and glued with Eastman 910 adhesive. Then the lead wires were soldered and a layer of wax was put on the gage. A protective layer of Epoxy served as the outside cover. The insulation and resistance were then checked.

B.5 Loading Apparatus

Various methods of loading were tried at the beginning of this investigation. It was necessary to maintain symmetric behavior. This was found to be best achieved by the arrangement finally adopted.

The one-inch diameter high strength steel tensioning rod was cast unbonded in the concrete. On one end, a steel bearing block with a bearing area of 6 by 3 in. was used. A 50-ton center hole jack pressed on the steel block with the reaction supplied by a nut on the end of the rod. The jack was operated by a Blackhawk pump.

On the other end, the bearing area was 6 by 1.5 in. A dynamometer was placed between this block and the nut. It had been calibrated and had a sensitivity of 310 lbs. corresponding to one dial division on the strain indicator. This end of the beam has been denoted as the "test end". It can be seen in Fig. B.4. The testssetup is shown in Fig. B.6.

It was found by the reversal of the ends that the bond was negligible and the loads were nearly equal at the two ends.

The bond tests were carried out with two lines of loading systems. The single pull-out tests were made in the manner described in Reference 29. The twin pull-out specimens were loaded by a small jack pressing against the center of the block on an area of 4 by 4 in. on one end and against a dynamometer on its other end. This can be seen in Fig. B.5b. On one bar a strain gage was mounted to have a check on the distribution of the total load between the two bars. The slip was measured with a travelling microscope as described in Reference 29.

B.6 Test Procedure

In the beam test the applied load was measured by a dynamometer. The strain distribution in the concrete was given by electric strain gages and mechanical gages (whittemore plugs). Dials were used to determine the crack width at some locations. Electric strain gages measured the strains in the reinforcement at the crack.

The development of the cracks was noted and the cracks were marked. Photographs were taken at significant stages of the test. The load was applied in about 15 increments to failure or to 50 kips, whichever was reached first. Each test took less than two hours.

In the bond tests, the load was measured by the dynamometers. An electric strain gage on one of the bars in the twin pull-out specimens served as a check on the loads in the symmetrically placed bars. A travelling microscope was used to measure the amount of slip. The load was applied in 10 equal increments up to yielding of the bar. Each bond test took less than 40 minutes.

TABLE B1

PROPERTIES OF RECTANGULAR SPECIMENS

Mark	Compressive Strength psi	Splitting Strength psi	Reinforcement (Distance from end) in.	Size of Reinforcement	Instrumentation*
R1	5630	460	-	-	C
R2	6130	450	-	-	C
R3	5200	360	-	-	C
R4	4500	380	0.5	No. 2 bar	W
R5	5500	390	0.5	No. 2 bar	W
R6	5300	400	1	No. 2 bar	W
R7	5800	410	1	No. 2 bar	D, W, S
R8	5900	380	0.5, 2	No. 2 bar	D, W, S
R9	5500	420	0.5, 3	No. 2 bar	D, W, S
R10	5300	420	0.5, 2.5	No. 2 bar	D, W
R11	5200	430	0.5	No. 2 bar	D, S
R12	5450	390	0.5	No. 2 bar	D, S
R13	4900	380	0.5, 2	No. 2 bar	D, S
R14	4900	380	0.5	No. 7 USSWG	D, S, W
R15	5700	430	0.5, 2	No. 7 USSWG	D, S, W
R16	6000	415	0.5	No. 7 USSWG	D, S
R17	5800	440	0.5	No. 7 USSWG	C, D, S

* C: Electric gages on concrete
W: Mechanical gages on concrete
S: Electric gages on reinforcement
D: Dials

TABLE B2

PROPERTIES OF SPECIMENS WITH I SECTIONS

Mark	Compressive Strength psi	Splitting Strength psi	Reinforcement (Distance from end) in.	Size of Reinforcement	Instrumentation*
T1	5500	350	-	-	-
T2	5500	350	-	-	C
T3	4400	390	-	- -	C
T4	5500	410	-	-	-
T5	5200	320	-	-	-
T6	5100	400	-	-	-
T7	4600	350	-	-	C
T8	5100	390	0.5	No. 2 bar	D
T9	5200	310	0.5	No. 2 bar	D, W
T10	5400	460	1	No. 2 bar	D, W, S
T11	5350	390	0.5, 2	No. 2 bar	D, W
T12	5200	420	1	No. 2 bar	D, S
T13	4650	400	0.5	No. 2 bar	D, S
T14	4500	400	0.5	No. 2 bar	D, S
T15	4700	370	0.5, 2	No. 2 bar	D, S
T16	5600	450	0.5	No. 7 USSWG	D, S
T17	5200	360	0.5	No. 7 USSWG	D, S
T18	5000	370	0.5	No. 7 USSWG	D, S

* C: Electric gages on concrete
W: Mechanical gages on concrete
S: Electric gages on reinforcement
D: Dials

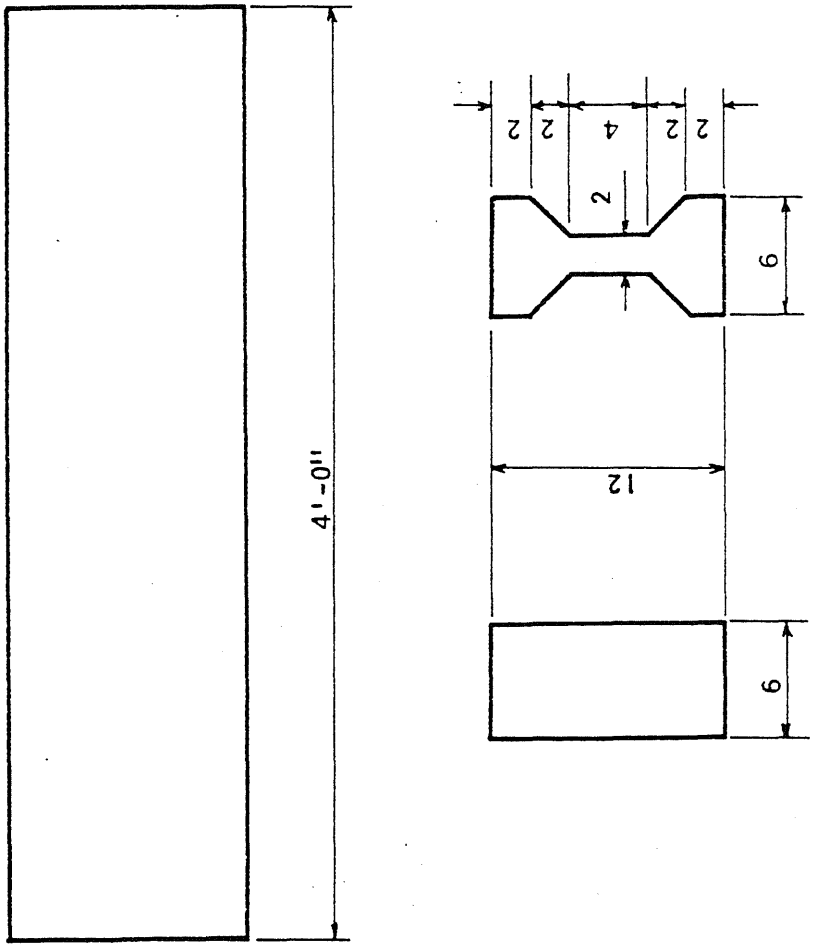

FIG. B.1 NOMINAL DIMENSIONS OF TEST SPECIMENS

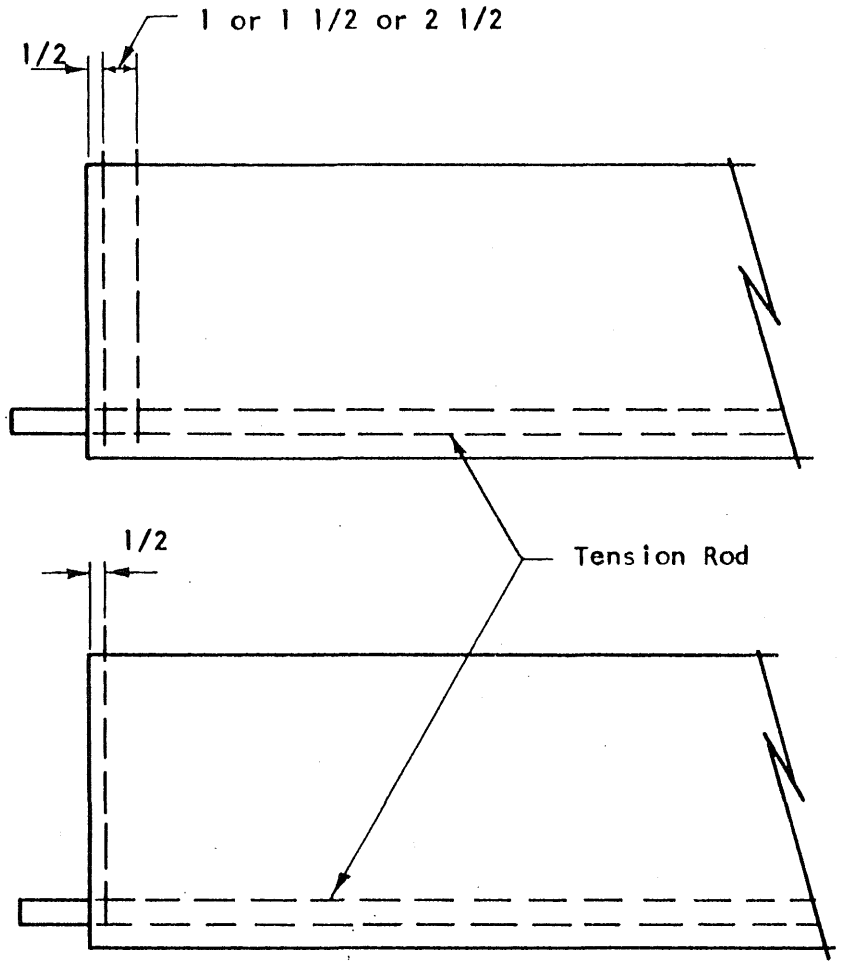

Reinforcement: No. 2 Bars, or
No. 7 USSWG

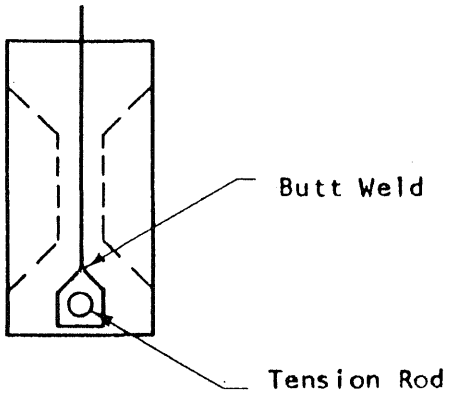

FIG. B.2 DETAILS OF REINFORCEMENT

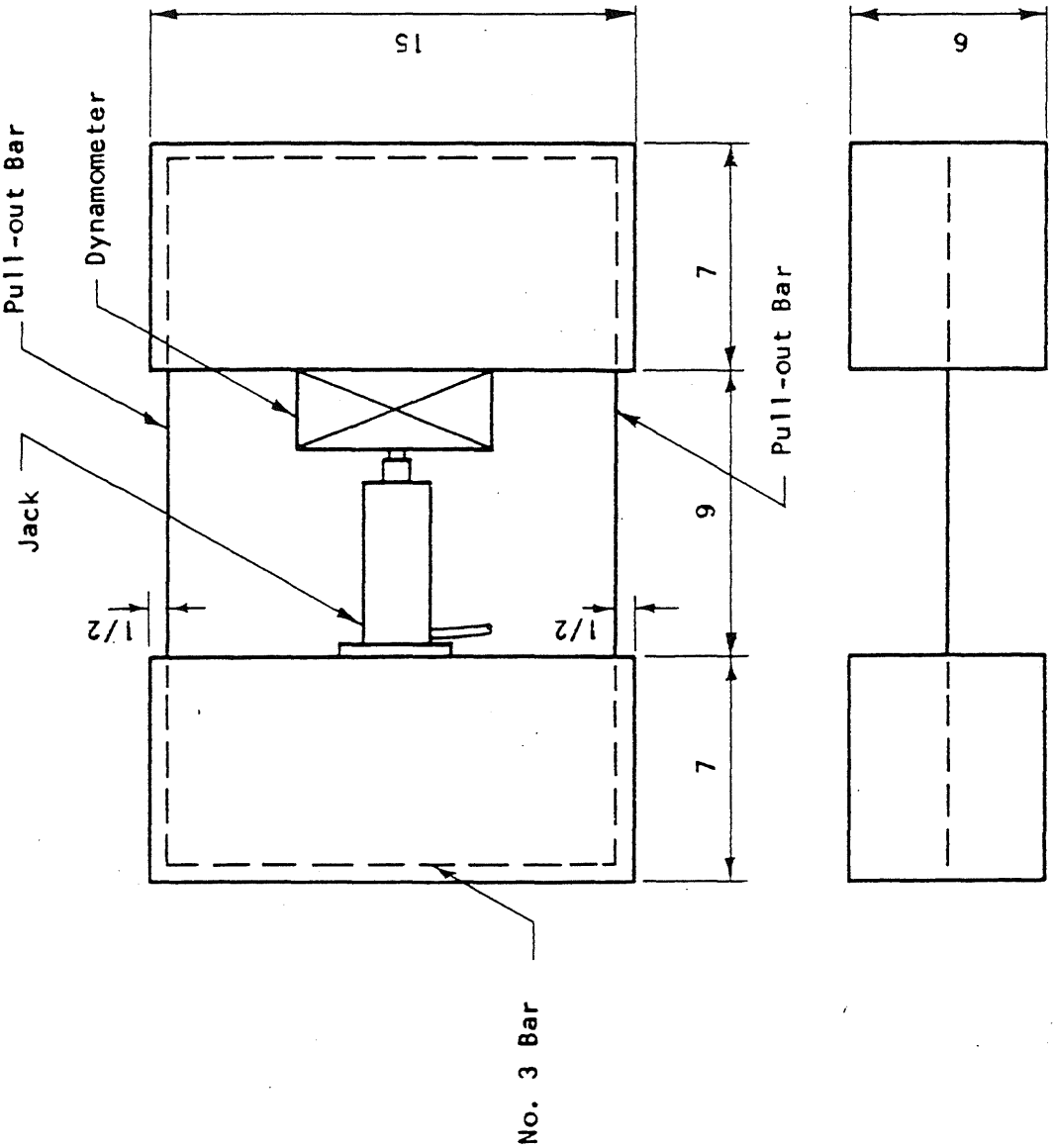

FIG. B.3 TWIN PULL-OUT SPECIMEN

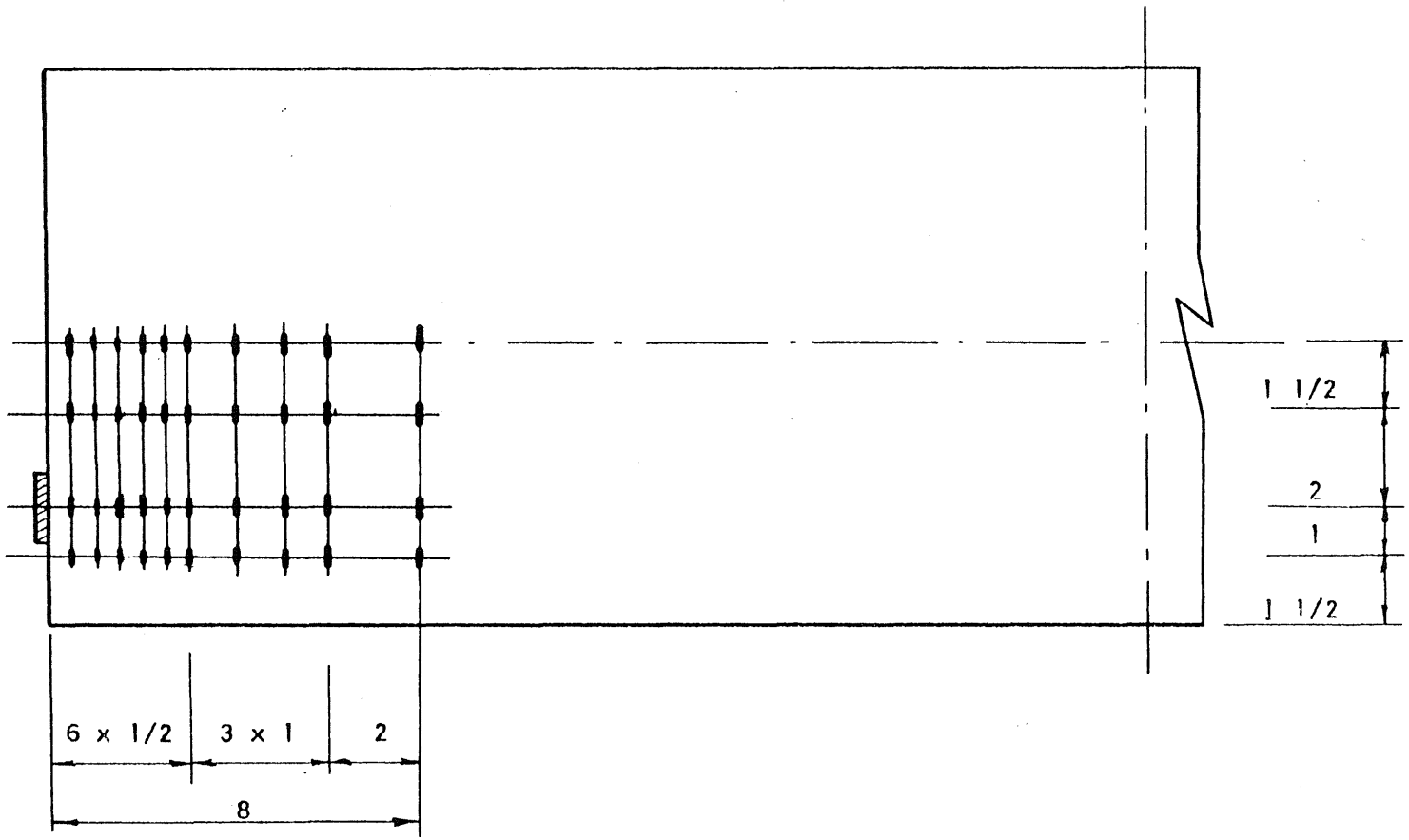

FIG. B.4 TYPICAL GAGE PATTERN

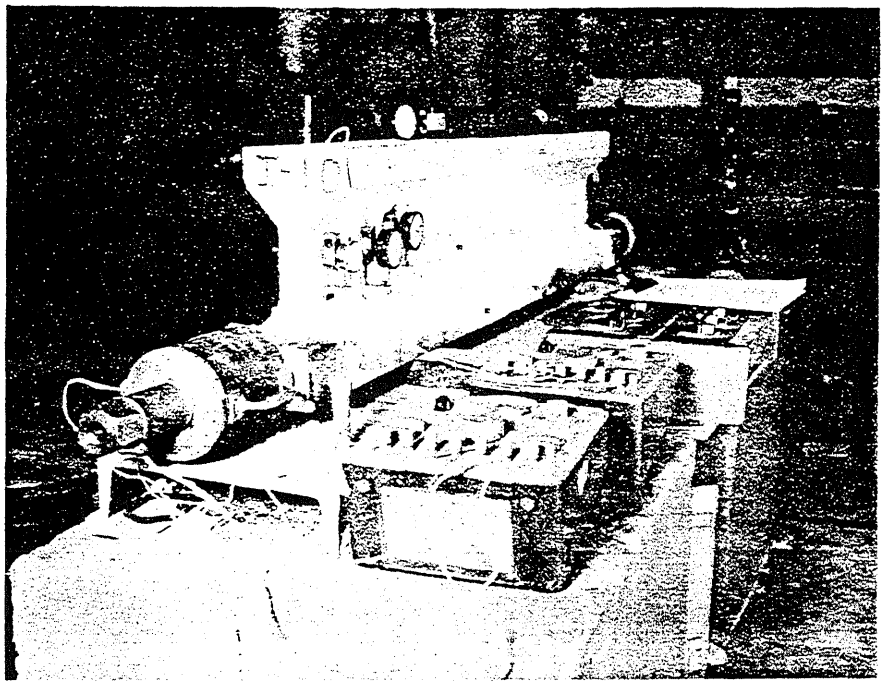

(a)

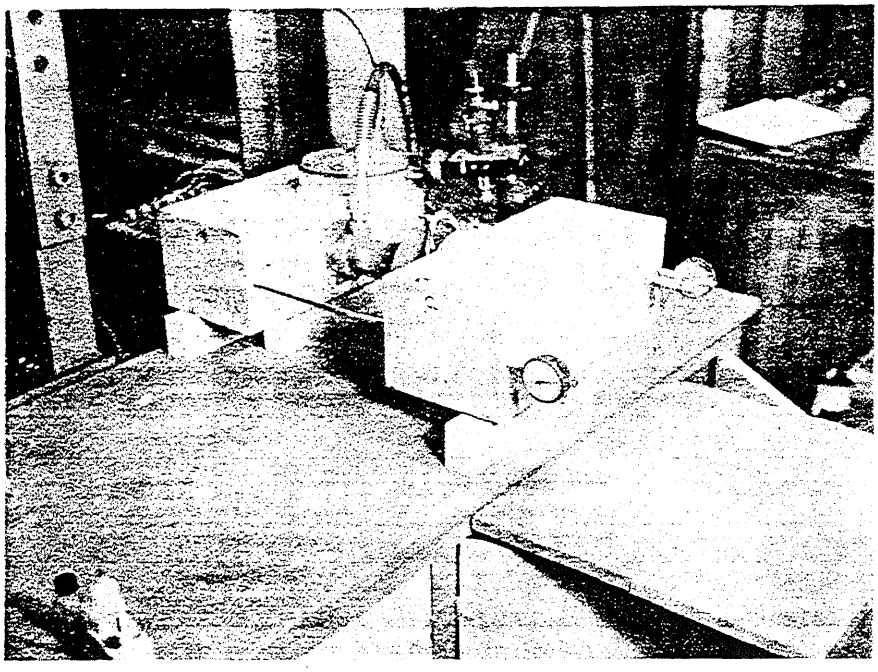

(b)

FIG. B.5 PHOTOGRAPHS OF BEAM AND TWIN PULL-OUT SPECIMENS

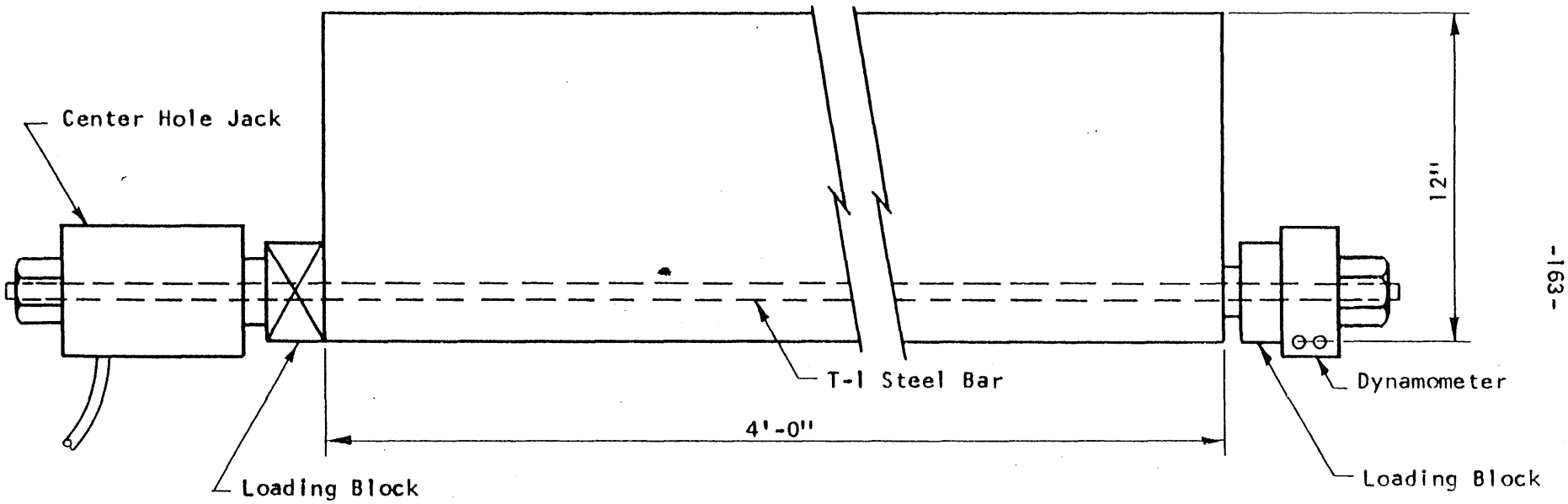

FIG. B.6 TEST SETUP

APPENDIX C

DESCRIPTION OF COMPUTER PROGRAM

C.1 Introductory Remarks

A high speed computer was used to achieve higher accuracy in the numerical procedure than other investigators obtained. The simplifying assumptions could thus be eliminated and the number of grid points could be increased.

A first solution was obtained using an IBM 650 computer but the time required to obtain sufficient convergence was prohibitive. For a symmetrical loading this machine would have been satisfactory but in the present investigation symmetry could not be utilized.

The final solution was done on the Control Data Corporation No. 1604 electronic digital computer.

A description of the numerical method is given in Section C.2. The input data are listed in Section C.3. The flow diagram is described in Section C.4. The output data and the validity of the program are presented in Section C.5.

C.2 Details of Numerical Procedure

As it was mentioned in Section A.2, the Airy stress function method was used in many analytical investigations. Some studies employed finite difference methods to execute the calculations. However, in all known cases some simplifying assumptions limited the confidence in the results. When no such assumptions were used, the answers were not given for the non-symmetric case and at a sufficient number of points. Some of these methods were discussed in Section A.2. The outline of the present procedure is described in Section 2.2 together with the assumptions and the theory behind it.

The biharmonic differential operator $\nabla^4 F = 0$ is replaced by the corresponding finite difference operator. Since the stress gradient is large around the load, a fine grid is necessary to get satisfactory answers. Symmetry conditions must be utilized as fully as possible to reduce the number of points and thus greatly facilitate the computations.

If the single eccentric load is considered to be made up of two loadings, one symmetrical and one anti-symmetrical as shown on Fig. C.1, then the calculations are not simplified. In the symmetrical case only one quarter of the region has to be considered. However, in the anti-symmetrical case no such simplification exists and half of the region must be included.

In the present procedure the region shown in Fig. 2.1 was treated. A grid of 1/2 by 1/2 in. yielded 897 grid points inside the region. An iterative method was applied to solve the problem. The biharmonic finite difference operator, that is shown on Figs. C.2, was applied successively to every inside grid point. This slow procedure could be used because of the availability of the high speed computer.

The boundary values were given in Section 2.2. Everything was calculated for P/A = 1, that is, for P = 72 kips. The corresponding boundary values of the stress function and its normal derivatives are given in Fig. 2.1. The normal derivatives established the necessary relation between the values of the stress function immediately outside and immediately inside the boundary.

The first iteration lasted 500 cycles. The shape of the stress function was then estimated to get a better approximation for the second run. For example, linear stress distribution of the longitudinal stresses was assumed from y = 0 to y = 14 in. To achieve better convergence in the significant parts of the region, the iteration was modified to do more cycles in these sub-regions for one full cycle. One cycle involved iteration

on the whole, the top half, the top third and the unloaded quarter corner of the region. In the final run all this was done 1000 times. The time between was 48 minutes and 23 seconds. Similar calculation on the IBM 650 would require over 48 hours.

After the end of the last cycle, the transverse stresses, the longitudinal stresses, the transverse strains and the residuals were calculated and printed by the computer. The residuals and the sum of the residuals gave an indication of the convergence of the procedure. The method of calculation of these quantities was described in Section 2.2. In the final run these quantities were calculated and printed after 750 cycles to serve for comparison with the final values.

C.3 Input Data

The values of the stress function on the boundaries were given by the boundary conditions. The values at the imaginary points immediately outside the boundaries were related to the values at the points immediately inside the boundaries. These correlations were coded on the cards together with the other initial values. Values were assumed for inside points as described in Section C.2. For the final run these values were punched on cards or were duplicated by the computer where that was possible.

The number of cycles was changed for every run to suit convergence and duration of run.

The value of Poisson's ratio was fixed for each run.

C.4 Flow Diagram

The flow diagram of the program is presented in Fig. C.3. The detailed flow diagram is not much more complex than the general one, hence

more of the details are included in Fig. C.3. The FORTRAN coding system simplifies most of the problems involved in cyclic computations.

The stresses, strain, and residuals were calculated and printed after a certain number of cycles as well as after the last cycle. This was done for all 897 points.

C.5 Output Data

The output consisted of the print-out of the following quantities: transverse stresses, longitudinal stresses, transverse strains, values of the stress function, and residuals. These were given for all 897 grid points. Also the time required and the number of cycles were printed.

In the last run all the above was calculated and printed after the 750th and after the 1000th cycle. The residual with the largest absolute value was -0.00205. The corresponding value of the stress function was 5.739. The smallest absolute value of the stress function in the critical regions was 0.0371 (at all other points of interest this value was considerably larger). The residue at this point was -0.000038. These proportions seemed to hold or were better at other points.

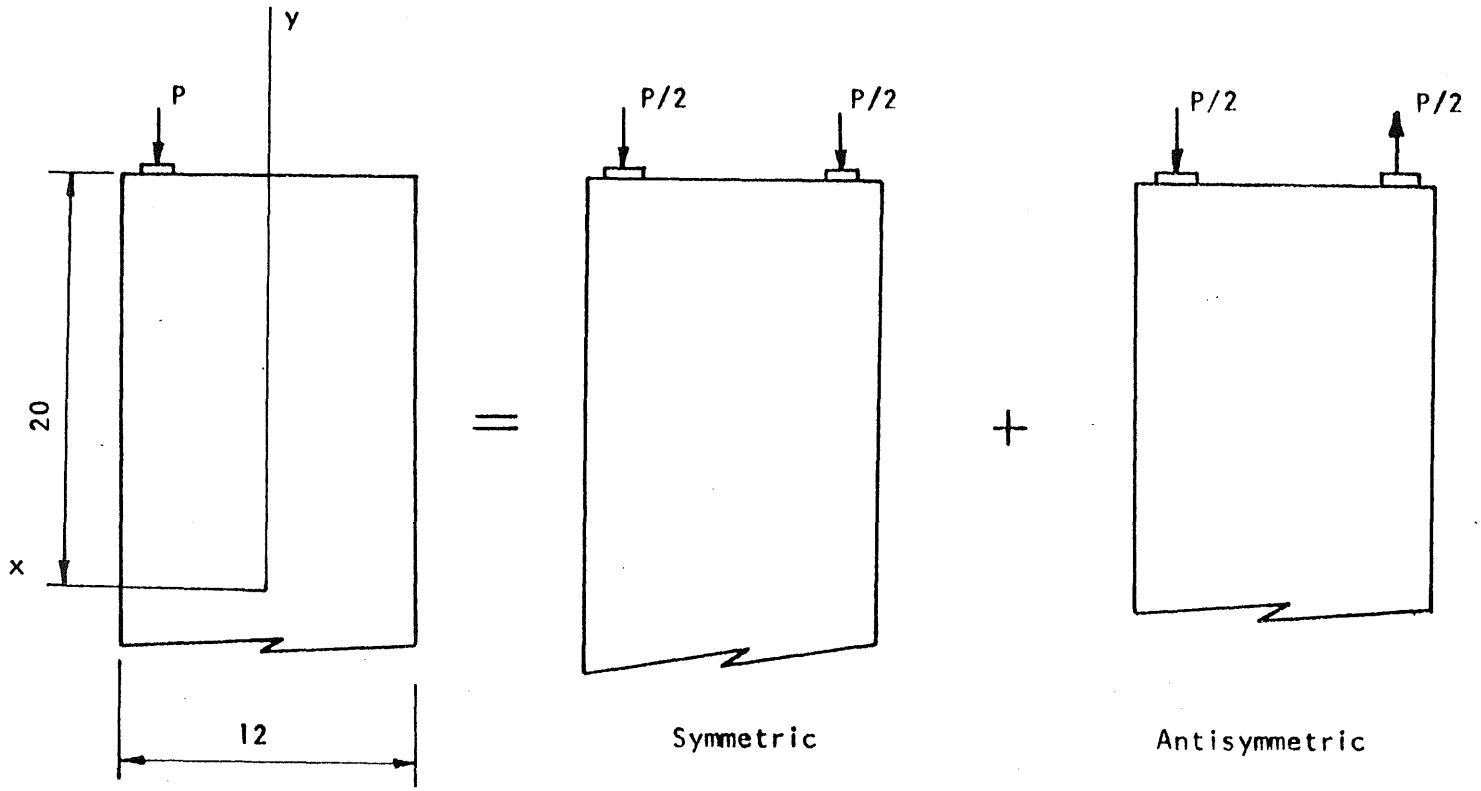

FIG. C.1 SUPERPOSITION OF LOADINGS FOR NUMERICAL SOLUTIONS

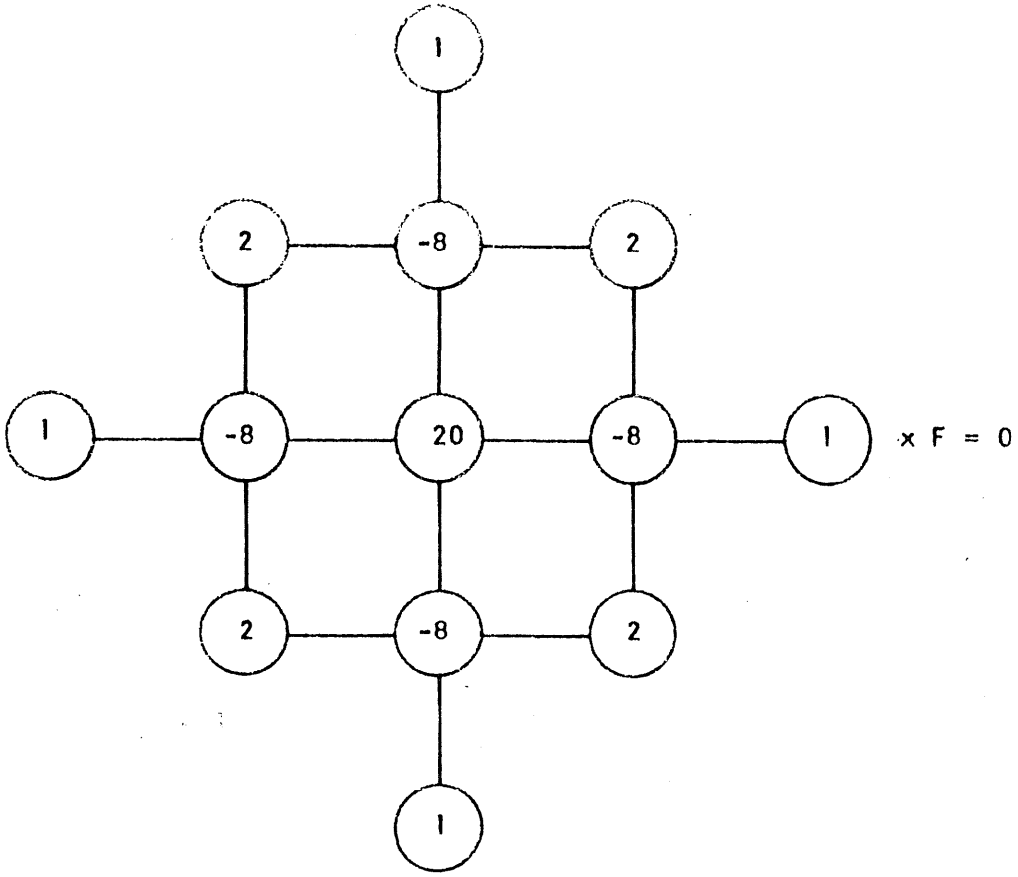

FIG. C.2 BIHARMONIC FINITE DIFFERENCE OPERATOR

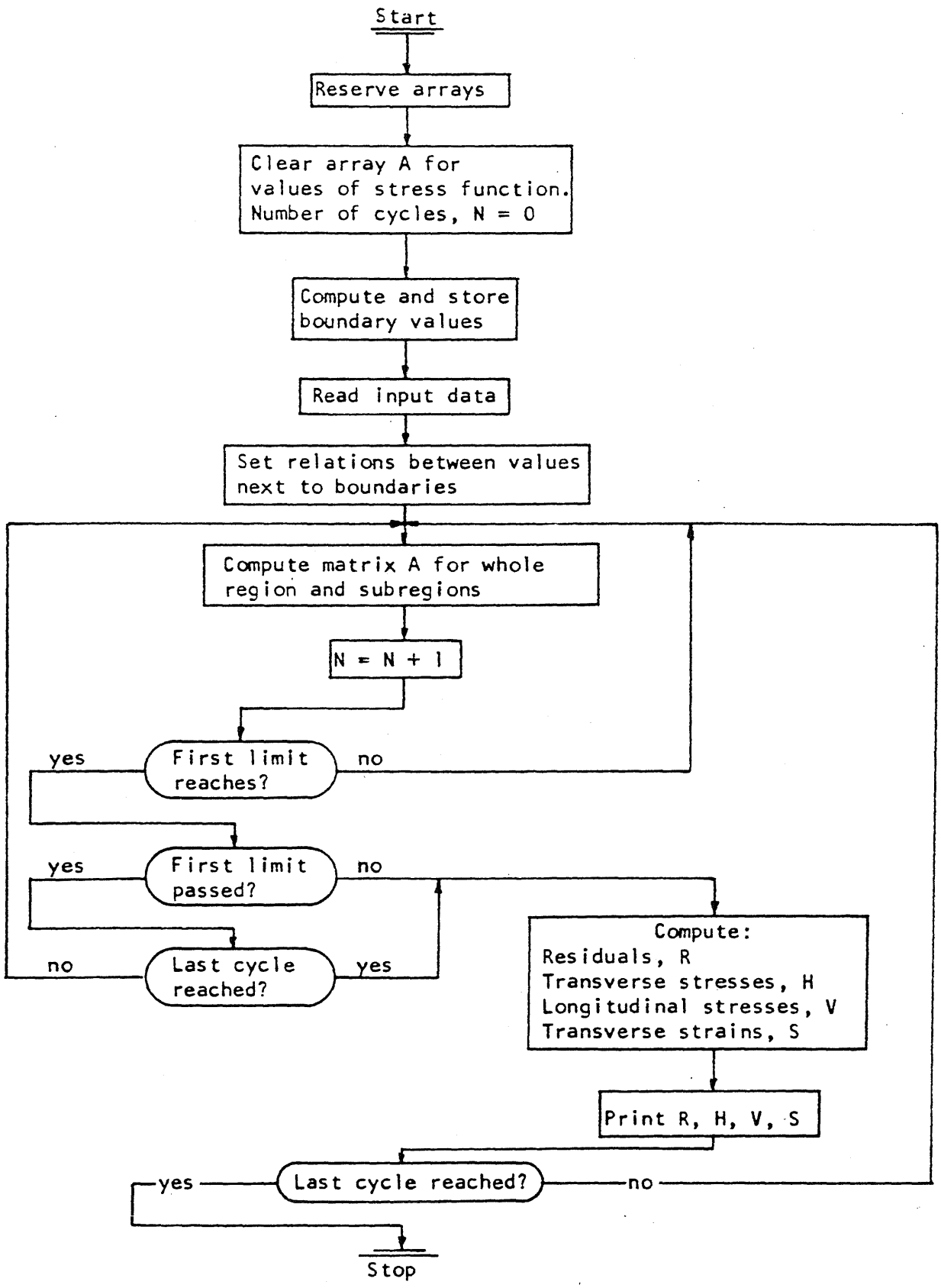

FIG. C.3 FLOW DIAGRAM